THE INFLUENCE OF DAMAGE ON THE CREEP BEHAVIOUR OF ICE SUBJECT TO MULTIAXIAL COMPRESSIVE STRESS STATES

SHAWN PATRICK KENNY

The Influence of Damage on the Creep Behaviour of Ice Subject to Multiaxial Compressive Stress States

by

© Shawn Patrick Kenny, B.Eng.

A thesis submitted to the School of Graduate Studies
in partial fulfillment of the requirements for the degree of
Master of Engineering

Faculty of Engineering and Applied Science
Memorial University of Newfoundland
May 25, 1992

St. John's Newfoundland Canada

ISBN 0-315-82653-3

Abstract

Medium-scale indentation tests, such as Pond Inlet (1984) and Hobson's Choice Ice Island (1989,1990), have shown that during rapid crushing events the failure zone can be characterized by distinct sub-regions. The behaviour of the damaged ice and crushed material located at hard spots or 'critical zones' of moderate to high confining pressures during interaction events is seen as the key to dynamic fluctuations in load and local peak pressures.

Consequently, an experimental program investigating the influence of microcracks on the creep response of polycrystalline, granular freshwater ice subject to hydrostatic confinement was conducted. The main objective of the test program was to better understand the creep behaviour of damaged ice generated at the contact zone during ice–structure interactions. A series of compressive stress pulses, which ranged from 0.3 MPa to 2.6 MPa, were applied to intact and pre-damaged samples under confining pressures of 0, 4, 10 and 20 MPa. The damage state was nominally uniform for all tests which was developed by loading the ice sample at a constant displacement rate of 10^{-4} s^{-1} to 2% axial strain.

Although the elastic response was marginally influenced by the pre-damaging path, the magnitude and rate of creep strain was significantly enhanced independently of the hydrostatic pressure. Also, the creep deformation was non-linear with applied deviatoric stress and exhibited a tendency for viscous processes to dominate at higher load levels. One of the key findings was the magnitude of lateral strain, hence volumetric deformation, and shear strain developed independently of the confining pressures investigated. The considerable enhancement and non-linearity of creep strain evident in the experimental program has significant implications when considering full-scale events. Furthermore, the findings point to possible simplifications to ice-load models and constitutive relationships that may be utilized in continuum analysis of ice–structure interaction.

Acknowledgements

The author greatly appreciates the academic guidance and friendship, throughout the course of this work, from my supervisor, Dr. Ian Jordaan. Special thanks to Dr. Garry Timco, National Research Council Canada (IME), for thoughtful input and suggestions. Also, Dr. Stephen Jones and Mr. Trent Slade, National Research Council Canada (IMD), must be recognized for their co-operation and assistance. Finally, thanks to Mr. Jing Xiao, Memorial University, for helpful comments and interesting discussions on ice engineering.

Financial assistance for this work was provided by Atlantic Accord Career Development Awards Board and NSERC.

Contents

List of Figures

List of Tables

Nomenclature

A	- constant, reference strain-rate per unit stress ($mm \cdot mm^{-1} \cdot s^{-1} \cdot MPa^{-1}$).
b	- power index $\approx 1/n$.
c_1	- constant for reference grain size (mm).
d	- material grain size (mm).
d_1	- reference grain size.
$D(t-\tau)$	- creep compliance function.
e	- equivalent strain ($mm \cdot mm^{-1}$).
$\dot{e}$	- equivalent strain-rate ($mm \cdot mm^{-1} \cdot s^{-1}$).
E	- elastic modulus (MPa).
E_k	- elastic modulus of the Kelvin unit (MPa).
E_m	- elastic modulus of the Maxwell unit (MPa).
E_o	- is the initial modulus of intact material (MPa).
$f(S_\sigma)$	- damage effect parameter.
m	- constant.
n	- power law constant, typically taken as 3.
N_A	- number of grains per unit area.
$\dot{N}$	- is the rate of crack nucleation.
$\dot{N}_o$	- is the rate constant.
p	- hydrostatic pressure (MPa).
q	- stress exponent.
s	- constant = 1.
S	- von Mises stress (MPa).
S_σ	- Schapery's damage parameter.
t	- time (s).
T_m	- melting point (° Kelvin).
α	- inverse relaxation rate (s^{-1}).
ϵ	- strain ($mm \cdot mm^{-1}$).
$\epsilon(t)$	- time-dependent deformation ($mm \cdot mm^{-1}$).
ϵ_c	- viscous strain ($mm \cdot mm^{-1}$).
ϵ_d	- delayed elastic strain ($mm \cdot mm^{-1}$).
ϵ_e	- elastic strain ($mm \cdot mm^{-1}$).
ϵ_{ij}	- deviatoric strain ($mm \cdot mm^{-1}$).
ϵ_v	- volumetric strain ($mm^3 \cdot mm^{-3}$).
$\epsilon_{1,2,3}$	- principal strains ($mm \cdot mm^{-1}$).
$\dot{\epsilon}$	- strain-rate ($mm \cdot mm^{-1} \cdot s^{-1}$).
$\dot{\epsilon}_c$	- reference viscous strain-rate ($mm \cdot mm^{-1} \cdot s^{-1}$).
$\dot{\epsilon}_o$	- reference strain-rate ($mm \cdot mm^{-1} \cdot s^{-1}$).
$\dot{\epsilon}_v$	- volumetric strain-rate ($mm^3 \cdot mm^{-3} \cdot s^{-1}$).

λ	- is the damage parameter.
σ	- applied stress (MPa).
σ_c	- critical stress for crack nucleation (MPa).
σ_{ij}	- deviatoric stress (MPa).
σ_o	- normalizing or unit stress (MPa).
σ_v	- volumetric stress (MPa).
τ	- applied shear stress (MPa).
η_k	- viscosity of the Kelvin unit ($MPa \cdot s^{-1}$).
η_m	- viscosity of the Maxwell unit ($MPa \cdot s^{-1}$).

Chapter 1

Ice–Structure Interaction: Rationale for Ice Mechanics Research

The majority of Canada's offshore natural resources, such as mineral deposits and hydrocarbon reserves, are situated on the continental margins. Exploration and recovery of these resources, in Arctic and sub-Arctic waters, presents a formidable challenge to the engineering and scientific disciplines. One of the most important factors to consider in design is the magnitude of ice pressure exerted on offshore structures and vessels. Estimating reliable design ice loads is essential to ensure structural integrity and economy of design.

The development of interaction models based on how ice deforms and ultimately fails appears to be a relatively straightforward engineering design problem. However, past investigations have shown that average global ice pressures range from 10 MPa in small-scale laboratory tests to 0.5 MPa for impacts of multi-year sea ice with artificial islands. This pronounced variation between measured index me-

chanical properties and full-scale ice behaviour is known as the *scale effect.* The phenomenon has been generally associated with non-simultaneous, brittle failure and statistical distribution of flaw size; see for example Iyer (1989) or Sanderson (1988). Consequently, prediction of ice forces is typically empirical in nature and based on extrapolation of data by considering the contact area or aspect ratio (Figure 1.1). Moreover, ice–structure interaction events are complex and depend upon many factors, such as inherent material and mechanical properties of ice, degree of confinement, structural compliance and contact geometry. Also, recent laboratory and field investigations have indicated that friction or pressure melting and sintering are active mechanisms. Although the crushing mode of failure is generally observed during interaction events, the process can be compounded by mixed-mode deformation (i.e. crushing coupled with splitting, out of plane flexure, spalling, or buckling). Typically during crushing events, regions of damaged and crushed ice are generated at the contact zone and discrete particles are ejected at the free surface.

Experience with small-scale indentation tests (Kry, 1978), lighthouses (Määttänen, 1977) and Cook Inlet platforms (Blenkarn, 1970) revealed that during a predominantly crushing mode of failure, there was a cyclical variation in the load accompanied by structural vibrations. Although recognizing the significance of ice-induced vibrations, past design philosophy considered that only narrow, flexible structures would be susceptible. In the winter of 1986, however, the Beaufort Sea structure *Molikpaq* experienced severe vibrations due to the repeated crushing failure of a multi-year ice floe which produced an eight metre high pile of pulverized ice adjacent to the structure (Jefferies and Wright, 1988). A prominent feature of the

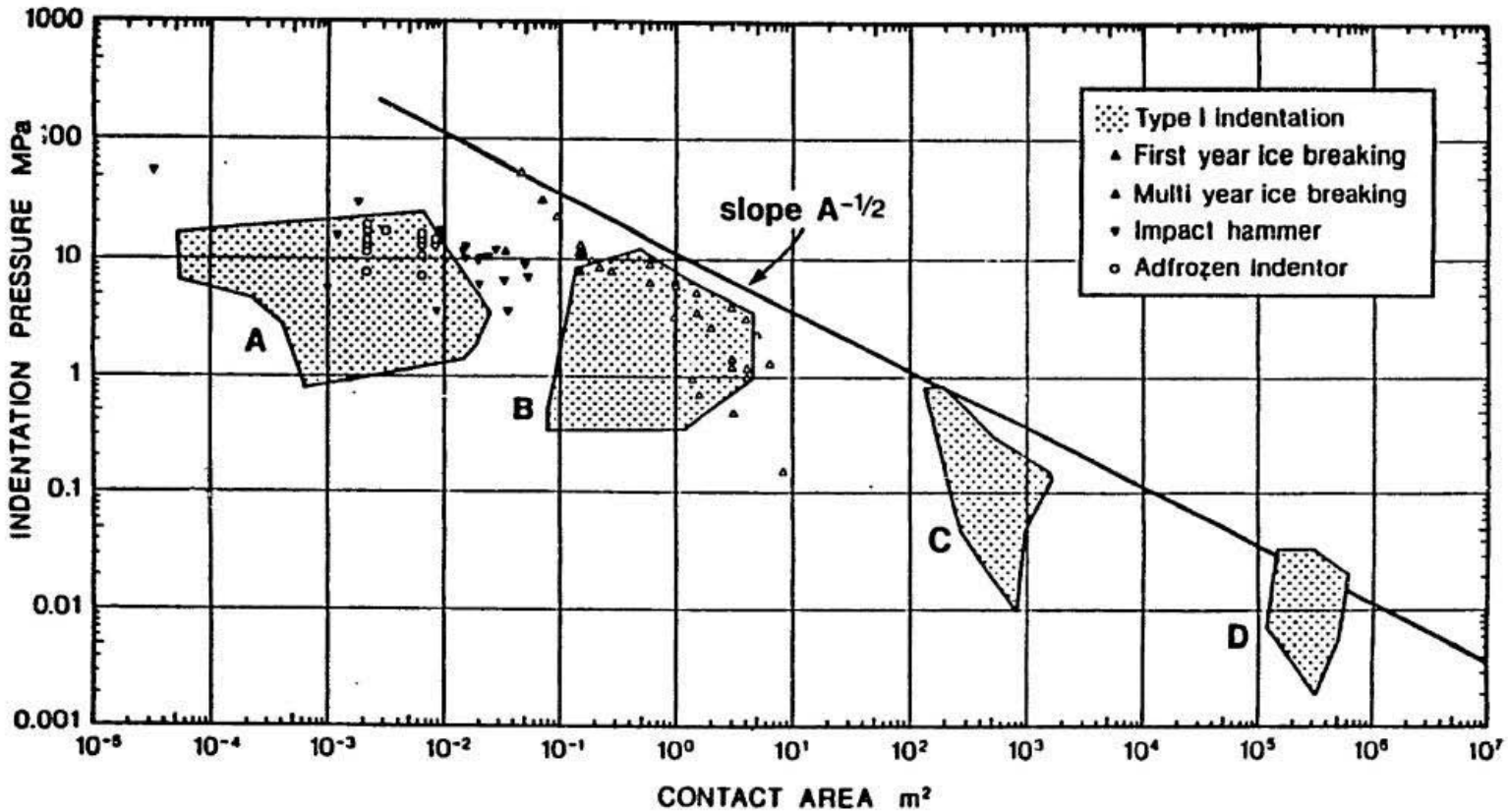

Figure 1.1: Pressure–Area Curve for Ice Illustrating the *Scale Effect* Phenomenon. The Dataset is Compiled From Various Interaction Scenarios and Only Indicates a General Observed Trend. *Sanderson (1988).*

interaction was a *phase-lock* phenomenon which enhanced the peak ice loads and increased the amplitude of vibration.

In an effort to understand the scale effect and dynamics of the ice crushing crushing process, a number of medium-scale indentation tests, such as Pond Inlet (Johnson and Benoit, 1987) and Hobson's Choice Ice Island (Frederking et al., 1990) have been jointly undertaken by government, industry and university research establishments. Typical average global pressures exerted were on the order of 3–5 MPa, whereas local peak pressures attained magnitudes of 60 MPa or more which had a characteristically varied spatial and temporal distribution accompanied with steep pressure gradients.

Clearly, the design of offshore structures to resist ice forces is a demanding task which must consider average global pressures (foundation, stability), magnitudes and distributions of peak local pressures (framing members, plates) and dynamic vibrations (working conditions, structural integrity). The complexity of ice-structure interactions has hindered the development of any rigorous method for the calculation of design ice forces. Although there are many empirically based methods oriented toward deterministic or probabilistic design loads, the difficulty lies within the development of a 'simplified' ice load model based on index mechanical properties and field data which accurately predicts full-scale behaviour for a number of scenarios.

Consequently, in the development of constitutive laws and failure criteria for ice, numerical techniques, such as the finite element method (FEM) appear to be most promising. However, any analytical or numerical model is dependent on the quality of input parameters and basic understanding of ice mechanics. Only by investigating

the underlying failure mechanisms involved can one develop a more realistic approach in ice mechanics to analyse interaction events and establish a foundation upon which accurate and reliable ice loads can be determined.

The focus of this thesis is to investigate the influence of microcracks on the creep deformation of granular, freshwater ice subject to triaxial compressive stress states. The experimental program aims to 'simulate' the behaviour of the highly damaged crushed material, subject to volumetric and deviatoric stress states, which is created at the contact surface during ice–structure interactions. Using this approach, the ultimate goal is the development of a realistic ice load model to aid in the design of offshore structures. The scope of the work presented herein may be summarized as follows:

1. Literature review of the damage process in ice with specific reference to laboratory and field data concerning compressive failure.
2. Description of the test program including laboratory apparatus and experimental procedure.
3. Analysis and discussion of the test data.
4. Critical assessment of the major findings and recommendations for future research.

Chapter 2

Deformational Behaviour of Ice

Recent investigations have shown that the dynamics associated with ice–structure interaction events can be, in part, related to the physical attributes of the contact zone. The process whereby an intact ice feature progressively damages and crushed material is subsequently extruded with continued deformation is presently the subject of considerable interest.

The scale effect necessitates the combination of full-scale observations, field measurements and controlled laboratory experiments whereby key parameters for the development of an ice–load model can be characterized.

2.1 Continuum Viscoelastic Response

Unlike most engineering materials, ice naturally exists at high homologous temperatures, typically $\geq 0.85\ T_m$, where T_m is the melting point in degrees Kelvin. Similar to metals, concrete and rock at high temperatures, ice will creep when subjected to any stress other than a purely hydrostatic stress state. This is evident in the flow of glaciers, where the strains experienced at the base, subject to enormous confining pressures, has essentially the same deformational response when ice is loaded under uniaxial conditions. Although creep is generally associated with a continuum process, at higher loading rates it is significantly influenced by the presence of cracks.

Long-term creep is developed through three stages of varying strain-rates; an initial transient creep rate, secondary steady-state phase and, finally, an increasing creep rate (Figure 2.1). There is some debate as to whether the secondary or minimum creep rate is a fundamental material property or merely marks the transition from the primary to tertiary stages — see for example Sinha (1990a). The tertiary stage is often associated with microcracking and large strains, which results in accelerated deformation rates and possible failure (Gold, 1972). This has also been evident in the time-dependent deformation of brittle rock (Costin, 1985). However, Sanderson (1988) points out that dynamic recrystallization can also initiate tertiary creep. Thus it is difficult to differentiate between the intrinsic deformational response and that due to damage.

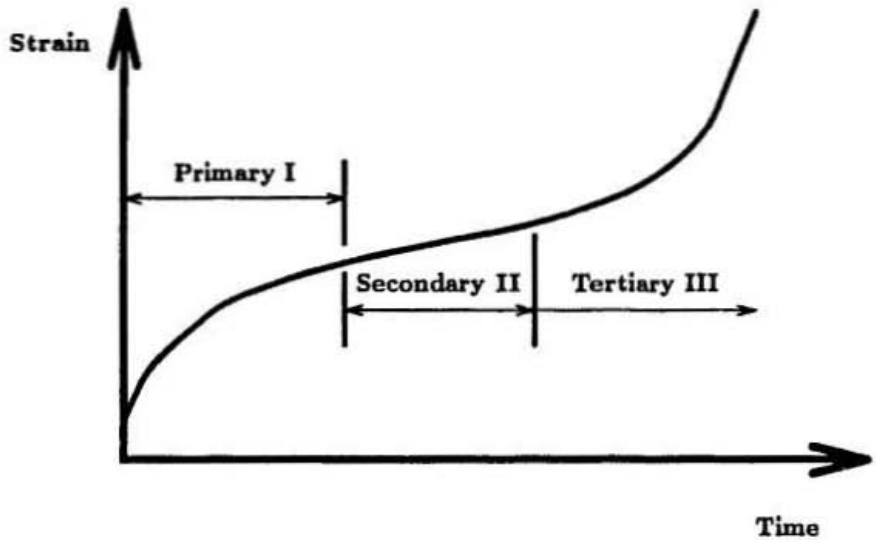

Figure 2.1: Long-Term Creep for Polycrystalline Granular Ice Marking the Three Stages, Primary I, Secondary II and Tertiary III.

The time-dependent deformational behaviour of ice under load, modeled as a linear viscoelastic solid under a uniaxial stress state, can be expressed as,

$$\epsilon(t) = \int_0^t D(t-\tau)\frac{\partial \sigma}{\partial \tau} d\tau, \tag{2.1}$$

where $0 \leq \tau \leq t$ and $D(t-\tau)$ is the creep compliance (ratio of ϵ/σ) when a constant stress is applied at time $t = 0$. Mechanical models simulating the viscoelastic behaviour of materials typically employ the combination of spring (Hookean) and dashpot (Newtonian) elements; see Figure 2.2.

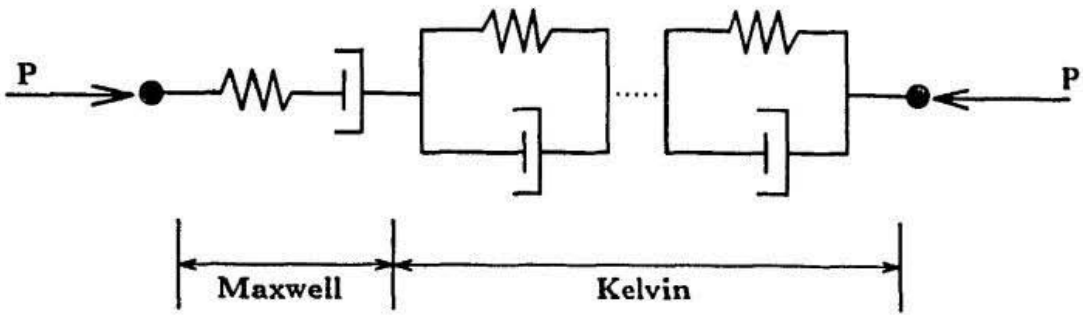

Figure 2.2: Generalized Viscoelastic Model. The First Two Elements, a Single Spring and Dashpot, Comprise the Maxwell Body and the Sequence of Parallel Elements Correspond to Kelvin Units.

The creep compliance for the rheological model shown in Figure 2.2 is given by (Flügge, 1967),

$$D(t-\tau) = \frac{1}{E_m} + \sum_{k=1}^{n} \frac{1}{E_k}\left[1 - exp\left(\frac{-E_k}{\eta_k}(t-\tau)\right)\right] + \frac{t-\tau}{\eta_m}, \tag{2.2}$$

where E is the elastic modulus,

η is the viscosity and

$\frac{\eta}{E}$ is the inverse retardation time.

Jordaan et al. (1990a) and Schapery (1991) point out that for the series of Kelvin units a spectrum of retardation times with a distribution function is required. However, in practice, the determination of such a formulation proves to be difficult and one resorts to approximate methods — see Jordaan and McKenna (1988).

During continuous ice crushing and clearing events the force-time history is dynamic in nature (1–60 Hz) and the time of loading can be considered rapid. The creep

response can be thus generalized by considering the primary and secondary terms and the total deformation expressed as,

$$\epsilon = \epsilon_e + \epsilon_d + \epsilon_c \tag{2.3}$$

where ϵ_e is the elastic strain,

ϵ_d is the delayed elastic strain and

ϵ_c is the viscous flow.

Delayed elasticity (transient or primary creep) is a recoverable strain process whereby grain boundary sliding occurs, through diffusional flow, due to the shear stresses generated between grains. Viscous flow (power-law or secondary creep), however, is non-recoverable deformation as a result of intragranular dislocation movements. The reader is referred to Hobbs (1974) and Sinha (1978) for further discussion on the physics of creep in ice.

On discussing the creep process in ice, the approach taken in this thesis is to describe the nonlinear viscoelastic behaviour by a four-element Burgers model (Figure 2.3). The absence of a Kelvin series, to describe the the non-linear deformational characteristics of ice, precludes simple closed-form solutions using linear viscoelastic theory based on the basic Burgers model. Consequently, Jordaan and McKenna (1988) and Szyszkowski and Glockner (1985) propose that the viscosities be considered stress-dependent.

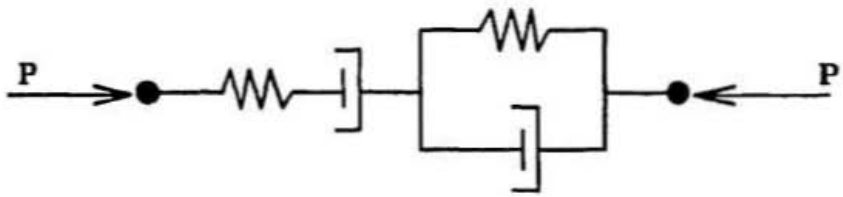

Figure 2.3: Four Element Rheological Model for Polycrystalline Ice. The Burgers Model is a Combination of a Kelvin Unit, which Corresponds to Delayed Elastic Strain, and a Maxwell Body, which Represents Elastic Deformation and Viscous Flow.

There are many phenomenological and constitutive models proposed for the creep behaviour of ice; see for example, Ashby and Duval (1985) and Duval et al. (1991). Although there is general agreement on the form of a secondary creep expression (i.e. power law), the time-dependent deformation is less well characterized. This is a consequence of the early work on creep of ice which concentrated efforts on the long term flow of glaciers. The basic relationship more commonly adopted, as in this thesis, for creep compliance is that due to Sinha (1978).

$$\epsilon(t) = \frac{\sigma}{E} + c_1 \left(\frac{d_1}{d}\right) \left(\frac{\sigma}{E}\right)^s \left(1 - exp\left[-(\alpha_T t)^b\right]\right) + \dot{\epsilon}_c t \left(\frac{\sigma}{\sigma_c}\right)^n \qquad (2.4)$$

where σ is the applied stress at time $t = 0$, E is the bulk elastic modulus, c_1 is a constant for a given reference grain size (d_1), d is the ice grain size, α_T is the inverse relaxation rate, $\dot{\epsilon}_c$ is the reference viscous strain-rate at σ_c and b, s, and n are constants.

The semi-empirical equation is valid for isotropic polycrystalline ice in which the microstructure has not deteriorated due to the presence of voids or fractures. As will be discussed in more detail later, the creep response is significantly influenced by microcracking.

2.2 The Progressive Damage Process in Ice

Damage connotes a change in structural integrity which results in the weakening of a material by reducing the effective modulus or stiffness. There are many microstructural characteristics which can be attributed to damage; these include, nucleation and growth of cavities which cause grain boundary embrittlement, the creation of fracture surfaces, and even the presence of voids, solid inclusions or pre-existing defects, such as brine pockets and drainage channels. For the purposes of this investigation, the damage process associated with microcracks is of primary importance and a description based on laboratory and field experience will be presented.

2.2.1 Microcrack Evolution Under Compressive Stress States

Ice is a unique material, in that it can behave as a viscoelastic solid and yet exhibit extreme brittleness under high loading or deformation rates. The propensity for fracturing can be appreciated by the low values of fracture toughness (150–200 $kPa \cdot m^{1/2}$) and strain energy release rate (0.5–2.0 $J \cdot m^2 \cdot s^{-1}$), which is of the same order as glass. The splitting of ice floes several kilometres in dimension markedly illustrates the brittle behaviour of ice (Figure 2.4). Although this describes a scenario different from that of a progressive damaging process under compressive stress states, it nevertheless demonstrates the extent to which fracturing may take place.

Recently, there has been significant research effort conducted on the characterization of events leading up to initial crack formation and the subsequent damage process in ice. These investigations include Cole (1985,1991), Hallam (1987) and Sinha

Figure 2.4: Photograph of a Multiyear Floe Impacting Hans Island. Note the Large Tensile Fracture which Has Propagated the Length of the Ice Floe ($\approx$ 2 kilometres) Causing the Ice Feature to Rotate Away From the Island.

(1984,1990b). The compressive fracture process can be essentially divided into two distinct events: crack nucleation and crack coalescence. Unlike deformation under tensile stresses where a single crack dominates sudden failure, an array of stable microcracks is formed under compression and the nucleation is considered to be, at least initially, independent of neighbouring events. Generally speaking, for high deformation rates ($\dot{\epsilon} \geq 10^{-4}$ s^{-1}), the initial cracks form at approximately 0.05% strain which corresponds to stress initiation levels on the order of 2 MPa (Cole, 1991). The cracks grow rapidly relative to the loading rate and show no tendency to propagate after formation (Hawkes and Mellor, 1972). Thus their evolution can be considered instantaneous growth to full size which is on the order of a grain facet. Kalifa et al. (1990) studied crack nucleation through video recording and determined that the nucleation of a crack occurs within 0.07–0.14 seconds. Also, a number of investigations on polycrystalline freshwater ice have shown that the cracks developed are predominantly aligned parallel with the principal compressive stress axis and randomly oriented in a plane perpendicular to the stress axis; see for example Kalifa et al. (1989) or Cole (1991). Interestingly, Jordaan and Timco (1988) showed that, during small-scale indentation tests, cracks oriented parallel to the loading direction were generated along lines of maximum shear. Continued deformation causes the crack density to increase whereby interaction or coalescence occurs and possibly culminating in abrupt failure. Although the characterization of the microcracking process in ice is well understood, there is still debate on the physical mechanism(s) responsible for the generation of cracks.

Gold (1972) was the first to conduct a comprehensive experimental study on the failure process in ice where an analysis on the dependence of microcracking activity with stress, strain and time was presented. It was observed that the cracking activity consisted of two independent distributions: one population of cracks was a function of the strain level and the other independent of strain. The former was considered to be associated with a dislocation pileup mechanism, based on the Smith-Barnby model, due to a resolved shear stress on the slip plane, and the latter was related to the inhomogeneous crystalline structure.

Sinha (1984) proposed that a critical grain boundary sliding displacement was responsible for the onset of cracking activity. Analysis on hundreds of grains showed that dislocation glide did not play a role in the formation of microcracks. Furthermore, it was stated that the contribution of delayed elastic and viscous creep components indicated that the fracture process was not truly brittle. However, this could also be attributed to the relatively low strain rates employed in the experiments ($\approx 10^{-5}$ to 10^{-4} s^{-1}) since there was a sharp decrease in strain to first cracks over a narrow range of increasing stress. This is also supported by observations made by Gold (1972) and Kalifa et al. (1989), where at higher loading and deformation rates, the cracks were predominantly generated at grain boundaries. Obviously, since ice is a viscoelastic solid, the influence of the creep components on fracture events is significantly dependent on time or rate processes.

The increasing fraction of intergranular cracks at higher deformation rates was associated with the anistropy of elastic material properties for neighbouring ice crystals within the solid matrix, that is, random orientation of the c-axis (Cole, 1988; Sunder

and Wu, 1990). When a remote stress is applied, nonuniform strain energies develop due to the incompatibilty associated with neighbouring grains which leads to stress concentrations and the formation of cracks. Unfortunately, location does not necessarily dictate the mechanism for crack nucleation since dislocation glide will produce both inter- and intragranular fractures. Also, similar grain size dependencies make it difficult to determine the source of the microcracking events (Cole, 1988).

With increasing deformation, cracks may begin to interact or coalesce at higher strains, but Cole (1991) did not observe growth of pre-existing cracks past the peak strength. However, experience with other brittle materials, such as ceramics, concrete, PMMA, and rocks, there has been observed growth of wing cracks — see for example Ashby and Hallam (1986), Cannon et al. (1990), Horii and Nemat-Nasser (1985). Wing cracks are out of plane extensions of pre-existing cracks inclined to the major compressive stress axis (Figure 2.5). A tensile stress zone develops at the tip of the fracture surface due to resolved shear stress and the crack is reoriented in the direction of the major stress axis. Further increase in strain energy causes the crack growth which could possibly propagate through the sample ends causing failure.

From a scientific viewpoint, the understanding of physical mechanisms responsible for cracks nucleation is important; however, for engineering purposes only the end effect on material behaviour is critical. A parallel can be drawm to plasticity theory where only the effects of dislocation movements are accounted for in the analysis. In any event, it would be practically impossible to follow the myriad of microcracks which are generated during the progressive damaging process in ice. The key devel-

opment is the structural deterioration due to a network of cracks which reduces the effective modulus of the material resulting in a loss of deformational resistance.

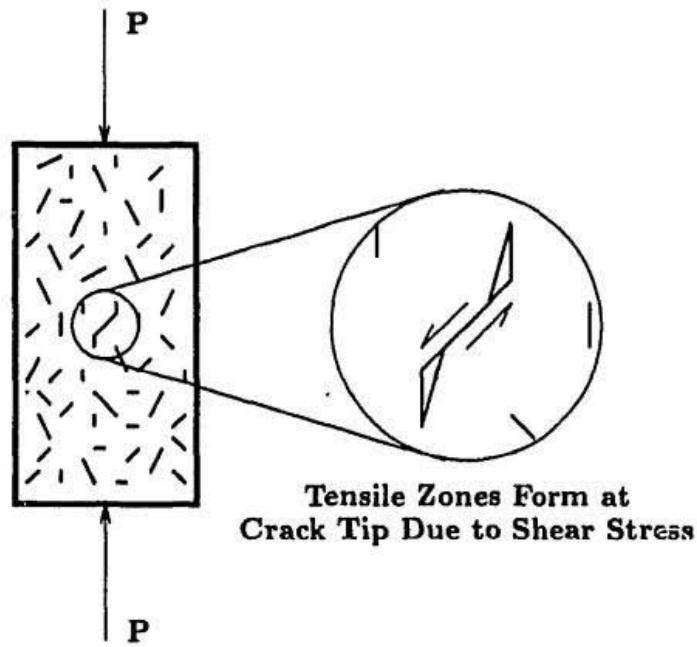

Figure 2.5: Schematic Illustration of Wing Crack Development in a Solid.

2.2.2 Macromechanics of the Ice Crushing Process

Present knowledge of the mechanical behaviour of ice has been founded on field measurements, controlled laboratory tests, as well as, past design experience. With the development of Arctic oil fields, early ice mechanics research (1960-70's) concentrated on peak forces and found not only considerable scatter in the data but also that ice strength was dependent upon a number of parameters. Indeed, Brown (1926) was one of the first to recognize this: "... the term compression or crush-

ing strength of ice is meaningless in-itself. The behaviour of ice in compression is different at the same rates of loading at different temperatures and at different rates of loading at the same temperature. The time factor is the all important quantity." Brown's insight on the deformational response of ice is shown clearly in Figure 2.6. Depending mainly on confinement and deformation rate, ice can behave as a nominally ductile creeping solid or an extremely brittle material.

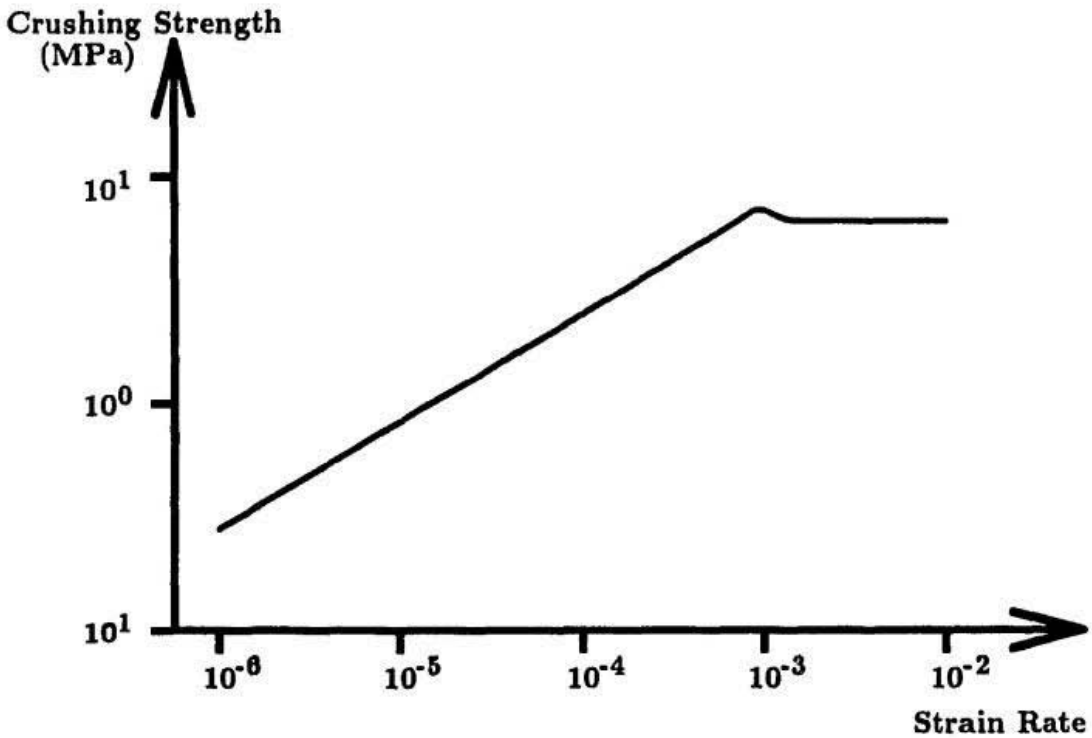

Figure 2.6: Logarithmic Plot of the Variation in Uniaxial Crushing Strength of Ice with Increasing Strain Rate.

For increasing strain-rates there exists a corresponding trend for higher peak strengths, with a maximum occurring around $\dot{\epsilon} \simeq 10^{-3}\ s^{-1}$. This region has been termed the ductile–brittle transition zone and is of particular engineering importance since the crushing strength is a maximum. The transition is related to a change in the observed deformational behaviour which can be mainly attributed to microcracking activity. This phenomenon is schematically illustrated in the generalized stress-strain curves for ice as shown in Figure 2.7.

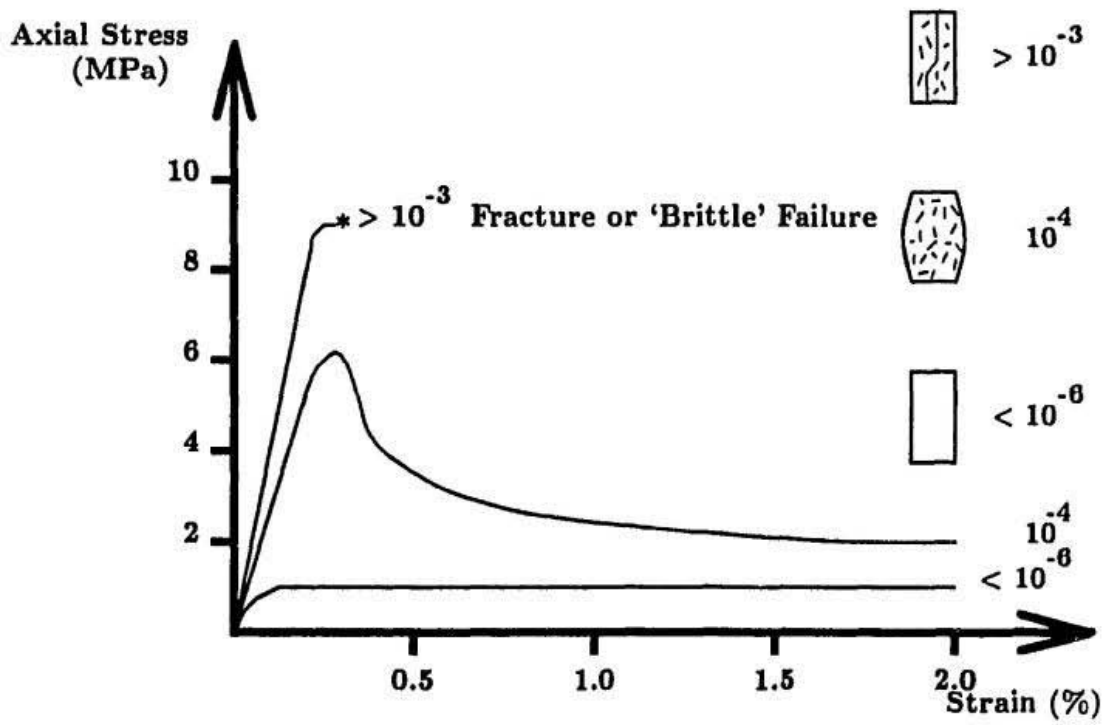

Figure 2.7: Schematic Illustration of the Stress–Strain Behaviour and Failure Modes for Ice under Uniaxial Compression with Increasing Strain Rates.

For the lower deformation rates ($\leq 10^{-6}$ s^{-1}) the behaviour is nominally ductile and continuum creep response is observed. As the strain-rate approaches the brittle regime, $\simeq 10^{-3}$ s^{-1} for uniaxial conditions, the propensity to form microcracks increases. Although peak stress is attained at relatively low strain level ($\simeq 0.002$), there is a considerable degree of damage due to the prescence of microcracks; this has been also observed by Cole (1991). Gold (1972) reported that when a rapid and extensive network of cracks developed, this caused a structural instability whereby the specimen loses resistance to deformation and creep is accelerated from the primary stage directly to tertiary behaviour. It should be noted that the transition strain-rate and degree of microcracking activity are dependent upon the same parameters. For example, Jones (1982) and Cole (1985) have shown that the transition strain-rate increases with confinement and finer grained ice respectively.

Prior to peak stress the cracks do not significantly influence the bulk mechanical properties. This can be appreciated by the slope of the stress–strain curve where microcracking leads to nonlinearity and 'strain softening' descending branch. This is also evident in other brittle materials like concrete and rock; see for example Dougill (1985). An important feature of the stress-strain curves shown in Figure 2.7 is the horizontal plateau reached after peak stress. This gives an indication of the active deformational mechanism; that is, one of continued energy dissipation through viscous creep ($\eta = \sigma/\dot{\epsilon}$). Also, if the sample is reloaded at the same strain-rate, then the plateau is followed and the stress–strain curve has become stabilized. However, with a subsequent increase in strain-rate the sample is further damaged and restabilizes (Figure 2.8).

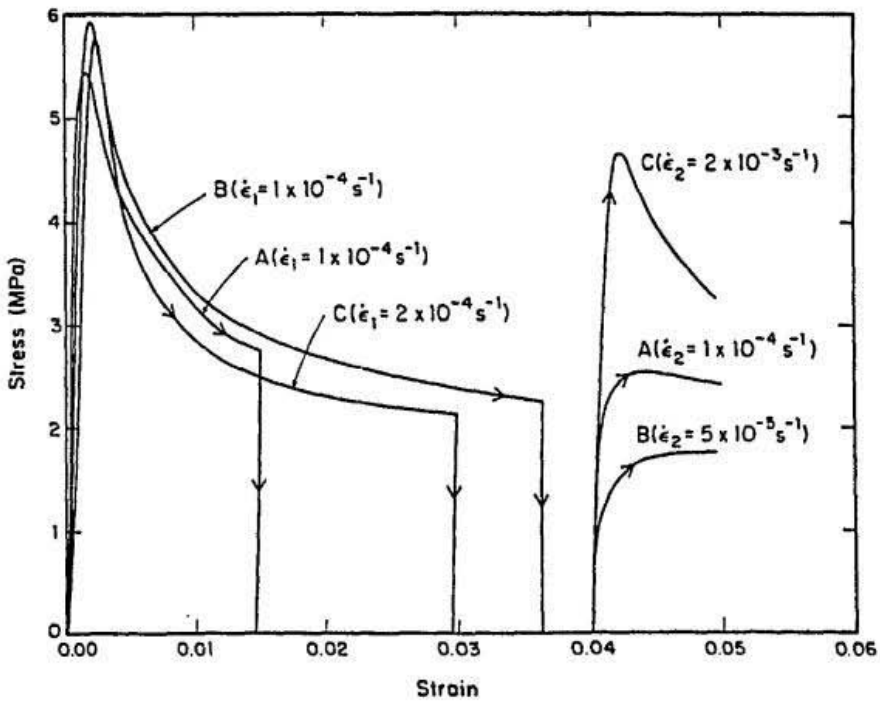

Figure 2.8: Typical Stress-Strain Curve for Polycrystalline, Granular Ice Loaded at Various Strain Rates. *Jordaan et al. (1990b).*

The direct effect of microcracking or damage is the degradation of the mechanical properties of the material, such as the loss in shear resistance (G) or bulk stiffness (E). Microcracking tends to reduce the overall structural resistance to deformation and enhances the basic creep response (Figure 2.9). Meyssonnier and Duval (1989) and Jordaan et al. (1990a) have shown that damage or prestrain causes a significant degradation in the mechanical properties of ice.

At high strain-rates ($> 10^{-3}$ s^{-1}), which are more applicable to dynamic ice-structure interaction events, phenomena known as slabbing or axial splitting can be observed in addition to microcracking. These events are associated with the out of plane extension of a pre-existing crack inclined to the major stress axis (Figure 2.5). The growth of wing cracks result in the reorientation of the crack surface par-

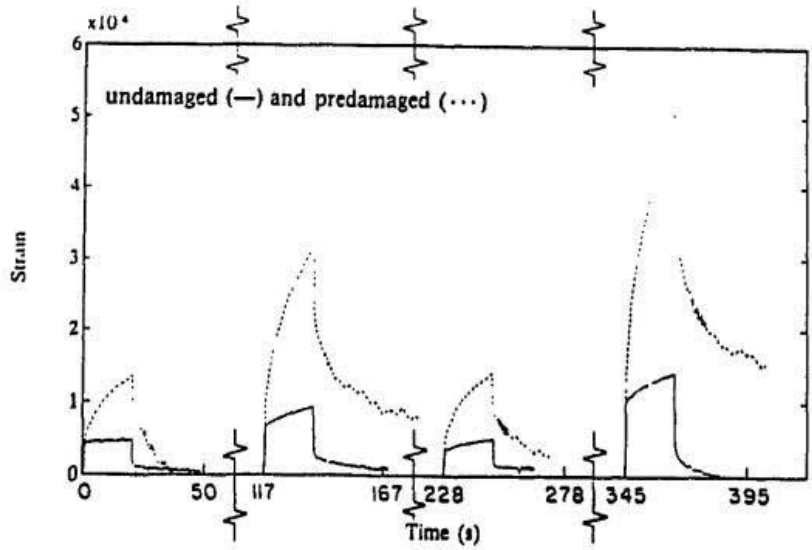

Figure 2.9: Creep Enhancement Due to Microcracking or Damage. *Jordaan et al. (1991a).*

allel to the principal stress direction; i.e., maximum tensile force is perpendicular to crack plane. At lower strain-rates ($\sim 10^{-4}$ s^{-1}) wing cracks are typically stable; however the imposition of a small, lateral tensile stress causes the cracks to propagate rapidly until failure. Evidence of wing cracks has been reported in other brittle materials, such as concrete, rock, sulphur, glass and PMMA. Wang (1981) observed this phenomenon in tests on multi-year sea ice.

The process of axial splitting or shear faulting, shown in Figure 2.10, is predominantly a function of confinement; see for example, Horii and Nemat Nasser (1985). Axial splitting occurs at high strain-rates, under nominally uniaxial conditions, with no platen–specimen end restraints, where a single fracture, typically associated with wing cracks, propagates through the material resulting in failure of the sample.

Conversely, slabbing dominates with increasing confinement or end effects where continued deformation causes the cracks to coalesce which results in the formation of a shear fault. This process is attributed to a family of stable wing cracks which has coalesced along the fault surface, whereby a matrix of coarse and fine powdered material is created — see Schulson (1990). The reader is also referred to articles by Cannon et al. (1990), Murrell et al. (1991) and Schulson et al. (1989) for further discussion and experimental evidence on the axial splitting and slabbing phenomenon. The shear zone is also evident during uniaxial compression testing of multi-year sea ice at lower strain-rates than when the phenomenon is observed in polycrystalline ice (Kenny et al., 1991). This could possibly be attributed to the early development of wing cracks at pre-existing defects, evident in rock mechanics, or that the internal porosity features (i.e. brine pockets, drainage channels) create a plane of weakness for the fault to develop. Ashby and Hallam (1986) developed a wing crack model to describe the failure of brittle materials and the concept of axial splitting and shear faulting.

The ice crushing process has been thus far discussed only in terms of the uniaxial behaviour; this hardly describes the complex stress states encountered during typical ice–structure interactions. Any realistic constitutive model must take into account the mechanical behaviour of ice under multiaxial stresses. For example, a biaxial stress state would describe a level ice field advancing against a wide offshore structure. On the other hand, a triaxial stress state is experienced during iceberg impacts or ramming of multi-year ridges. Figure 2.11 is a reproduction of the data from a test series conducted by Jones (1982). Laboratory grown, equiaxed, polycrystalline,

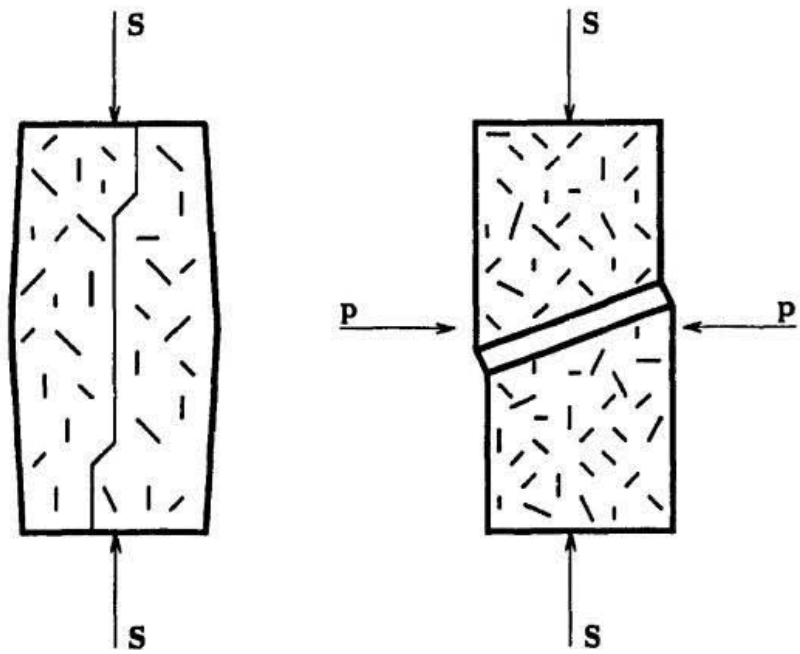

Figure 2.10: Failure Modes of Ice under Compressive Stress States at High Strain Rates ($> 10^{-3}$ s^{-1}) where S Represents the Applied Deviatoric Stress and p is the Confining Pressure.

freshwater ice was deformed at a constant strain-rate under hydrostatic confinement. There are essentially two main regions of interest: (1) the area bounded by lower confining pressures (< 20 MPa) and higher strain-rates (> 10^{-5} s^{-1}) and (2) the family of horizontal curves for all other data points.

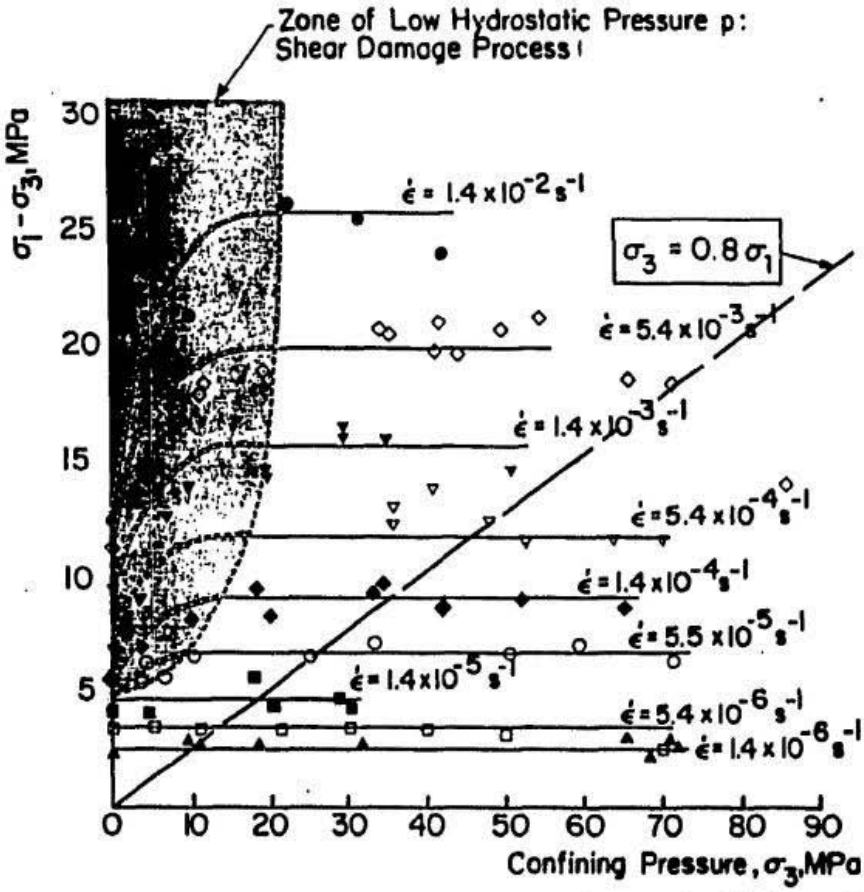

Figure 2.11: Dataset from Constant Strain Rate Tests under Hydrostatic Confinement Conducted by Jones (1982).

In the region of increasing peak differential stress, for a given strain-rate, the deformational behaviour is associated with a progressive damaging process. With higher confining pressures the peak stress stabilizes to a maximum, microcracking activity is inhibited and pure creep observed. Thus the creep response of ice is invariant with hydrostatic pressure and dependent only upon the differential or deviatoric stress, this is also exhibited by metals and concrete. The majority of studies investigating the behaviour of ice under multiaxial stress states are concerned primarily with the 'strength' of the material under constant strain-rate tests; see for example, Häusler et al. (1988), or Murrell et al. (1991). Understanding the damage process and deformational behaviour of ice under moderate to high confining pressures is seen as the key, since this is the principal mechanism involved during full-scale ice crushing events.

A characteristic of ice due to the high working temperature, is the relatively low magnitude of confining pressure required to induce a phase change. Jones (1982) states that with respect to the pressure melting temperature, the hydrostatic confinement has no influence on the creep strain-rate but merely changes the effective temperature. For further discussion on pressure melting the reader is referred to works by Kheisin and Cherepanov (1970) and Barnes et al. (1971). Using Jones' data, Nadreau et al. (1988) proposed that the tendency for the decrease in peak differential stress at higher confining pressures, is in effect, due to pressure melting (Figure 2.12). A teardrop model was developed to describe an anisotropic, three-dimensional failure surface for ice. Recently, Gagnon and Sinha (1991) have reported that pressure melting was evident during medium-scale indentation tests

where interface temperature measurements and thin sections revealed the presence of a melt.

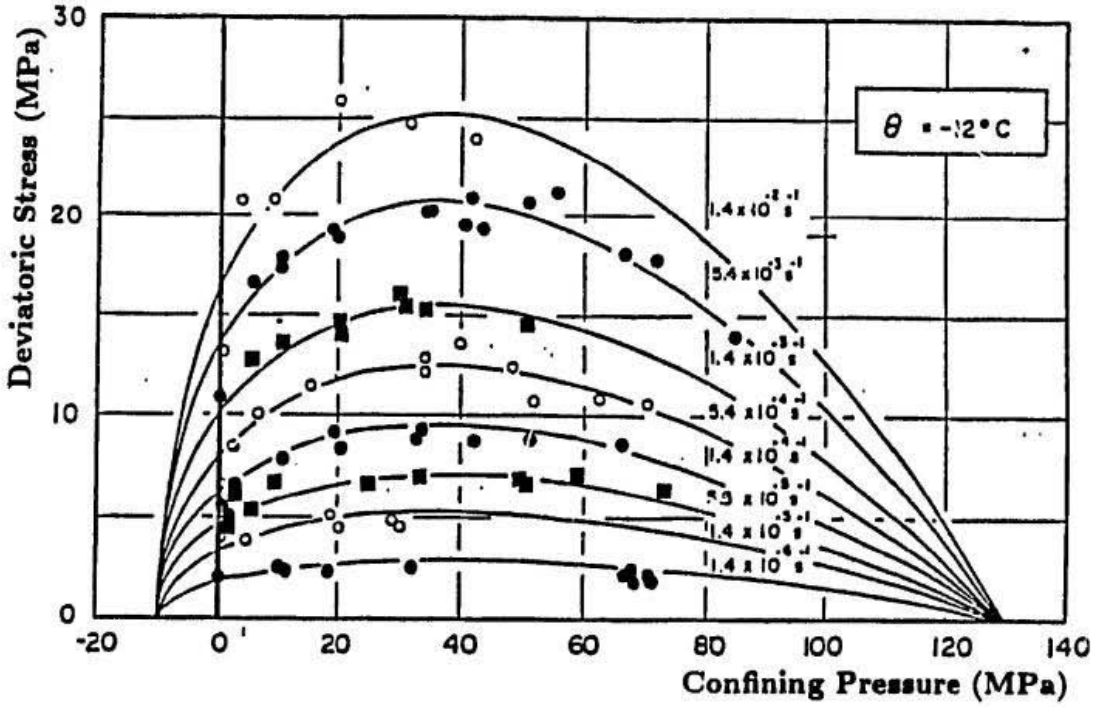

Figure 2.12: Teardrop Model Developed by Nadreau et al. (1988).

However, the teardrop model is empirical and does not attempt to explain the underlying physical mechanisms responsible for the observed mechanical behaviour. Conceivably the principal mechanisms involved during the deformation of ice under multiaxial stress states are schematically illustrated in Figure 2.13. Referring to Figure 2.11, for the lower hydrostatic pressures and higher strain rates there is a zone where a progressive damaging process associated with the development of microcracks. For a given strain-rate, upon the imposition of higher confining pressure the damage is eventually supressed with pure creep becoming the dominant mode of deformation. Further increases in the confinement, for a constant strain-rate and

temperature, would result in creep deformation and pressure melting with the end result being a phase change. Note that, during transitional periods there are stress states where the mechanisms compete for dominance. Also, pressure melting could be active on a localized level, for global stress states less than that required for a phase change, due to intense stress concentrations at crack tips and triple points or frictional mechanisms, such as shear along grain boundaries or crack surfaces.

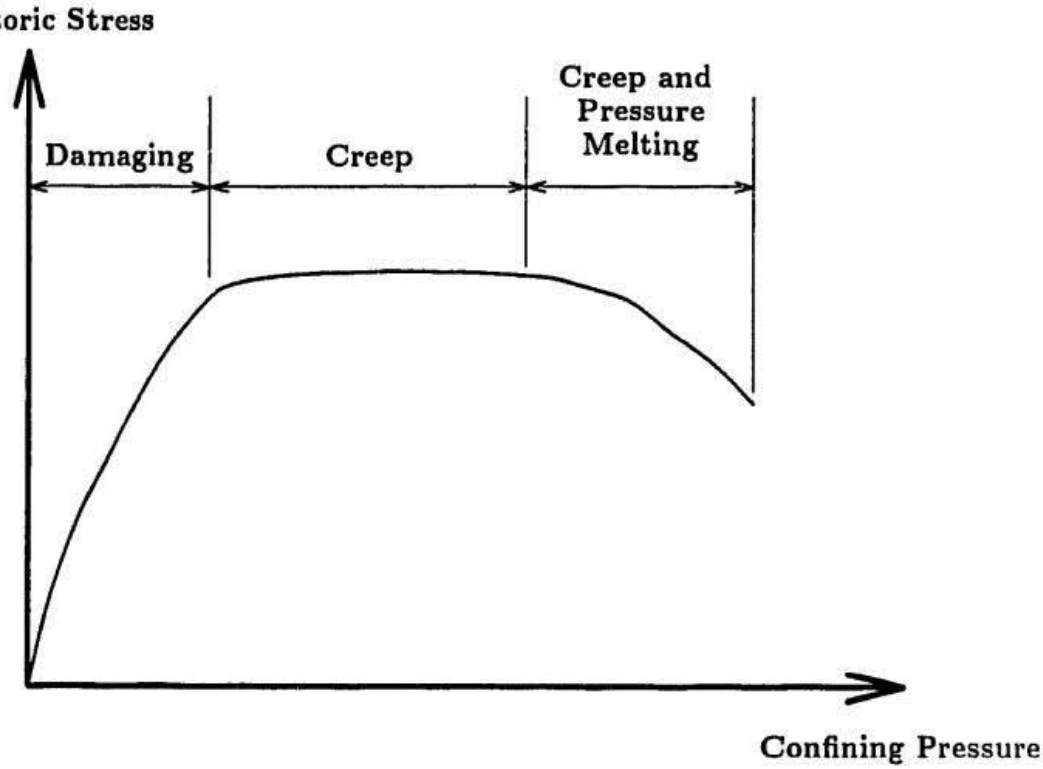

Figure 2.13: Multiaxial Deformation Mechanisms in Ice for a Constant Strain Rate

Although laboratory tests cannot directly model the interaction events at full-scale, one can develop a basic understanding of the failure process in ice, under nominally similar conditions, which could be the foundation for input into numerical or

analytical models. However, damaging or microcracking, in-itself, does not fully explain ice–structure interaction events. Likhomanov and Kheisin (1971) were among the earliest investigators to recognize this fact. During drop-ball impact tests it was observed that the specific crushing energy (i.e resistance to impact) was not a fundamental index property but depended upon elastic deformation, creation of fracture surfaces, frictional processes, clearing mechanisms and pressure melting. Clearly, the failure processes during even small-scale interaction events are highly complex and dependent upon a number of physical mechanisms. Consequently, primarily due to the scale effect, laboratory investigations must be verified by observations and experience gained at full-scale.

Previous field tests, Hans Island (1981), Pond Inlet (1984), and Hobson's Choice Island (1989,1990), have demonstrated the importance of large and medium-scale experimental programs. This has led to the development of new ice load models and significantly advanced the level of understanding of ice–structure interaction events. Hans Island dramatically showed that global ice loads exerted during impact of large multi-year floes (1-3 km diameter) was only on the order of 0.5 MPa. The medium-scale indentation tests, whose main objective was to study dynamic ice–induced vibrations, revealed that local peak pressures, which reached 60 MPa or greater, had a varied spatial and temporal distribution with steep pressure gradients. Generally, interaction models make assumptions regarding the physical characteristics of the failure zone; thus the development and enhancement of such models require detailed description. To better understand the interaction process during field events, an account of the test series conducted at Hobson's Choice Ice Island in 1990 will be

presented. Also, the discussion will bring to focus the logic underlying the present test program.

For all tests, crushing was observed during indentation and discrete ice particles were ejected from the free edges of the indentor (Figure 2.14). However, for several tests spalling or flaking events, associated with large macrocracks, were observed. Although a number of parameters were investigated in the test program, there were characteristic features common to all of the failure surfaces. Illustrated schematically in Figure 2.15 are the typical features associated with the failure zone after indentation.

There are essentially three distinct regions associated with the interaction zone; first, spall areas on the periphery of the contact surface, second, regions of crushed ice and discrete granular particles, generally but not exclusively associated with low pressures, where the material is eventually extruded from the free edges with continued indentation, and third, hard spots or critical zones consisting of damaged ice which are considered to be centers of extrusion. Macroscopically, this region appears to be 'intact' but thin section analysis revealed significant local damage (Meaney et al., 1991).

The crushed layer typically contained large, 25 mm diameter or greater, relatively undamaged particles surrounded by finely pulverized ice, suggesting a grinding action as the larger particles slide and rotate during extrusion. The development of a crushed layer during indentation seems to be analogous to the shear zone generated in the uniaxial and triaxial laboratory tests. The steep pressure gradients

Figure 2.14: Photograph During Penetration of a Rigid Indentor at 400 mm/s — Test SFR-01. Note the Particles Being Ejected from the Edges of the Ice–Indentor Interface.

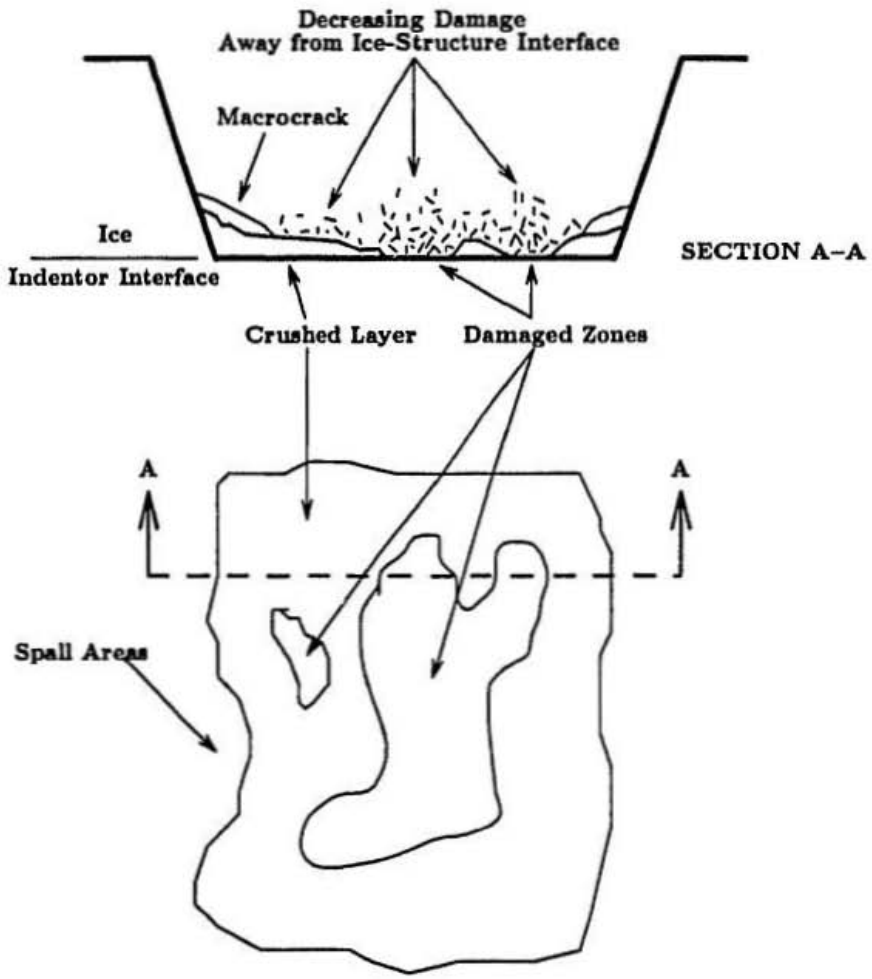

Figure 2.15: Schematic Illustration of a Typical Failure Surface Exhibited During the 1990 Medium-Scale Indentation Tests on Hobson's Choice Ice Island. The Test Face can be Subdivided into Three Major Zones; (i) Spall Areas, (ii) Regions of Crushed Material and (iii) Damaged Zones.

exhibited, which can be related to zones of intense shear, appear to be the driving force behind the grinding and pulverization of the ice, which is rapidly transported to the periphery of the ice–structure interface. Although the features of the failure surface suggest that peak pressures should correlate with the hard spots or critical zones, superimposing the final recorded pressures on the interface did not produce conclusive evidence for such a phenomenon. It is also important to note that the crushed ice layer appeared to have sintered or have experienced pressure melting. This was evident from density profiles of the failure zone and interface temperature measurements. Thus regions of the crushed layer could be considered competent material and experience significant loads during indentation.

Obviously, there has been a significant metamorphism in the material structure; that is a transformation from an intact solid continuum to a densely microcracked body and array of discrete particles. Not only the physical properties of the ice have changed but also the mechanical behaviour, since there is a gradual reduction in the stiffness and shear resistance in the ice matrix — see for example Stone et al. (1989). It is important to realize that any constitutive models must recognize this fact. For example, the degradation of ice properties can be analyzed using continuum damage mechanics and the crushed material, which lacks appreciable shear resistance, could be modeled as a viscous fluid or Mohr-Coulomb material.

Conceivably, the local strain-rates would increase substantially toward the ice-structure interface; i.e. from the parent ice, to regions of influence, to finally the highly damaged zones and crushed ice layer. Also, there would be varying degree of deviatoric stresses and confining pressures throughout the failure region. These

ideas are illustrated in Figure 2.16. Crushed layer thickness measurements, density profiles and thin section analysis of the failure zone (see Kenny et al., 1991) indicated that the bulk of the deformation, related to energy dissipated or expended, occurs within the near field. Jordaan and Timco (1988) have estimated that the energy consumed by the crushed layer developed during small-scale indentation test to be 99% of the total energy.

Early work by Kheisin and Cherepanov (1970) showed that the contact face was characterized by subregions of crushed and damaged ice which they characterized as a "distinct destruction surface". Similar failure zone features were also reported in small-scale ice crushing tests by Fransson (1991), Riska (1991) and Lindholm et al. (1990), as well as, ship–ice interactions by Riska et al. (1990). Hence, ice crushing events can be generalized into a number of observed mechanisms: (1) spalling events in regions of low confinement, (2) a damaging process within critical zones or hard spots, (3) flow or ejection of crushed material due to pressure gradients, and (4) pressure or friction melting and sintering. The behaviour of the crushed ice located at hard spots or critical zones is seen as the key to dynamic fluctuations in load and peak pressures exerted during interaction events.

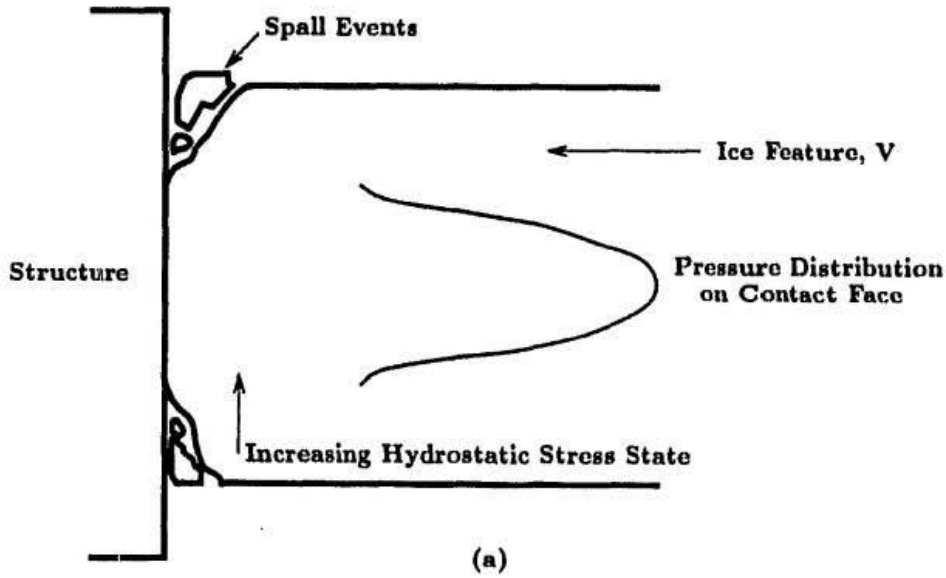

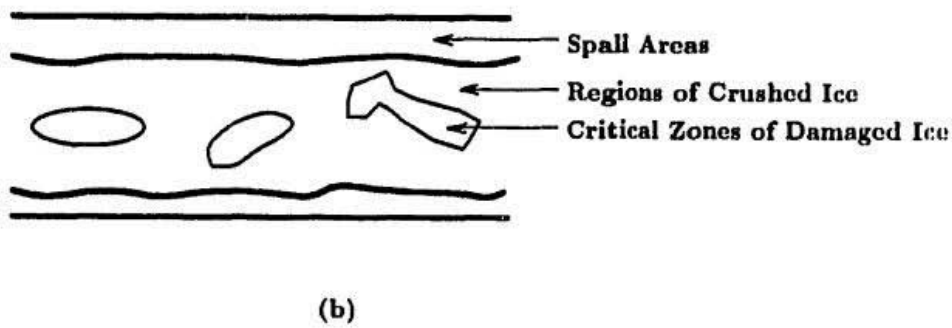

Figure 2.16: Idealization of Ice–Structure Interaction Events; (a) Shows the Pressure Gradient on the Contact Face and the Variation in Deviatoric and Volumetric Stresses, (b) Illustrates the Spatial Distribution of Pressure Zones with Elevation Across the Contact Face, such as Lower Pressures Associated with the Crushed Layer and Hard Spots or Critical Zones of Higher Pressure where Dynamic Effects are Occuring.

Clearly, the calculation of ice forces for offshore structures is an endeavour which requires knowledge from many fields of science. Although empirically-based models have proved their merit, albeit with simplifications for practical engineering design, development of laws based on physics of the deformation processes is required. This will enable the ice engineer to develop strategies for various structural configurations to be deployed under wide ranging scenarios.

Chapter 3

Experimental Program

Most laboratory investigations on the multiaxial behaviour of ice have investigated the 'crushing strength' under constant strain-rate loading conditions. To the author's knowledge there has been no systematic study on the deformational behaviour of damaged ice as a function of confinement and applied stress.

Evidence from medium-scale indentation tests showed that the contact zone was characterized by subregions of crushed or pulverized material and damaged ice. The behaviour of damaged ice and crushed material located at hard spots in zones of moderate to high confining pressures is seen as the key to the dynamics of the ice crushing process.

Consequently, a study on the creep response of intact and pre-damaged ice under hydrostatic confinement was conducted. With these thoughts in mind, the following discussion focusses on the experimental program.

3.1 Preparation of Test Specimens

All tests were conducted using laboratory prepared polycrystalline, equiaxed, fresh-water ice. Figure 3.1 schematically illustrates the equipment setup used during the molding process to manufacture ice samples. The system was housed in an anteroom which was maintained at a nominal temperature of 0° C.

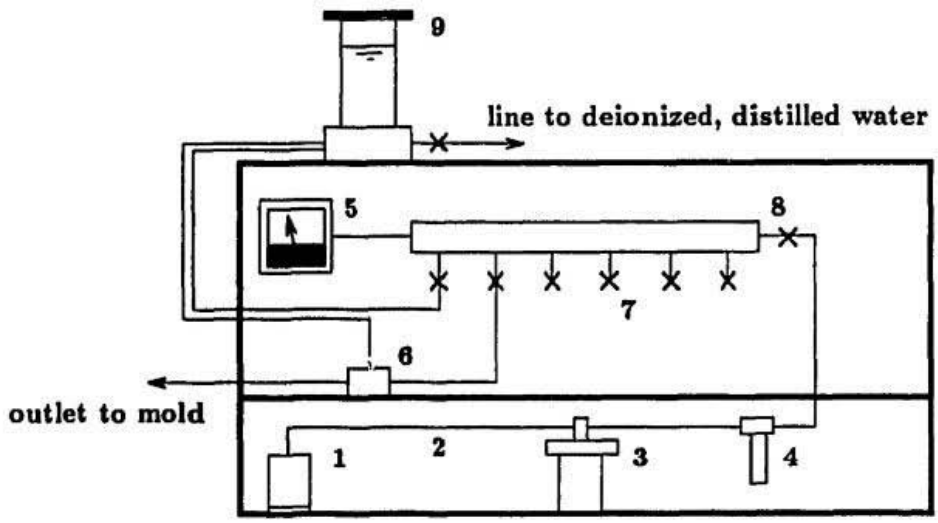

1. Vacuum pump	4. Dry trap	7. One way valve
2. Thick wall tubing	5. Vacuum gauge	8. Glass manifold
3. Cold trap	6. Three way valve	9. Deaerator

Figure 3.1: Schematic of Equipment Used in the Manufacturing of Ice Samples.

To ensure quality and repeatability of the ice samples the following procedure was adopted. Pure water, obtained by filtering and distilling municipal tap water, was used throughout the manufacturing process. The measured resistivity of the pure water was on the order of 10 $M\Omega \cdot cm^{-1}$. The next stage was to develop samples which

were uniform and homogeneous in grain size, thereby ensuring isotropic mechanical behaviour. Dictating grain size can be easily achieved by the introduction of a nucleating agent; such as, seed ice. Bubble free columnar grained ice, grown from unidirectional freezing of pure water, was crushed using a, *Clawson Model #PC-75*, commercial mechanical ice crusher and then sieved. Ice particles which passed the #4 US (4.75 mm) screen and retained on the #6 US (3.35 mm) sieve were used as seeds. The seed ice was then placed in a tapered, rectangular, fibreglass mold (Figure 3.2) which was used to set the seed ice–pure water mixture. The bottom of the mold was bolted to an aluminum plate and the mating sealed by a rubber gasket. To develop the vacuum, a flexible membrane fabricated from a weather balloon was used to cover the mold. Snow was then placed on top of the seed ice to act as a protective buffer so that the membrane would not be punctured. A seal was ensured using elastic bands and high vacuum silicon grease.

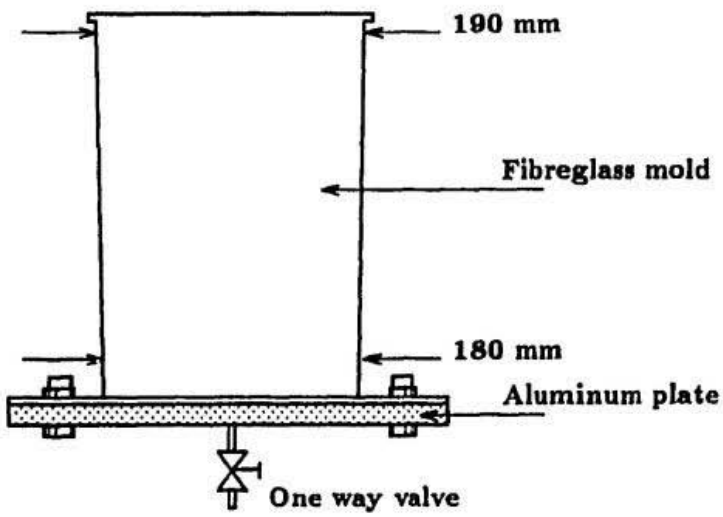

Figure 3.2: Mold for Maturing Ice Samples.

Subsequently, the mold and tubing system, shown in Figure 3.1, was placed under a vacuum for approximately 2 hours and brought to a gauge pressure of 0.5 mm Hg. The deaerator was then filled with distilled deionized water, cooled to 0° C, and the chamber was evacuated for 10–15 minutes. Finally, the mold was filled with the deaerated water through the evacuated tubing. After flooding, the mold was covered by an insulating jacket leaving the bottom aluminum plate exposed to encourage unidirectional freezing. Typically, the ice would mature in 3 days at -10° C and would then be removed from the mold by allowing the fibreglass shell to warm slightly. Once removed from the mold, the ice sample was sealed in plastic bags and temporarily stored at -30° C until the day before a test. The ice block would then be allowed to equilibriate to -10° C overnight prior to machining of individual test specimens.

This molding technique would produce equiaxed, granular polycrystalline ice having a random c-axis orientation. Cole (1986) presents experimental evidence on the role in which grain size dictates the mechanical behaviour of ice, where variance in the grain diameter changed the bulk failure mode of the specimen from ductile to brittle for the same deformation rate. The mean grain diameter for the ice samples was 4.3 mm which was calculated using the expression,

$$d = \sqrt{\frac{6}{\pi N_A}} \quad , \tag{3.1}$$

where N_A is the number of grains per unit area. Thin sections, essential in the

development of fabric diagrams, grains size analysis and damage characterization, were obtained by using a *Leitz* biological microtome and the double microtoming technique outlined in Sinha (1978) was employed. A typical horizontal thin section is shown in Figure 3.3.

Generally, there would be larger than average grains generated at the base of the mold and a concentration of fine air bubbles near the snow layer at top. Consequently, to ensure quality ice specimens, the top and bottom 75 mm were removed and discarded. The ice was then cut, using a bandsaw, into four equal sections. Individual samples were machined into right rectangular prisms, using a jointer and a milling unit, having dimensions of 60 $\pm$0.1 mm square and 120 $\pm$0.1 mm in length. The machining process produced samples with a very smooth surface and parallel ends — a critical parameter, particularly at higher strain-rates, which influences the mechanical behaviour of the specimen due to eccentric loading.

3.2 Test Equipment

A *Material Testing Systems (MTS) Corporation* Model # 311.31 test frame was used for all experiments and was housed in a standard cold room, which could maintain a working temperature within the range of 0° C to -40° C. Axial load, in-situ ice displacement, hydrostatic pressure, temperature and time were recorded on a personal computer, using the *Viewdac* data acquisition software package at a sampling rate of 200 Hz. Also, a hardcopy backup was recorded using a *Yokogawa 3066* pen recorder to measure, in real time, MTS load, triaxial cell pressure and temperature and a *Yokagowa LR4210* pen recorder was used to record the axial

Figure 3.3: Horizontal Thin Section of an Intact Ice Sample.

and lateral displacement of the ice sample. Figure 3.4 schematically illustrates the triaxial cell configuration used during the test program. Details of the mounting collars for the LVDT's and brass endcaps are presented in Appendix A.

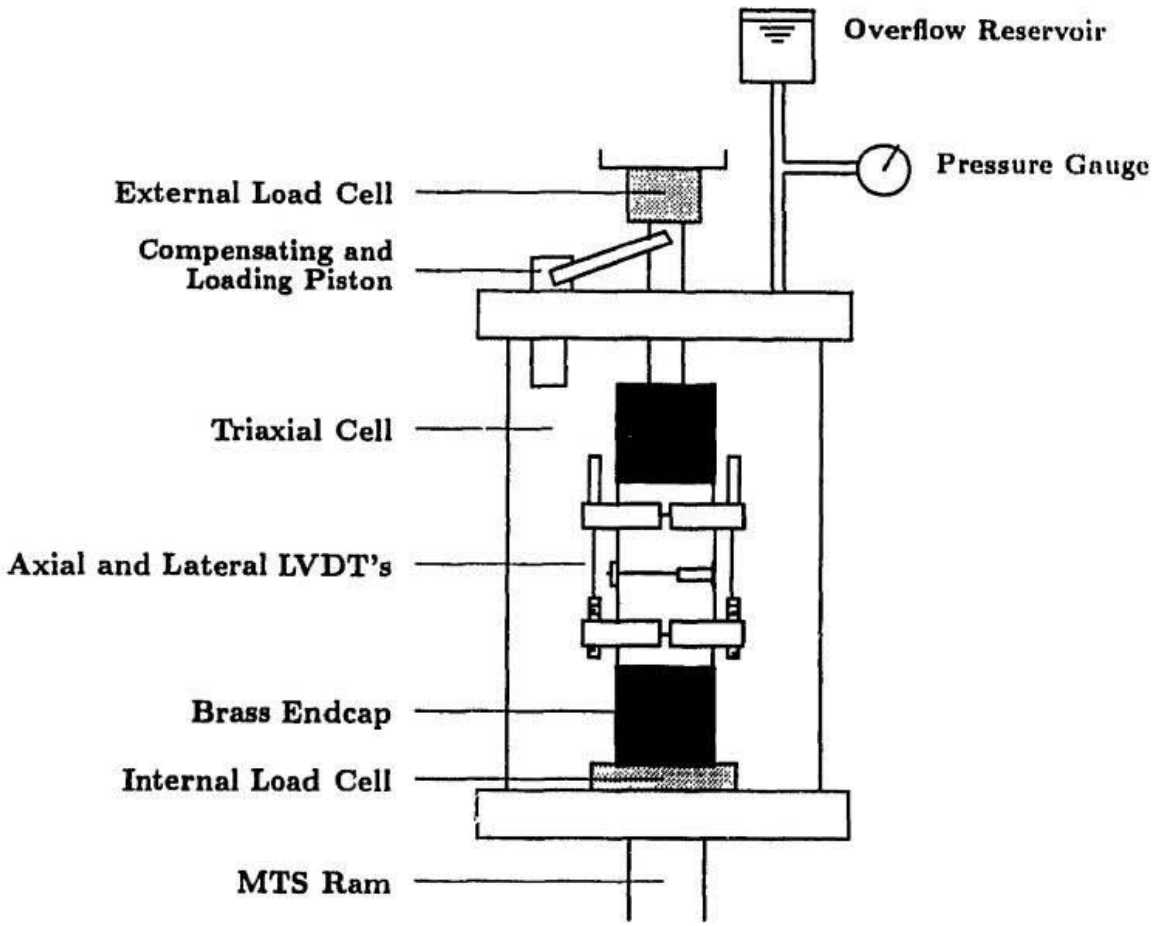

Figure 3.4: Schematic Illustration of the Triaxial Cell System Employed During the Test Program.

The triaxial cell, fabricated from stainless steel, was equipped with four portals: two with access for viewing or video monitoring the tests and two others used to

provide a light source to illuminate the cell interior. The viewing windows restricted the maximum confining pressure to 20 MPa (3000 psi). Constant pressure was maintained during the test by the use of a compensating piston which was attached to the actuator piston via a fulcrum — see Kalifa et al. (1989). A translucent silicone oil, with a viscosity of eight centistokes (20° C), was used as the pressurizing fluid. Two *MTS-661.23B-01* 250 kN capacity load cells, one internal and the other external of the cell, were used to measure the stress applied to the ice sample. The former directly measured the axial stress applied to the specimen and was used as the reference signal during load control phases. Two *Schaevitz* MHR-100 series linear variable differential transformers (LVDT), with a stroke of ±2.54 mm, were mounted on the sample, via an aluminum support collar with knife edges, to measure axial strains directly from the sample. Lateral strain was measured by a *Schaevitz* MHR-250 LVDT with a stroke of ±6.35 mm. The lateral gauge was attached to the sample by an aluminum mounting block, with 30 millimetres contact along the corners of the specimen, which was supported by elastic bands. The axial gauge length was 70 millimetres and the lateral gauge length was 55 millimetres. A photograph of an undamaged ice sample and a fully instrumented specimen is shown in Figure 3.5.

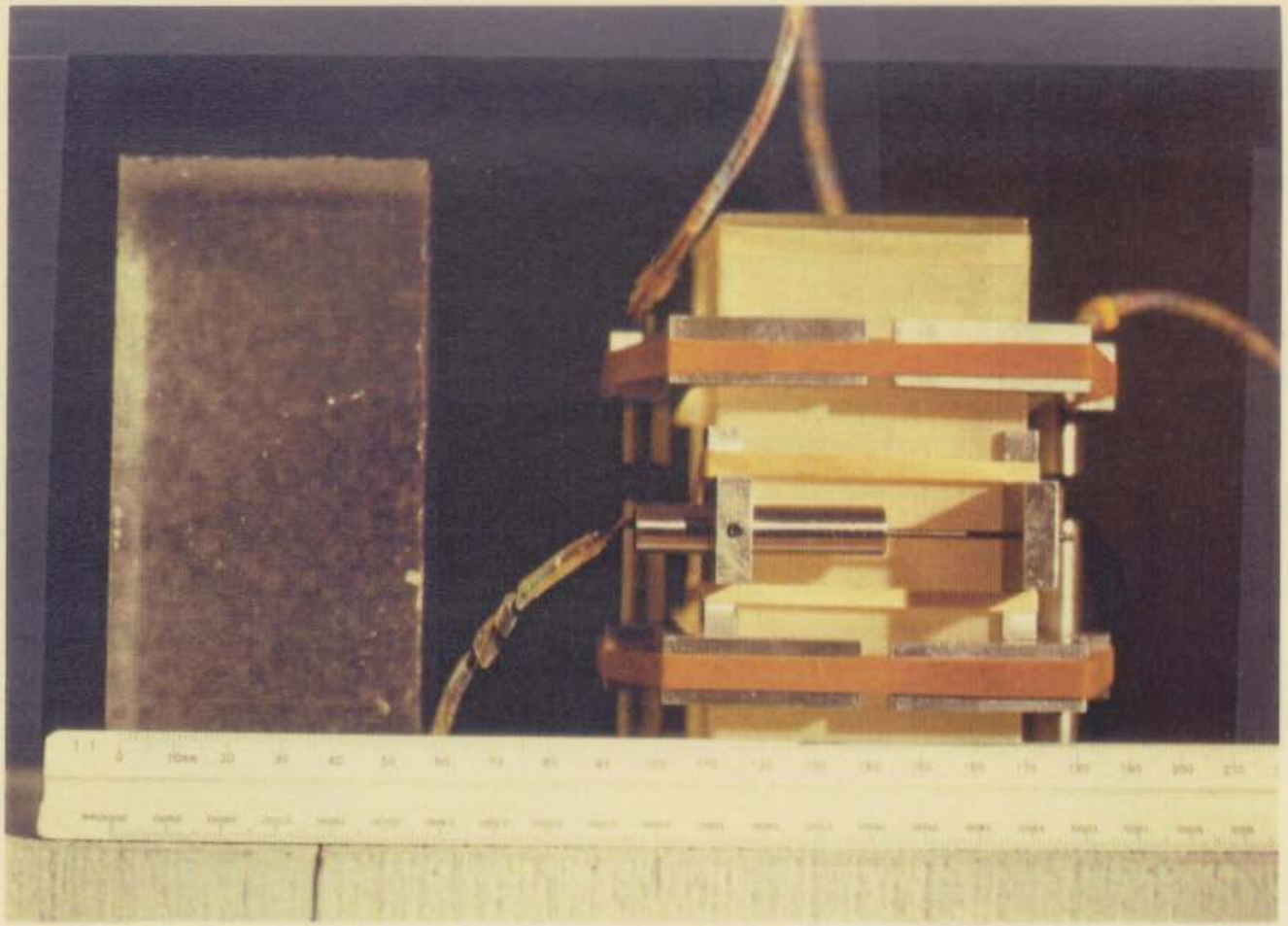

Figure 3.5: Photograph of an Undamaged Ice Sample and a Fully Instrumented Specimen. The Axial and Lateral LVDT Mounts are Fabricated From Aluminum and Attatched to the Specimen by Elastic Bands.

3.3 Test Program

All tests were conducted at the Institute for Marine Dynamics, National Research Council Canada in St. John's, NF. As stated earlier, the purpose of the investigations was to study the influence of damage on the creep deformation of polycrystalline, granular freshwater ice under hydrostatic confinement.

The experimental program consisted of applying a series of compressive loads to undamaged and pre-damaged ice samples at various confining pressures; whereby the subsequent deformational response of the specimens could be analysed with respect to the influence of microcracks on the strain developed under a multiaxial stress state. Pre-damaged samples were obtained by loading the specimen uniaxially at a constant displacement rate of 10^{-4} s^{-1} to an axial strain of 0.02. These parameters were chosen so that the creep response, under uniaxial conditions, could be compared to similiar tests conducted at Memorial University.

A typical stress–strain curve for the damaged ice is shown in Figures 3.6. To hinder the pressurized fluid from penetrating into the cracks of the pre-damaged specimens, all samples were jacketed by a latex membrane similar to those used in soil and rock mechanics. Figure 3.7 illustrates the dilatation typically developed when the ice sample was loaded uniaxially at a constant displacement rate of 10^{-4} to a total strain of 2%. Profiles of pre-damaged samples were measured, using a micrometer, which supported the LVDT measurements and revealed that the barreling was quite uniform. A thin section through a pre-damaged ice sample is shown in Figure 3.8. Note the fine grained structure developed between the grain boundaries which

could be the result of a grinding action between grains. Figure 3.9 is a photograph of a typical vertical thin section through a pre-damaged ice sample. A number of possible wing cracks were observed for several thin sections through different samples, although it is not known whether they were developed during the pre-damaging phase or load pulse series. Alternatively, the wing cracks features could have developed through the coalescence of grain boundary cracks.

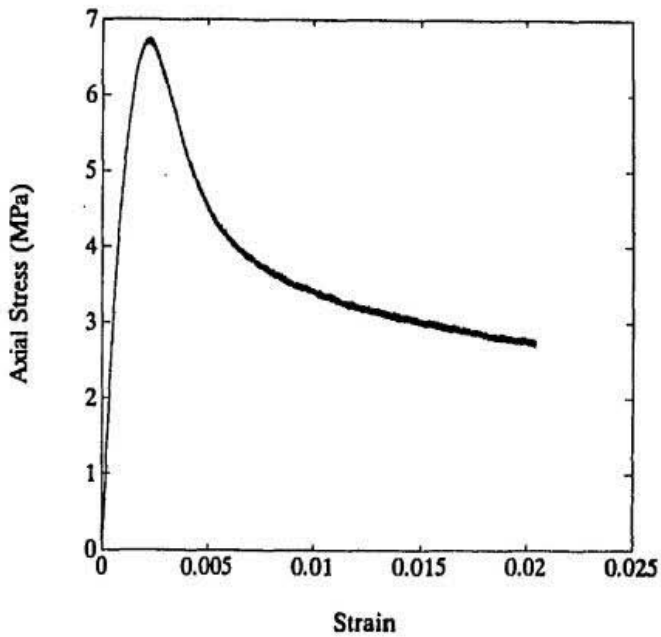

Figure 3.6: Typical Axial Stress–Strain Curve for Pre-Damaged Samples.

The confining pressures studied were 0, 4, 10 and 20 MPa and the applied deviatoric loads ranged from 0.5–1.5 MPa for uniaxial conditions and 0.3–2.6 MPa for triaxial stress states. Figures 3.10 and 3.11 illustrate the load pulses for the uniaxial and tri-axial cases respectively. The constant stress levels were applied, under load control, for 20 second duration which was followed by a relaxation period of approximately 150 seconds. Peak stress was attained in approximately 0.02 seconds.

Figure 3.7: Photograph of a Pre-Damaged Ice Sample.

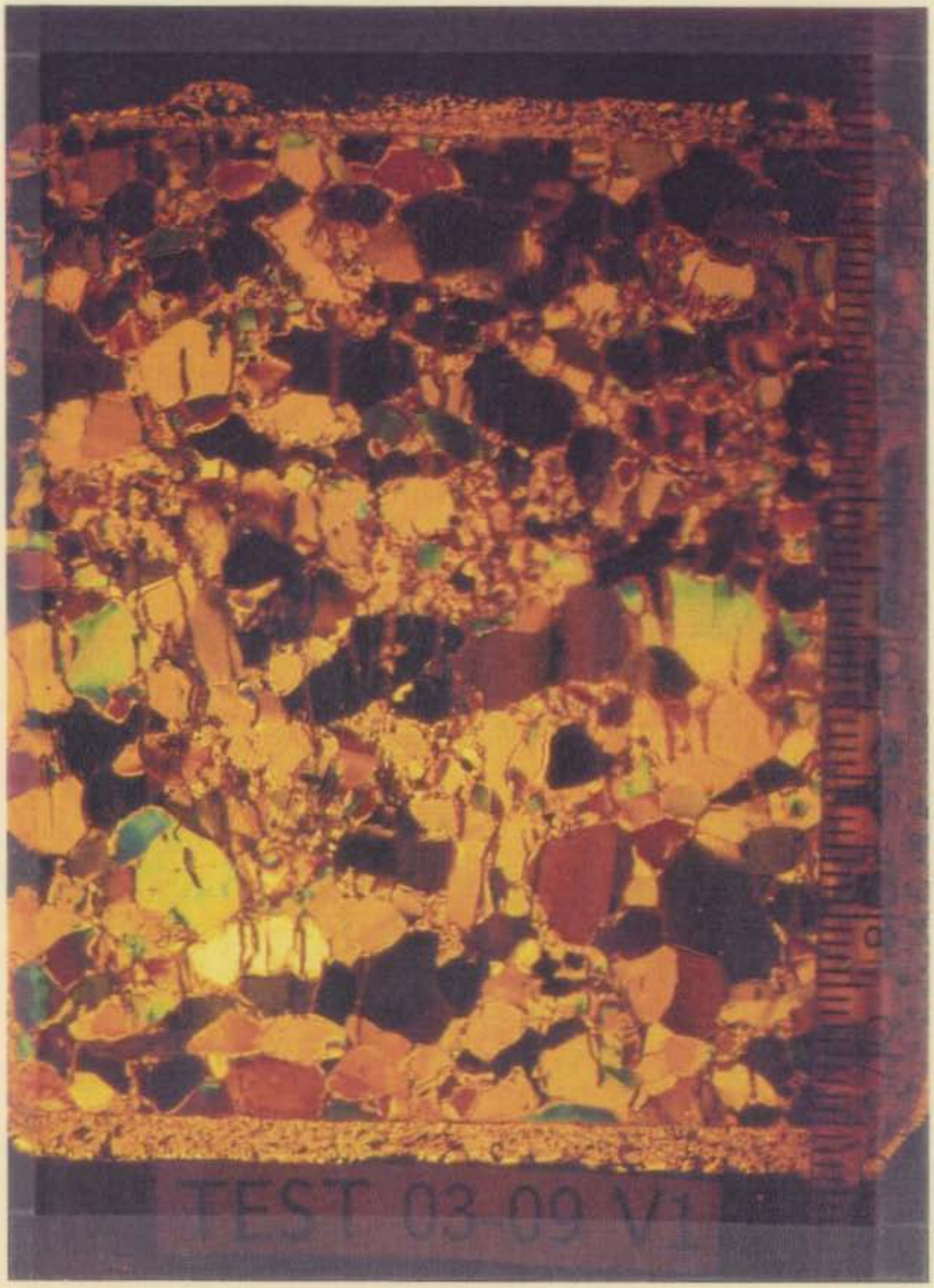

Figure 3.8: Thin Section through a Pre-Damaged Ice Sample. Note the Fine Grained Particles Dispersed Throughout the Sample between Individual Grain Boundaries.

Figure 3.9: Vertical Thin Section through a Pre-Damaged Ice Sample. Note the Presence of a Possible Wing-Crack Near the Center of the Photograph.

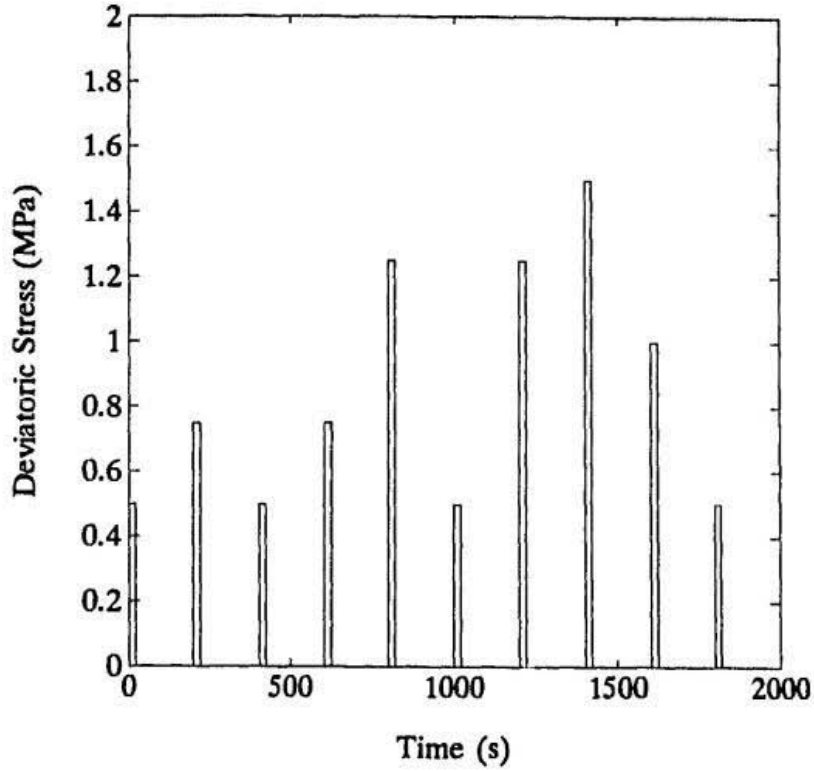

Figure 3.10: Command Signal for Unaxial Stress Pulse History.

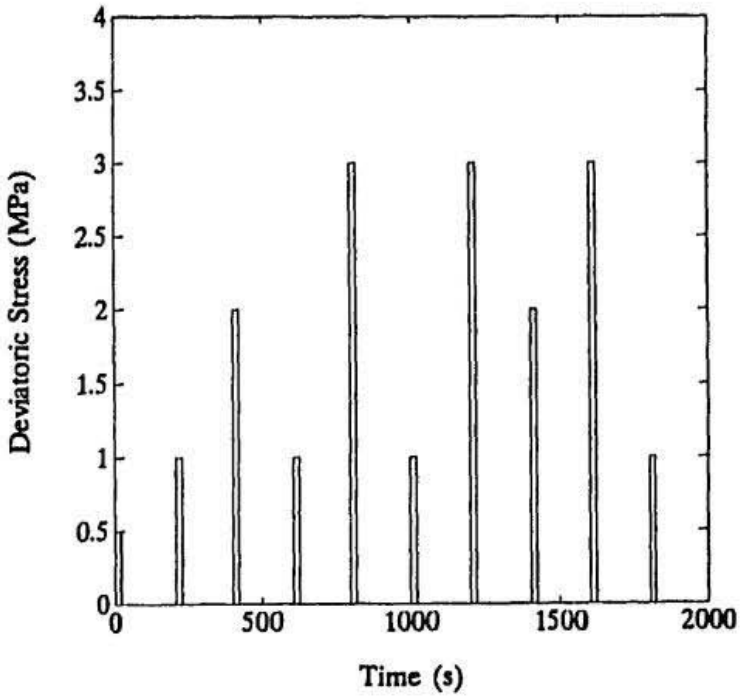

Figure 3.11: Command Signal for Triaxial Stress Pulse History.

Analysis of the pulse records measured by the two loads cells indicated that the actual stress applied to the ice was less than the reference signal, as measured by the external load cell, when the specimen was subject to hydrostatic confinement. The discrepancy between applied and measured stress was attributed to friction on the loading piston by the sealing gaskets which reduces the stress experienced by the ice sample. Table 3.1 summarizes the stresses for the test series, rounded to the nearest 0.05 MPa, for the reference signal (i.e. external load cell) and actual measured stress which was recorded by the internal load cell. Consequently, it is important to realize that the measured deformational response cannot be directly compared for different confining pressures.

For future experiments it is recommended that the internal load cell be used as the reference measurement with respect to the command signal. The stress magnitude measured by the internal load cell (measured deviatoric stress) will be used throughout the analysis of the experimental results.

Table 3.1: Reference Stress Signal and Measured Applied Deviatoric Stress

Confining Pressure (MPa)	Reference Deviatoric Stress (MPa)	Measured Deviatoric Stress (MPa)
0	0.50	0.50
	0.75	0.75
	1.00	1.00
	1.25	1.25
	1.50	1.50
4	0.50	0.30
	1.00	0.75
	2.00	1.60
	3.00	2.60
10	0.50	0.30
	1.00	0.75
	2.00	1.60
	3.00	2.60
20	0.50	0.30
	1.00	0.50
	2.00	1.40
	3.00	2.40

Chapter 4

Analysis and Discussion of Experimental Results

In earlier chapters, it was shown that the progressive damaging process plays an important role during ice–structure interactions. Recently has there been significant effort to relate the observed stress–strain behaviour of ice; from laboratory tests and field programs, to the development of a constitutive ice–load model — see for example Winkler and Dorris (1990), and Jordaan et al. (1990b). The following section will focus on the presentation of the experimental results and subsequent analysis.

4.1 Creep Enhancement under Triaxial Stress State

4.1.1 Axial Deformation

The observed deformational behaviour of pre-damaged ice under uniaxial conditions is shown in Figure 4.1. The applied constant stress pulse was previously illustrated in Figures 3.9 and 3.10. Although the ice has experienced considerable permanent or non-recoverable deformation, between the first and tenth load pulse, there is not any apparent influence on the deformational response for the same applied stress. Thus, one can assume that repeated loadings did not appreciably contribute to any further damage within the specimen. These characteristics are typical and were observed throughout the test program for all confining pressures and deviatoric stresses.

The significance of damage (i.e. microcracks) on the deformational behaviour of ice is illustrated in Figure 4.2, where the strain developed in the pre-damaged specimens is considerably enhanced and several times the magnitude experienced by the intact ice. This is in good agreement with Jordaan et al. (1990a), where similar results are presented, for uniaxial conditions using a different testing system. The effect of creep enhancement was markedly demonstrated during the triaxial tests where higher stress levels could be applied without subjecting the ice sample to further damage, Figures 4.3–4.5, since repeated loadings exhibited nominally similar deformational behaviour. These figures present the average axial deformational response, for each applied stress pulse, and compare the measured strains from the intact ice sample to the pre-damaged specimen for a given confining pressure.

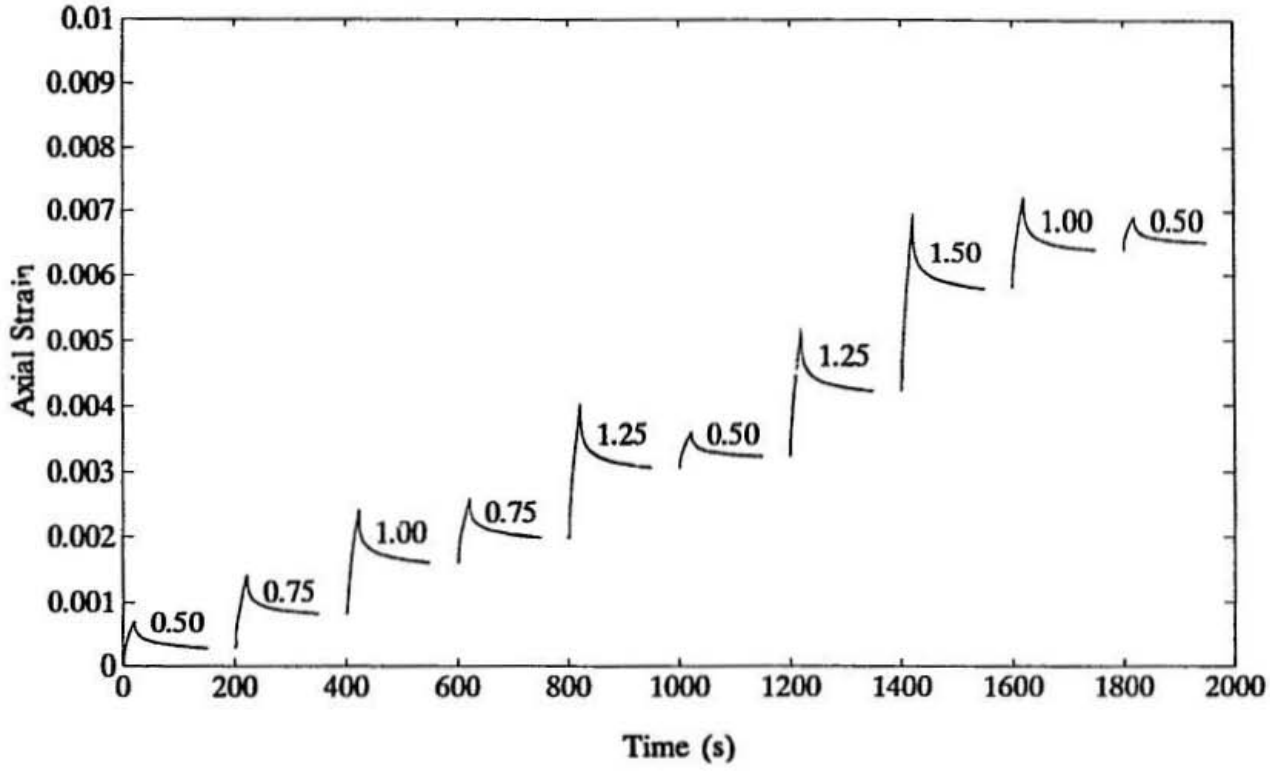

Figure 4.1: Typical Deformational Response for Pre-Damaged Ice Sample Subject to Sequential Uniaxial Compressive Loadings. The Numbers Listed Above Each Strain Curve Represents the Applied Deviator Stress in MPa.

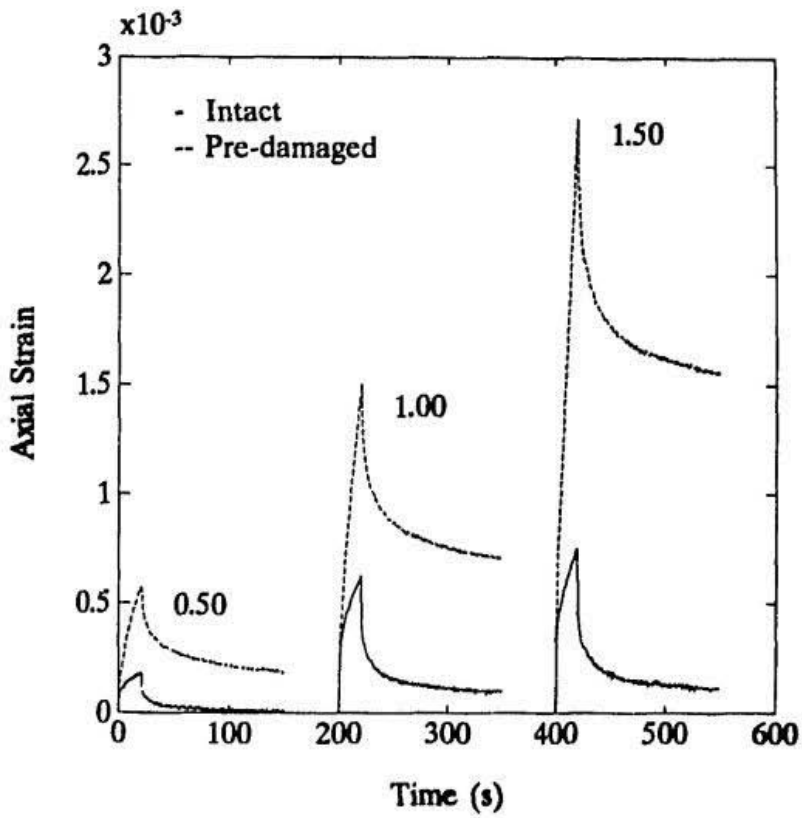

Figure 4.2: Axial Strain Response at 0 MPa Confinement for Intact and Pre-Damaged Ice Samples. The Numbers Listed Above Each Strain Curve Represents the Applied Deviator Stress in MPa.

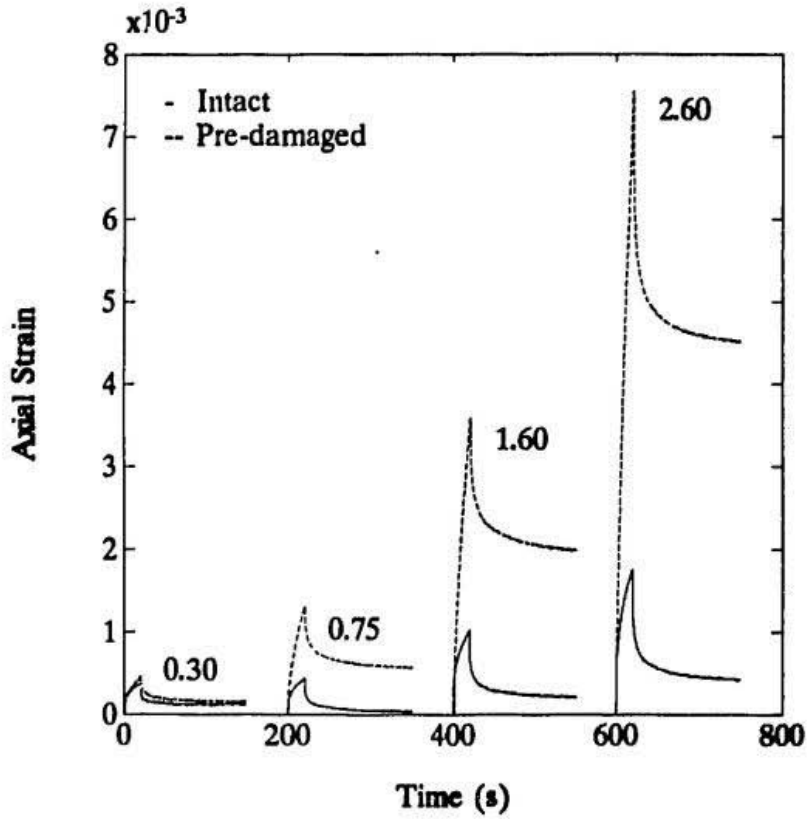

Figure 4.3: Axial Strain Response at 4 MPa Confinement for Intact and Pre-Damaged Ice Samples. The Numbers Listed Above Each Strain Curve Represents the Applied Deviator Stress in MPa.

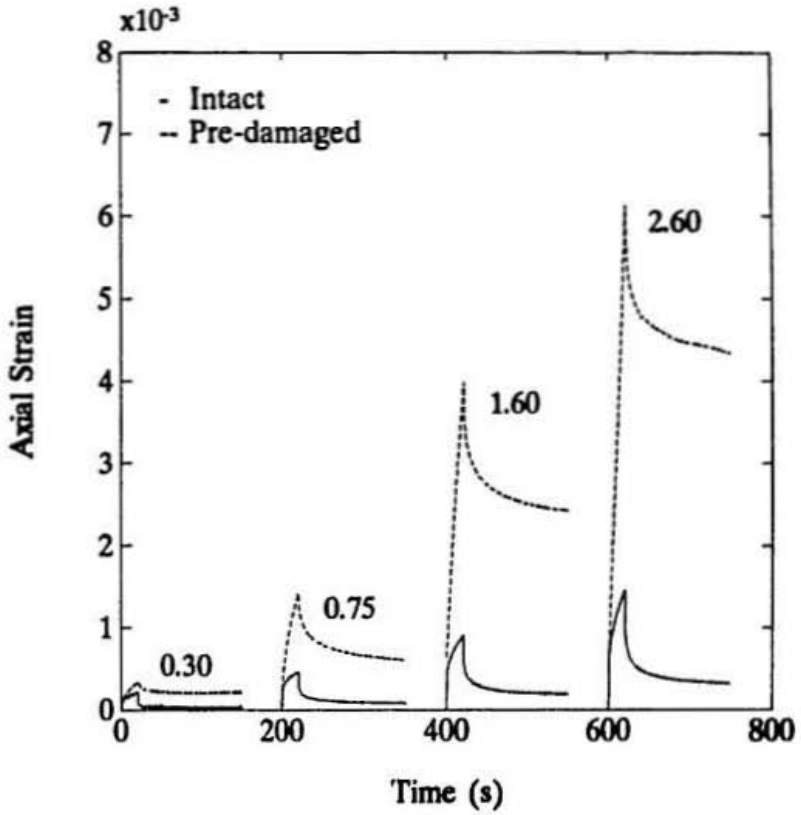

Figure 4.4: Axial Strain Response at 10 MPa Confinement for Intact and Pre-Damaged Ice Samples. The Numbers Listed Above Each Strain Curve Represents the Applied Deviator Stress in MPa.

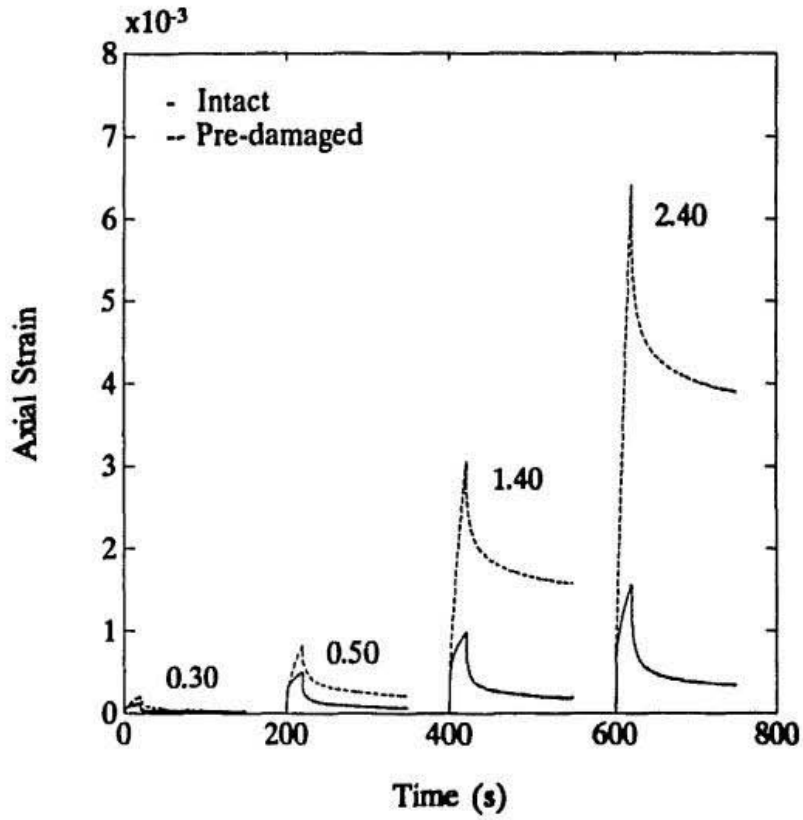

Figure 4.5: Axial Strain Response at 20 MPa Confinement for Intact and Pre-Damaged Ice Samples. The Numbers Listed Above Each Strain Curve Represents the Applied Deviator Stress in MPa.

Elastic moduli of both intact and pre-damaged ice were determined from the load pulse series for all tests. Sinha (1988) demonstrates the importance of considering applied stress rate when investigating the elastic modulus. Since ice creeps at any stress state, other than purely hydrostatic, for static loading conditions then time is the all-important factor. Analysis of the constant stress pulses indicate that the loading rate was in the range of 10–100 MPa·s^{-1}. The magnitudes of stress and strain for the determination of elastic moduli are shown in Figures 4.6 and 4.7. The mean modulus for intact ice was 9.16 ± 0.14 GPa, and ranged from 5.92 ± 0.10 GPa to 7.00 ± 0.11 GPa for the pre-damaged ice samples (Table 4.1). This is in good agreement with the data presented by Sinha (1988) and Jordaan et al. (1990a). Conceivably, the increase in stiffness for the damaged ice at 20 MPa confinement could be due to the partial closure of microcracks which induces traction or frictional sliding between crack surfaces. For further discussion see Horii and Nemat-Nasser (1983), where a criterion is developed such that a critical confining pressure to shear stress ratio is required to open microcracks which causes a change in the bulk modulus of the solid. The key finding is the significant enhancement, particularly at higher deviatoric stresses, of creep strain due to damage.

Referring to Figures 4.2–4.5 it can be seen that, although the elastic deformations for both intact and pre-damaged ice samples are on the same order, there is considerable difference in the magnitude of creep strain. The enhancement of both rate and magnitude of creep strain, for the pre-damaged specimens, could be attributed to the intense stress concentrations which may exist at crack tips resulting in accelerated

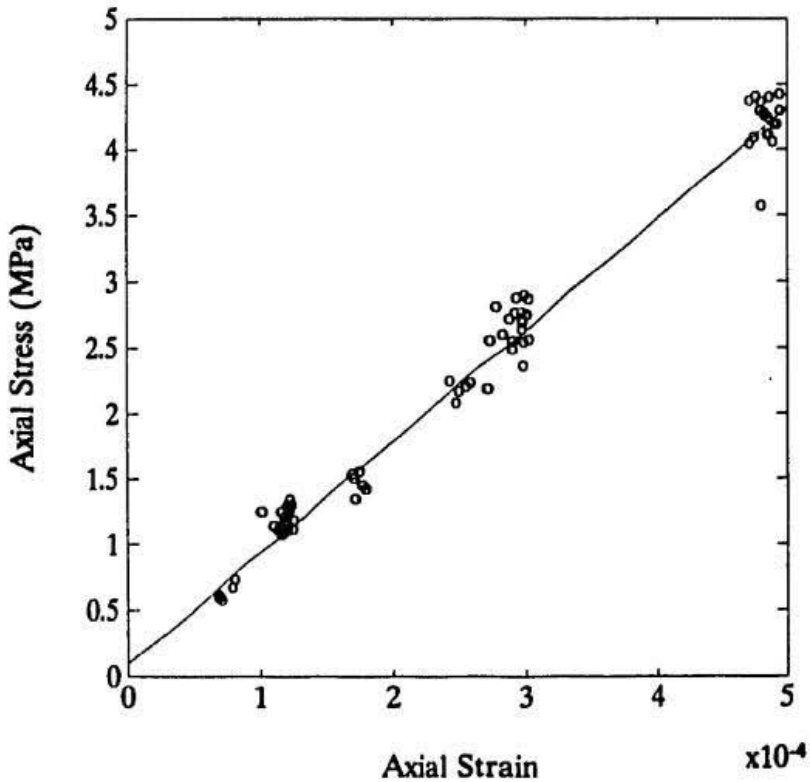

Figure 4.6: Determination of the Elastic Modulus from Stress-Strain Response for Intact Ice. The Superimposed Line is a Least-Squares Best Fit of the Data.

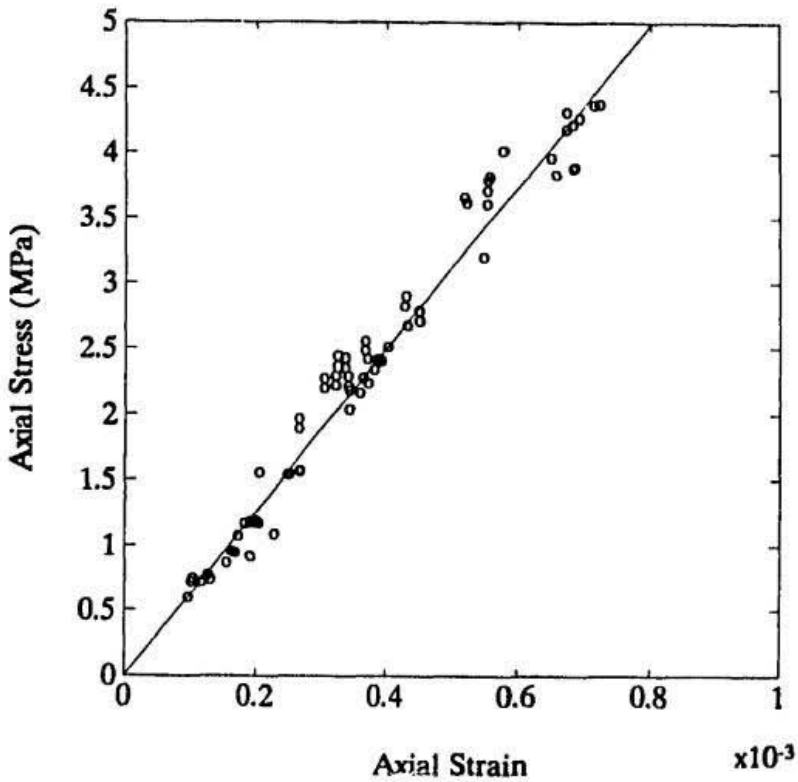

Figure 4.7: Determination of the Elastic Modulus from Stress-Strain Response for Pre-damaged Ice. The Superimposed Line is a Least-Squares Best Fit of the Data.

Table 4.1: Mean Elastic Moduli

Ice Type	Confining Pressure (MPa)	Elastic Modulus (GPa)
Undamaged Ice	0, 4, 10 & 20	9.16
Pre-Damaged Ice	0	6.27
Pre-Damaged Ice	4	6.10
Pre-Damaged Ice	10	5.92
Pre-Damaged Ice	20	7.00

deformation through traction and power law creep. Although there is a modest increase in the elastic modulus at 20 MPa, the creep enhancement appears to be independent of the confining pressure for the range investigated. Also, evident is the tendency for viscous processes to dominate the response at higher applied stresses as the proportion of elastic plus delayed elastic strain to total strain decreases with increasing load. Interestingly, early work by Kurdyumov and Kheisin (1976) and Likhomanov and Kheisin (1971) idealized the crushed material generated during drop-ball impact tests as a viscous layer.

Further, a more subtle characteristic, is the observed non-linearity in strain with applied stress as shown in Figure 4.8. The axial strain response is non-linear and apparently independent of the confinement. The stress pulses around 4 MPa were loaded on a 'sacrificial' sample, from the same batch as the specimens used in the experimental program, to determine the range of deviatoric stresses which could be applied to pre-damaged samples without inducing further damage. Although some caution should be used in interpreting these two data points, it seems that the magnitudes correspond with the overall trend.

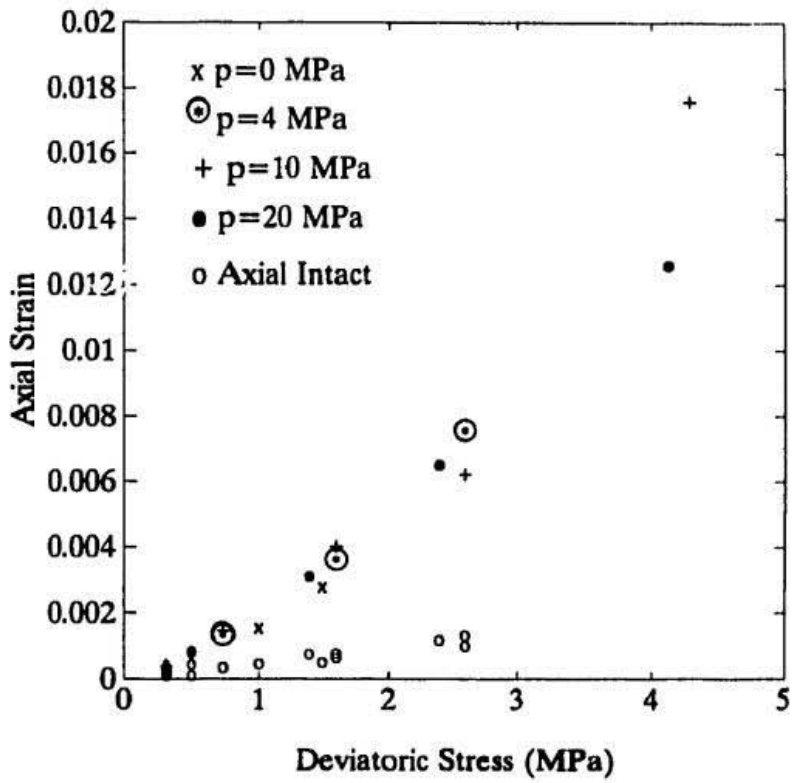

Figure 4.8: Non-Linearity of Axial Strain as a Function of Deviatoric Stress for Intact and Pre-Damaged Samples at Time, t=20s.

Clearly, the significance of damage on the axial deformation of ice under triaxial stress states has been demonstrated. Surprisingly, one of the key features which is responsible for the significant creep enhancement has not been thoroughly addressed; that is, the bulk volumetric expansion due to microcracking. Only recently has there been a more concerted effort to investigate the dilatancy in ice and the influence on the mechanical behaviour subject to a multiaxial stress state.

4.1.2 Lateral Deformation and Dilatation in Ice

Observations of the ice failure surface after penetration by an indentor, during the Pond Inlet (1984) and Hobson's Choice Ice Island (1989,1990) field experiments, revealed that material located at the periphery of the contact face was less consolidated than more central regions. Field investigations by Kenny et al. (1991) have shown that the density of the crushed ice layer ranged from 749 $kg \cdot m^{-3}$, at the free edges, to 864 $kg \cdot m^{-3}$, near the center of contact. The density of the parent structure varied between 858 $kg \cdot m^{-3}$ and 890 $kg \cdot m^{-3}$. In fact, the material on the periphery of the failure surface could be broken away from the test face with minimal effort. This implies that dilatational mechanisms are active during ice–structure interaction events. Experiments conducted by Wang (1981), Sinha (1991) and Dorris (1991) have also demonstrated the importance of volumetric expansion due to microcracking.

Since the axial strain is influenced by damage, it is not surprising the the lateral strain, which is directly related to the formation of microcracks, is considerably enhanced. Furthermore, a significant observation was that at higher deviatoric stresses the lateral deformation dominates the strain response of the material. Figures 4.9–4.12 present the measured lateral deformational and corresponding axial strain for the pre-damaged ice specimens. Unfortunately, the lateral strain for intact ice cannot be presented because the resolution of the system was on the same order as the measured signal. This resulted from a combined influence of the data acquisition board and required stroke range of the lateral LVDT for the pre-damaged samples. However, by comparing the lateral and axial strains for the damaged ice samples it is possible to appreciate the significant enhancement in lateral creep strain since the Poisson's ratio, i.e. ratio of lateral to axial strain, for intact ice is known to be on the order of 0.3 (Sinha, 1988) and assumed to be 0.5 for creep.

Perhaps as should be expected, the lateral strain response exhibits much the same characteristics as that shown by the axial deformation curves, such as accelerated creep rate due to damage, non-linearity with stress and a tendency for viscous behaviour to dominate at higher applied stresses. For all confining pressures, at relatively low applied deviatoric stresses (0.5–1.0 MPa) the lateral and axial strains are on the same order, however, as the stress pulse is increased to the 2.0–3.0 MPa range, the lateral strain can be almost double the axial response. Similarly, elastic plus delayed elastic recovery for both axial and lateral strain response is on the order of 40% for the higher deviatoric stresses. The most striking feature is the magnitude of lateral strain developed independent of the hydrostatic confinement for the higher deviators. The large proportion of permanent lateral strain could

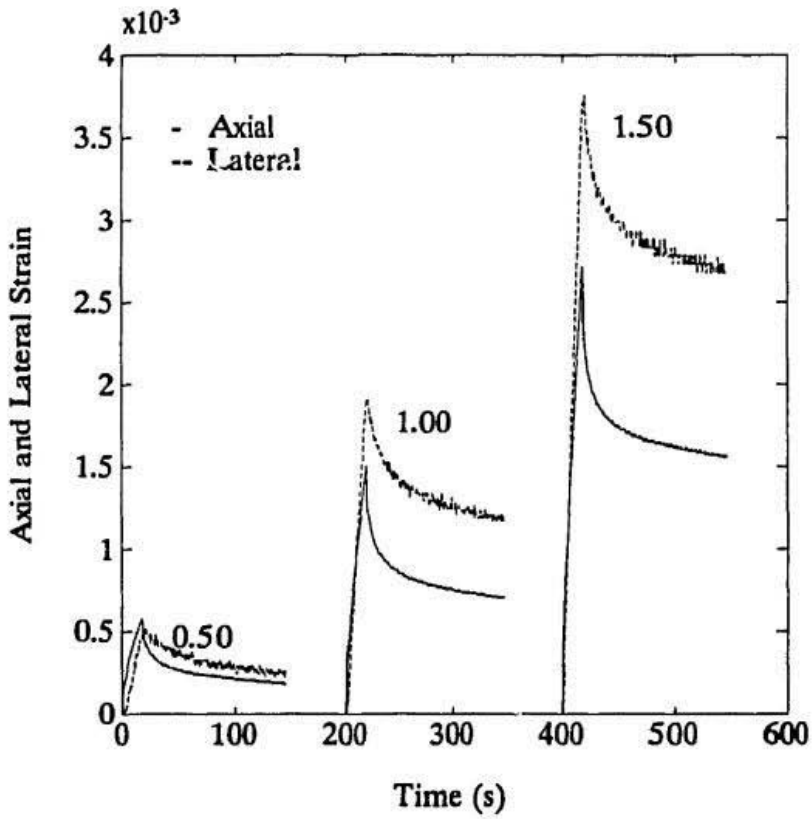

Figure 4.9: Lateral and Axial Strain Response under Uniaxial Loading Condition for Pre-Damaged Ice Sampes. The Number Listed Above Each Strain Curve Represents the Applied Deviator Stress in MPa.

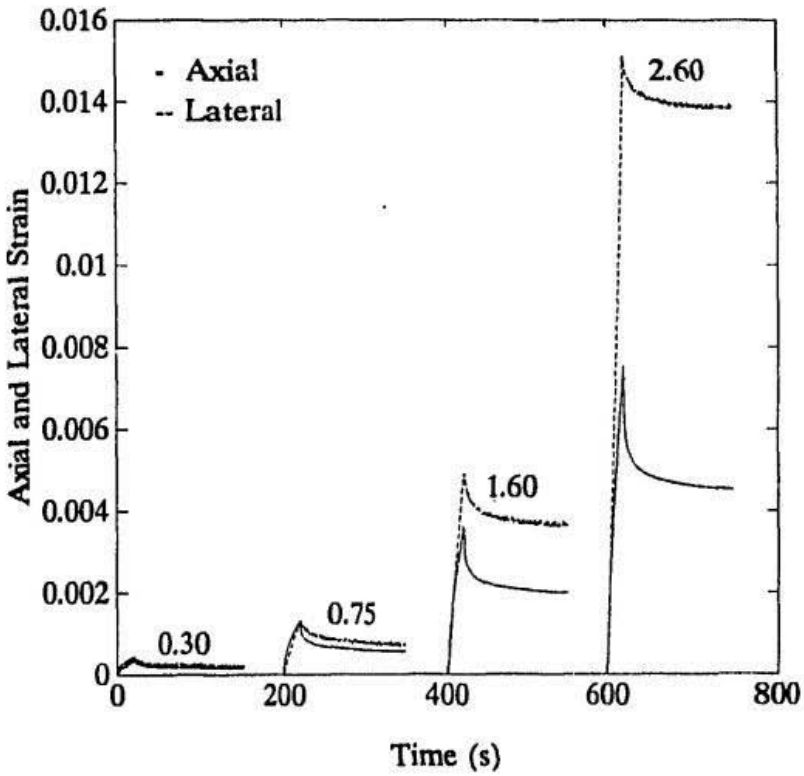

Figure 4.10: Lateral and Axial Strain Response at 4 MPa Confinement for Pre-Damaged Ice Sampes. The Number Listed Above Each Strain Curve Represents the Applied Deviator Stress in MPa.

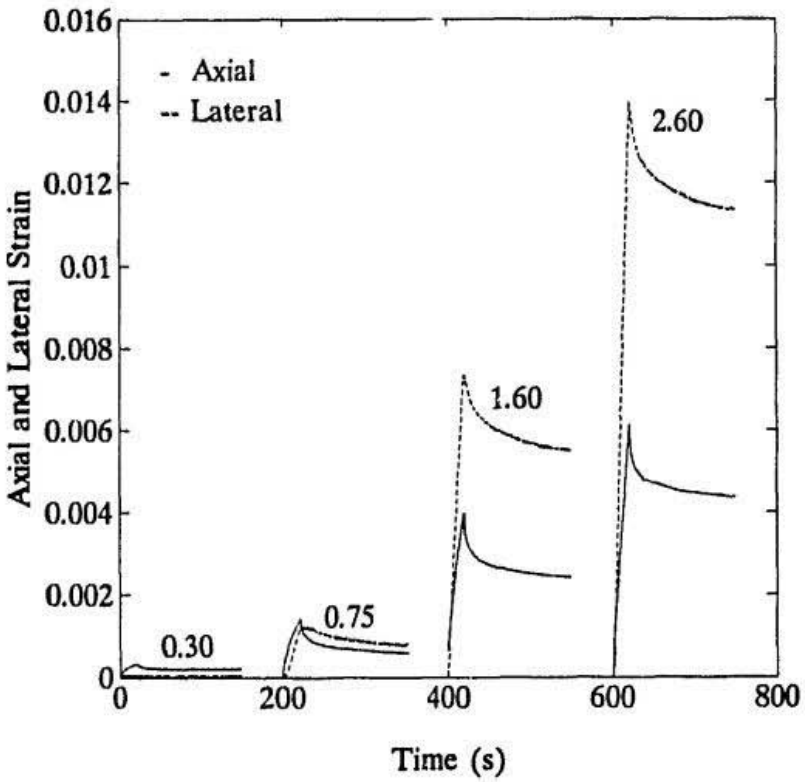

Figure 4.11: Lateral and Axial Strain Response at 10 MPa Confinement for Pre-Damaged Ice Sampes. The Number Listed Above Each Strain Curve Represents the Applied Deviator Stress in MPa.

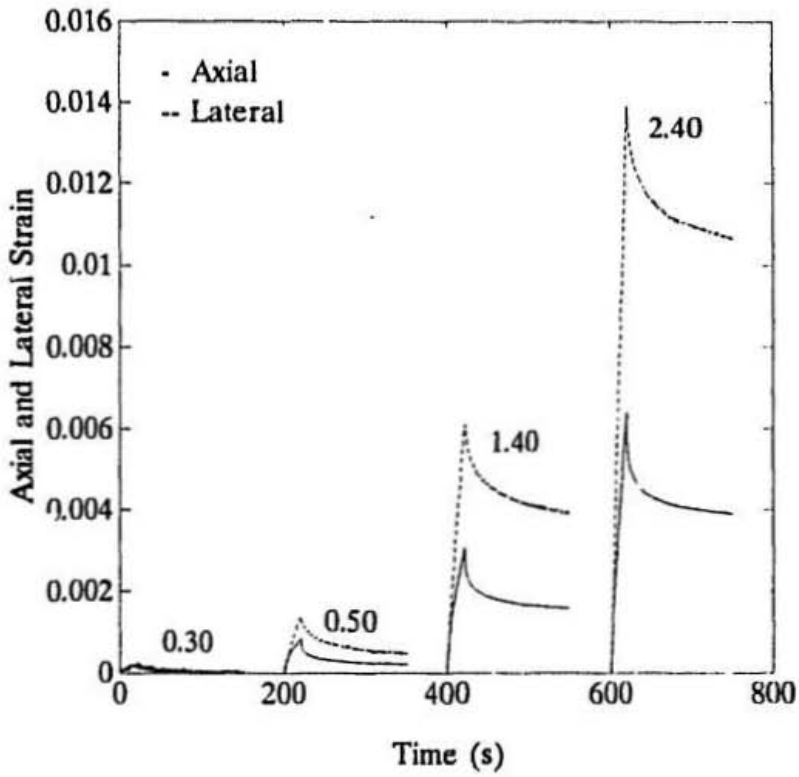

Figure 4.12: Lateral and Axial Strain Response at 20 MPa Confinement for Pre-Damaged Ice Sampes. The Number Listed Above Each Strain Curve Represents the Applied Deviator Stress in MPa.

be attributed to intense creep at crack tips which causes distortion or enlargement of the microcracks. Also, since the cracks were introduced under uniaxial loading conditions and subsequently confined, the degree of crack closure could be less than if the damage was induced under triaxial stress states. In other words, one must consider the stress-path and the influence on the damage level.

Similar to the axial strain response, the lateral deformation appears to be independent of the confinement and non-linear with deviatoric stress. This is illustrated in Figure 4.13 where the lateral strain response of pre-damaged samples is compared to intact ice at 20 s after the initial application of the stress pulse. The results show an overall trend independent of the imposed hydrostatic stress state. Although there appears to be as drop in the lateral strain for $p = 20$ MPa and $\sigma = 4.12$ MPa, as mentioned earlier, some caution should be taken with respect to these data points where limited information is available. Though it is conceivable that at higher confining pressures the lateral deformation would be inhibited.

Presently, there is limited information regarding the dilatational behaviour of ice under a multi-axial stress state. Wang (1981) investigated multi-year sea ice under constant strain-rates of 10^{-7}–10^{-2} s^{-1}, measuring both lateral and axial strains, noting the anisotropic nature of the strain ratio (i.e. apparent Poisson's ratio). Sinha (1991) conducted constant stress tests on laboratory grown S-2 type ice subject to uniaxial compressive loads of 1.2 to 3.0 MPa. Under the applied stress, the sample developed microcracks and dilatation was observed. The strain ratio reached a maximum on the order of 0.7 which indicates the presence of open cracks. Similar strain ratios can be determined from the data reported by Dorris (1991) where a

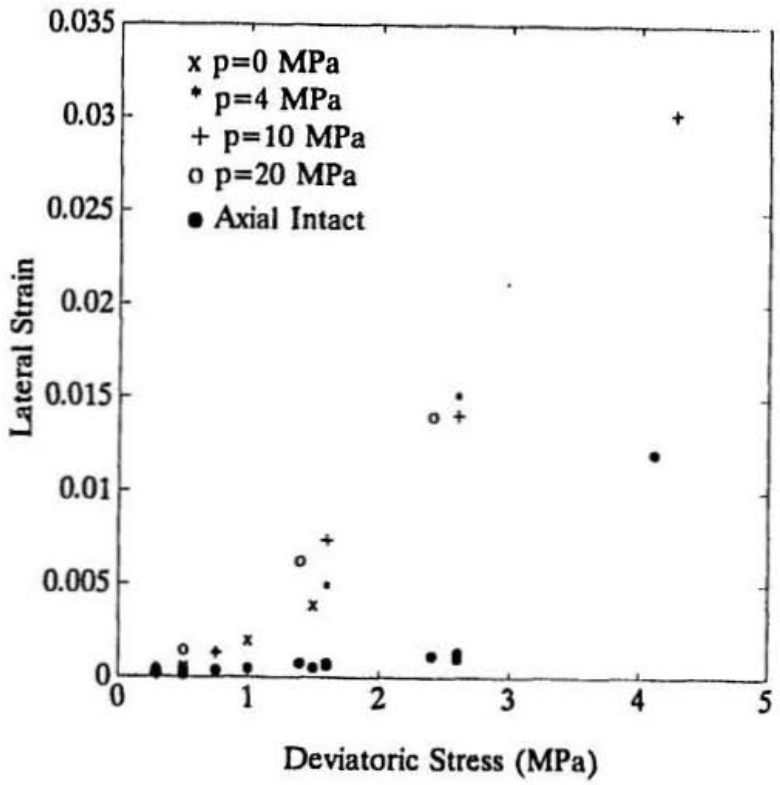

Figure 4.13: Non-Linearity of Lateral Strain as a Function of Deviatoric Stress for Pre-Damaged Samples at Time, t=20s. Note that the Axial Strain for Intact Ice is also Shown for Reference.

series of constant strain-rate tests (10^{-3} s^{-1} and 10^{-2} s^{-1}) under 2.62 MPa and 10 MPa hydrostatic confinement were performed on multi-year sea ice. Figure 4.14 shows that the strain ratio, calculated from Dorris' tests, increased from 0.5 to 0.7 with a decrease in confining pressure. The increase in strain ratio (> 0.5) indicates the progressive influence of microcracks and dilatational effects, where the limiting value points to a stabilization in the volumetric strain-rate and the horizontal plateau section of the stress-strain curve. Although in the present test program a series of constant stress pulses were applied to pre-damaged specimens, similar trends were observed and a typical curve is shown in Figure 4.15.

The difference in strain ratios, between Dorris' data and the present investigations, may be in part due to either the method for introducing damage into the ice or specimen size effect where the ratio of grain size to sample diameter may be reflected in the deformational behaviour. The present test series investigated pre-damaged polycrystalline granular ice deformed under uniaxial conditions to 2% strain and then subjected to constant loads under hydrostatic pressures. On the other hand, Dorris (1991) employed intact multi-year sea ice subject to constant strain-rate deformation under a triaxial stress to 10% axial strain.

Furthermore, the shape of the specimen may have also played a role in the creep deformation. First, effective sealing of the sample from the confining fluid, for example through the use of o-rings, was significantly inhibited due to the inherent corners on the square samples and endcaps. Although post-test inspection of the damaged specimens did not indicate the presence of oil, there is still a possibility that the deformation could be enhanced by lubrication through a reduction in the

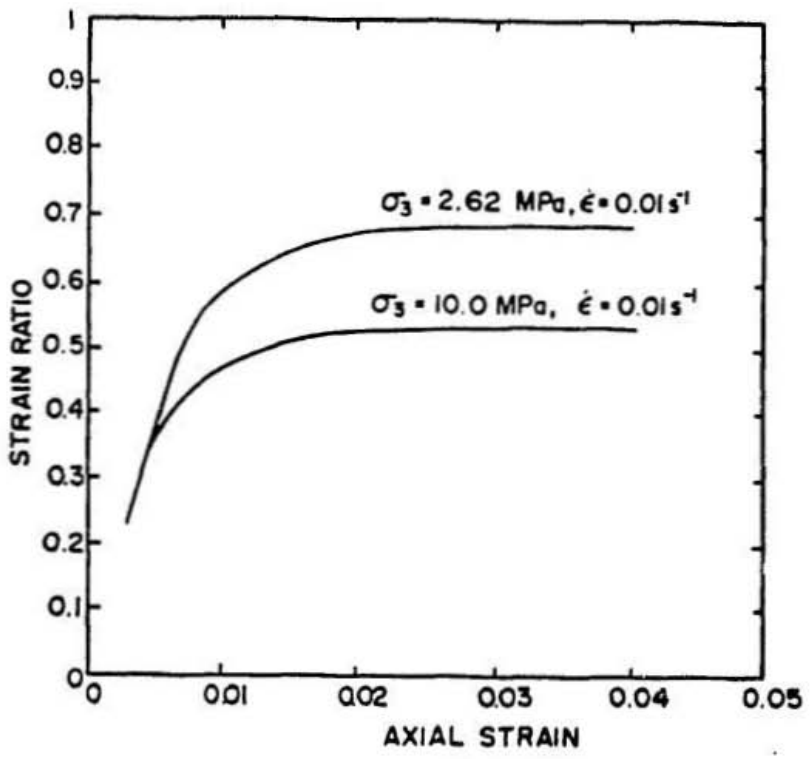

Figure 4.14: Strain Ratio of Multi-Year Sea Ice. *Jordaan et al., (1990b)*

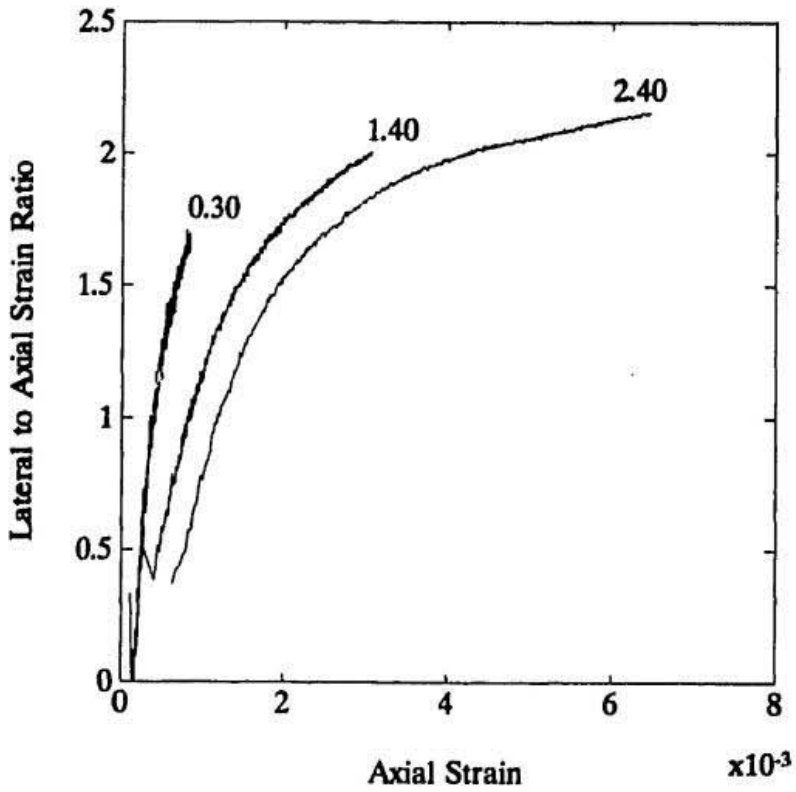

Figure 4.15: Strain Ratio for Pre-Damaged Ice at 20 MPa Confinement

frictional resistance to sliding across crack faces. Secondly, it was noted during the test program that end effects may have influenced the deformational response of pre-damaged specimens. Qualitative comparison of crack densities from the prismatic specimens of the present study with cylindrical samples from tests previously conducted at Memorial University, having nominally similar specimen diameter to length ratios and stress paths, indicated a greater degree of cracking near the ice-platen interface (Figure 3.7). This may have resulted in further "softening" of the specimen and enhancement of the creep strain-rate. Finally, slabbing or shear faulting may have occurred during the pre-damaging phase of the experiments which would influence the creep strain behaviour and may account for the high lateral strains developed under hydrostatic stress. Figure 3.7 shows an apparent fault line running along the face diagonal. The slabbing is probably due to the lipped depression of the brass endcap, which aids in alignment of the specimen, resulting in a confinement of the sample at the ice–platen interface. (Appendix A). In light of the present experimental results, a series of tests are currently being conducted at Memorial University with specific aims at investigating these areas of concern.

4.1.3 Triaxial Behaviour

The development of a realistic ice load model requires detailed knowledge of the confined behaviour of ice. The interaction between stress-path, damage state and subsequent material deformation needs to be thoroughly addressed. Analysis of the multiaxial behaviour was conducted assuming that the creep strain was isotropic and the deformation was comprised of independent deviatoric and volumetric components. Figures 4.16–4.19 illustrate the calculated volumetric and equivalent strains

developed in the pre-damaged ice samples for the range of confining pressures investigated. The volumetric strain is defined as,

$$\epsilon_v = \frac{1}{3}\left[\epsilon_1 + \epsilon_2 + \epsilon_3\right], \tag{4.1}$$

where ϵ_1, ϵ_2 and ϵ_3 are the principal strains. The equivalent strain is defined as,

$$e = \left[\frac{2}{3}\epsilon_{ij}\epsilon_{ij}\right]^{\frac{1}{2}}, \tag{4.2}$$

where ϵ_{ij} is the deviatoric strain developed in the material which can be also expressed as,

$$e = \sqrt{\frac{2}{3}}\left[(\epsilon_1 - \epsilon_2)^2 + (\epsilon_2 - \epsilon_3)^2 + (\epsilon_3 - \epsilon_1)^2\right]^{\frac{1}{2}}. \tag{4.3}$$

For volumetric strains, when the pre-damaged specimens are loaded at the higher stress levels, there is significant dilatation, on the order of axial strain, after the initial compaction phase, whereas the results reported by Dorris (1991) show volumetric deformation much less than axial. The large dilatational strains evident could possibly be attributed to the relationship between stress-path and damage state. For the given loading and damage conditions, the bulk of the microcracks may be fully or partially open, hence the observed viscous dominated strain could be related to intense creep causing distortion or enlargement of the microcracks. Conversely, intact samples loaded under triaxial stress states, as in Dorris (1991),

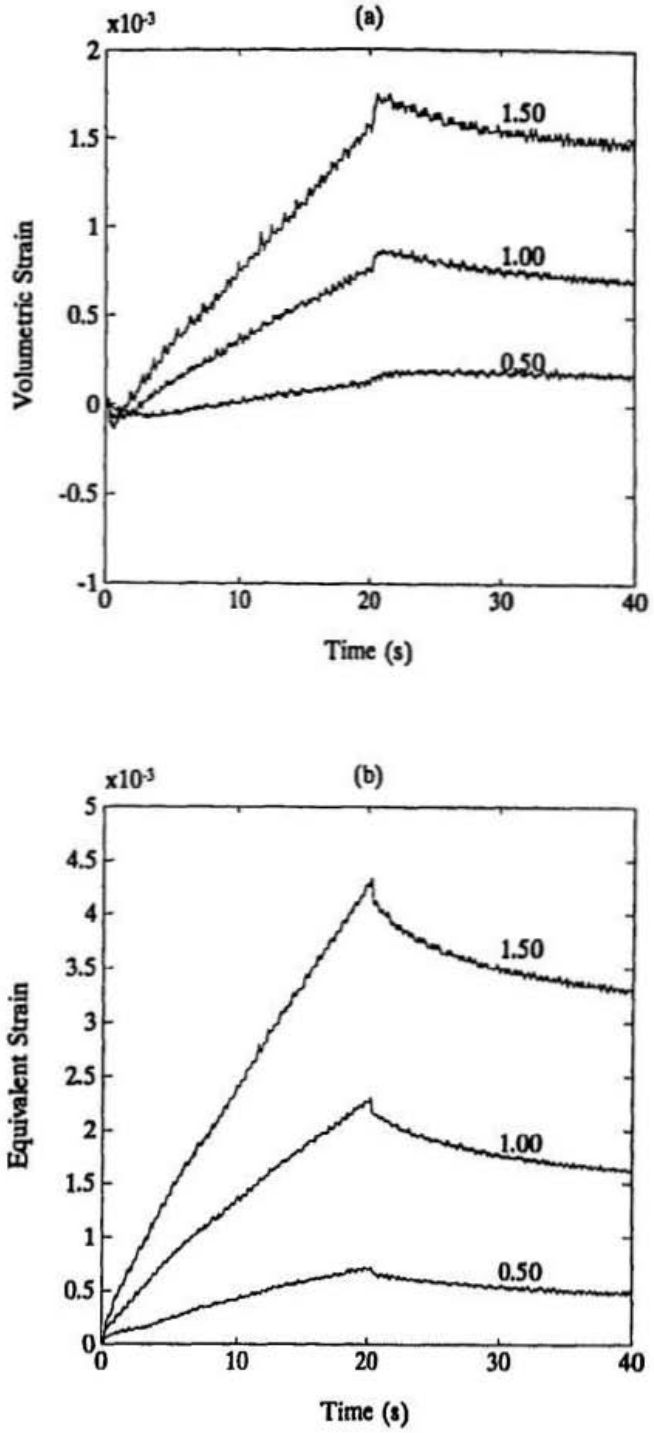

Figure 4.16: (a) Volumetric Strain for Uniaxial Loading Conditions, (b) Equivalent Strain for Uniaxial Loading Conditions. The Number Listed Above Each Strain Curve Represents the Applied Deviator Stress in MPa.

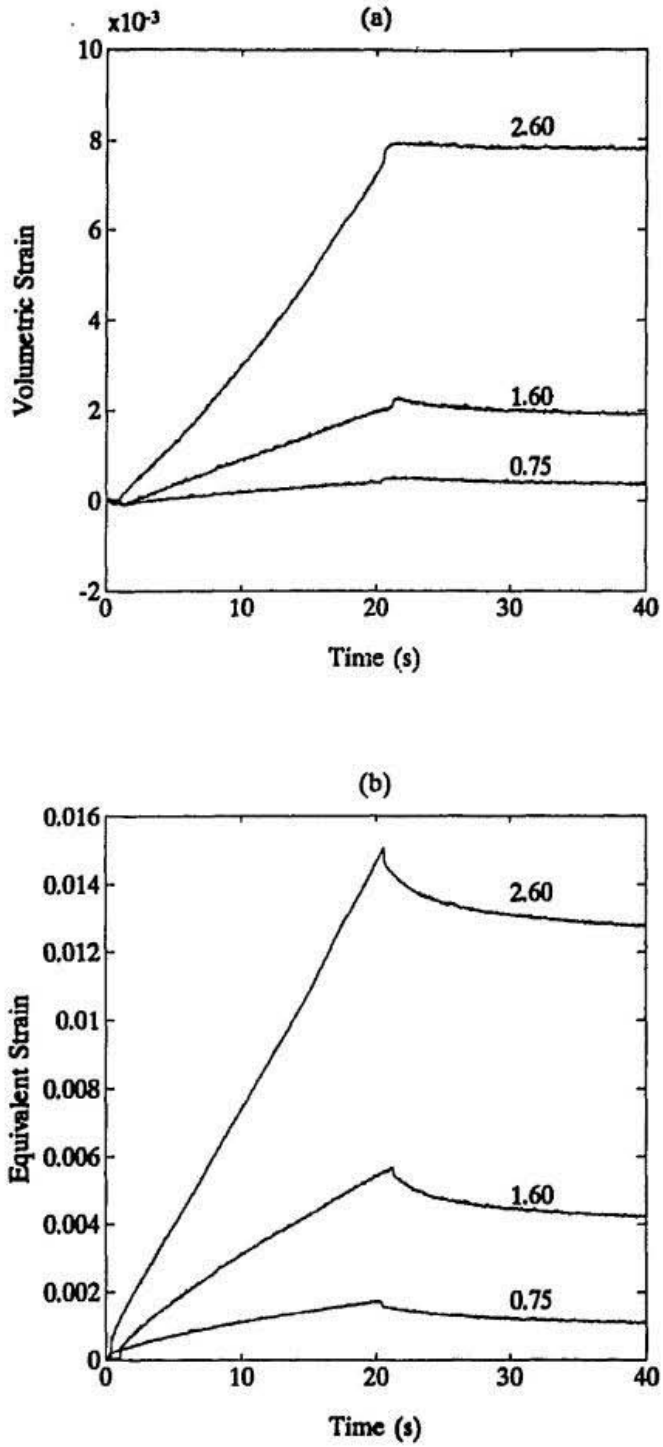

Figure 4.17: (a) Volumetric Strain for 4 MPa Confinement, (b) Equivalent Strain for 4 MPa Confinement. The Number Listed Above Each Strain Curve Represents the Applied Deviator Stress in MPa.

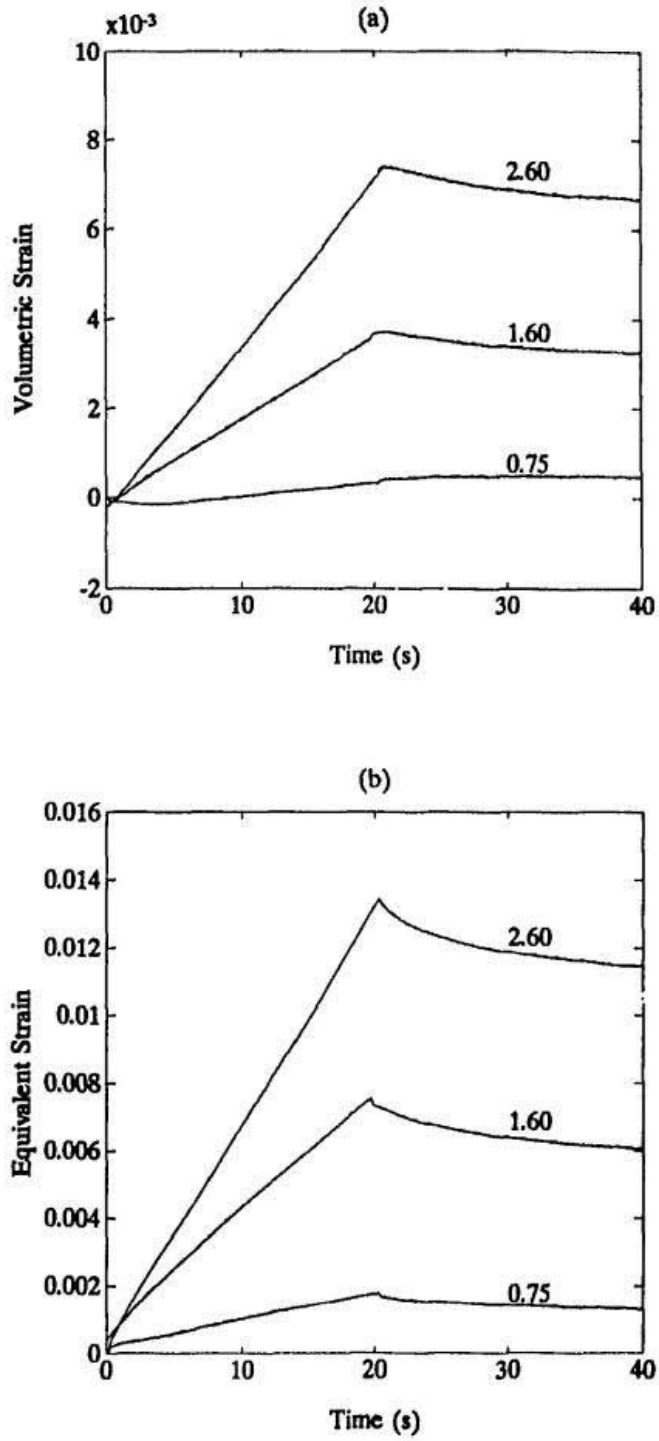

Figure 4.18: (a) Volumetric Strain for 10 MPa Confinement, (b) Equivalent Strain for 10 MPa Confinement. The Number Listed Above Each Strain Curve Represents the Applied Deviator Stress in MPa.

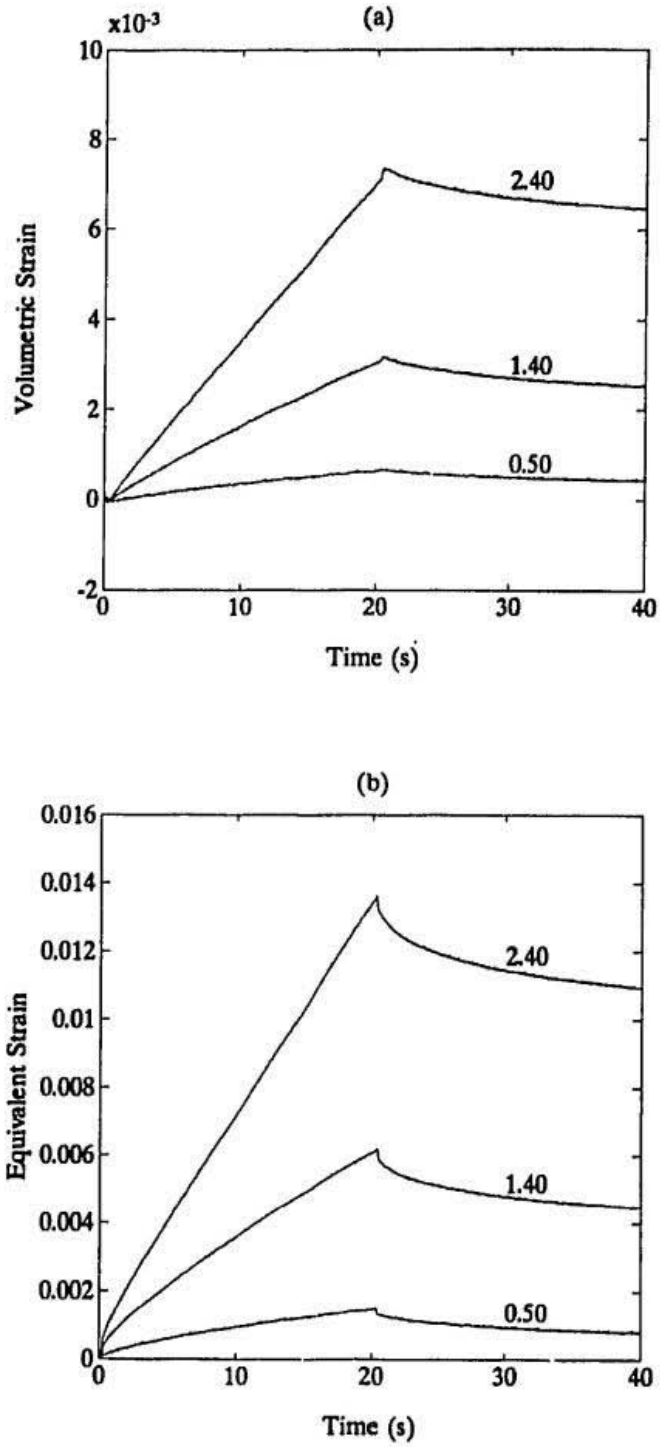

Figure 4.19: (a) Volumetric Strain for 20 MPa Confinement, (b) Equivalent Strain for 20 MPa Confinement. The Number Listed Above Each Strain Curve Represents the Applied Deviator Stress in MPa.

could have the majority of the cracks closed where primary creep and traction across crack faces would be the more significant deformational mechanism.

Figure 4.20 shows the relationship between dilatational strain-rate and volumetric stress. The rate was calculated from the volumetric strain–time curves when volumetric expansion was evident after the initial compaction phase; thus the elastic contribution and initial decrease in volume is not considered. The presence of microcracks or damage appears to influence the dilatational behaviour of the ice sample with respect to confinement, since the strain-rates are not constant for nominally constant volumetric stress states — for an intact solid the volumetric deformation is proportional to the mean stress. Consequently, the dilatational strain-rate was plotted as a function of deviatoric stress (Figure 4.21), which shows a non-linear relationship with shear stress.

Similarly, Figure 4.22 illustrates the non-linearity of equivalent strain-rate with deviatoric stress. Considering that roughly 60% of the equivalent strain response exhibited by the pre-damaged specimens for the higher stress levels was permanent secondary creep, the strain data was analysed assuming that a power law relationship, of the form $\dot{\epsilon} = A\sigma^n$, was appropriate to describe the deformation. The strain-rates were calculated from the strain–time curve, using numerical differentiation, over the 20 second load pulse while ignoring the initial elastic response. Long term creep experiments have shown that the magnitude of the exponent is typically taken as 3. Indeed, the debate over whether secondary creep exists in polycrystalline ice, as related to a fundamental material property, is considered to be dependent on the presence of microcracks. Figure 4.23 presents the shear strain-rate as a func-

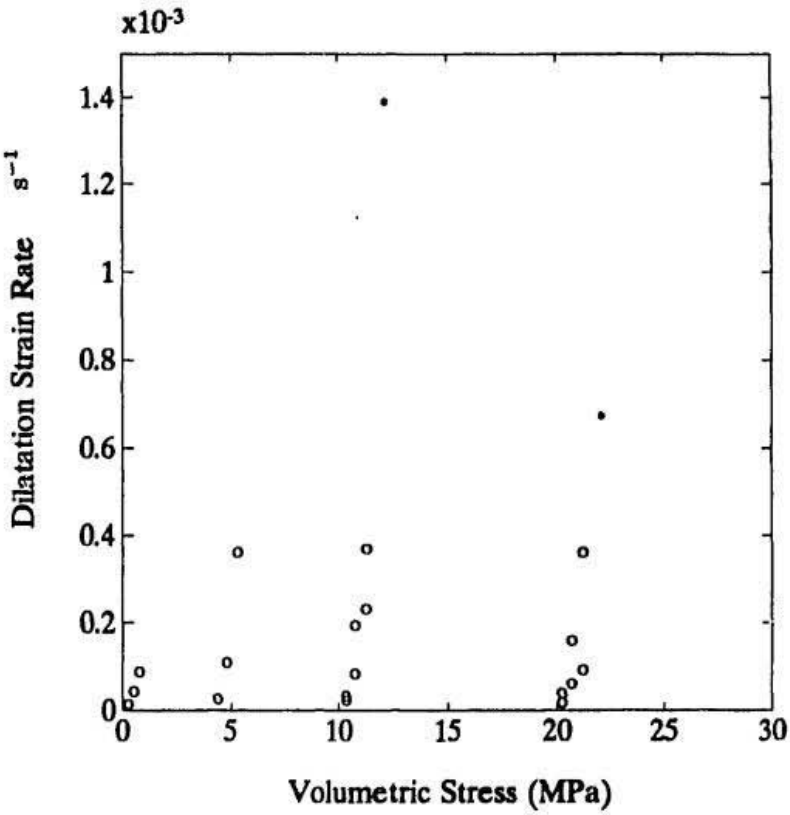

Figure 4.20: Dilatational Strain-Rate as a Function of Volumetric Stress

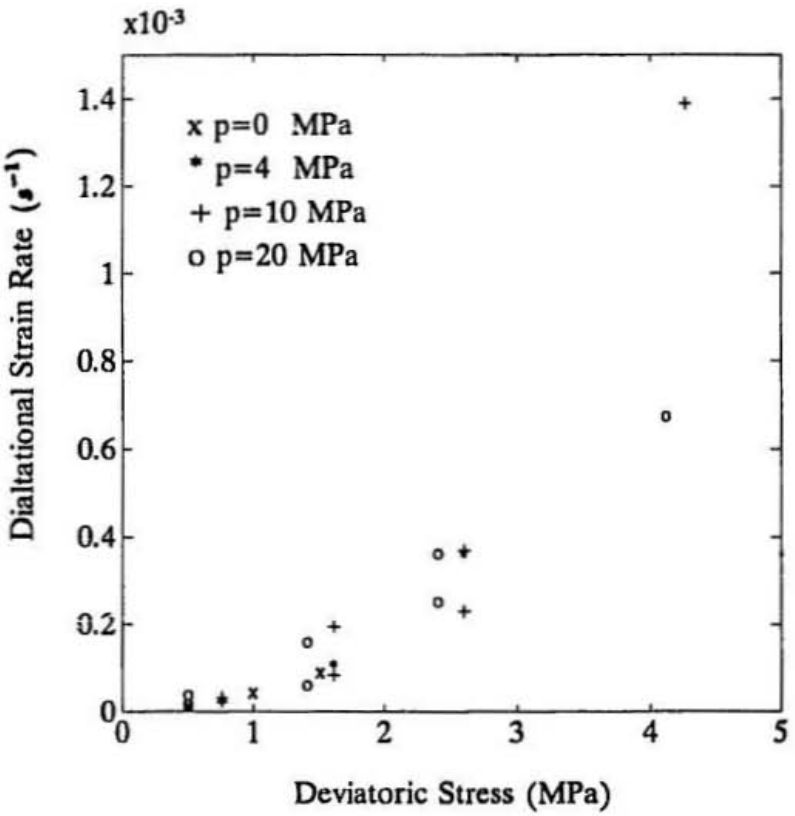

Figure 4.21: Dilatational Strain-Rate as a Function of Deviatoric Stress

tion of shear stress for uniaxial loading of polycrystalline ice. At higher stresses on the order of 10 MPa the creep flow exhibits power-law breakdown; see Sanderson, (1988).

Initial analysis of the least-squares best fit and logarithmic values of equivalent strain and deviatoric stress gave coefficients of A=1.4x10^{-4} and n=1.73 (Figure 4.24). The relatively low creep exponent observed during the present study may be explained in consideration of the underlying assumptions. Typically the determination of the power index is from long term creep measurements conducted over several minutes to hours, whereas in the present study, the stress pulse was applied for only 20 seconds. Also, due to the short time interval, the separation of transient and viscous response is complicated realizing that the elastic plus delayed elastic strain is at least on the order of 40% of the total deformation. The tacit assumption made here was that the overall creep response could be appropriately described by a power law equation representing an effective viscous element. The influence of the delayed elastic component tends to 'soften' the overall response, particularly at lower stress levels, which is reflected in the exponent, n. In effect, the compliance of the two creep terms is averaged and the viscosity of the Kelvin unit dominates the strain response. However, if one considers the behaviour at deviatoric stress levels greater than 1.0 MPa, the observed tendency for the dominating viscous behaviour is characterized by an increased exponent. Consequently, disregarding the lower stress values (i.e. $<$ 1.0 MPa), a fit of A=8x10^{-5} and n=2.34 — this is illustrated in Figure 4.24. The derived power-law relationships for equivalent strain-rate are shown in Figure 4.25.

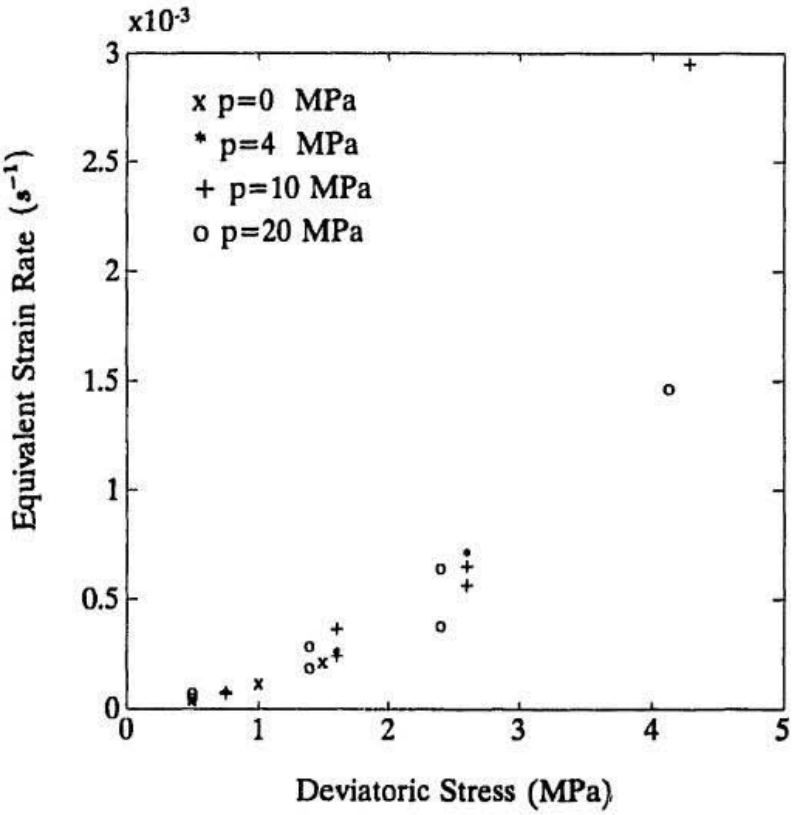

Figure 4.22: Equivalent Strain-Rate as a Function of Deviatoric Stress.

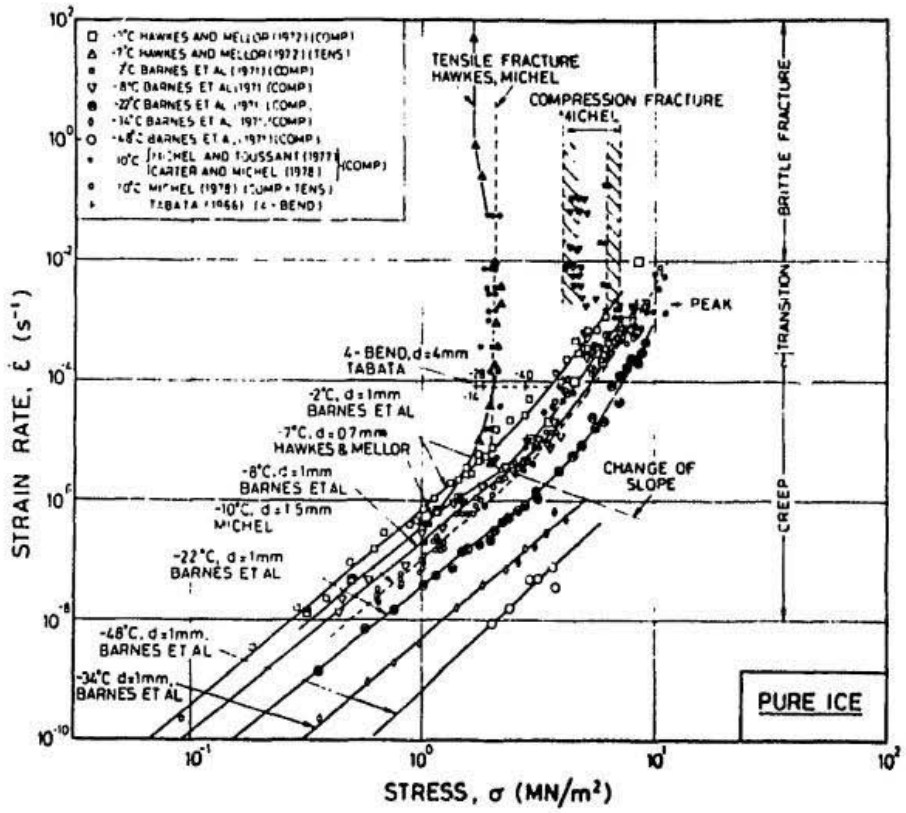

Figure 4.23: Logarithmic Plot of Shear Strain-Rate as a Function of Shear Stress. *Hallam, (1986)*

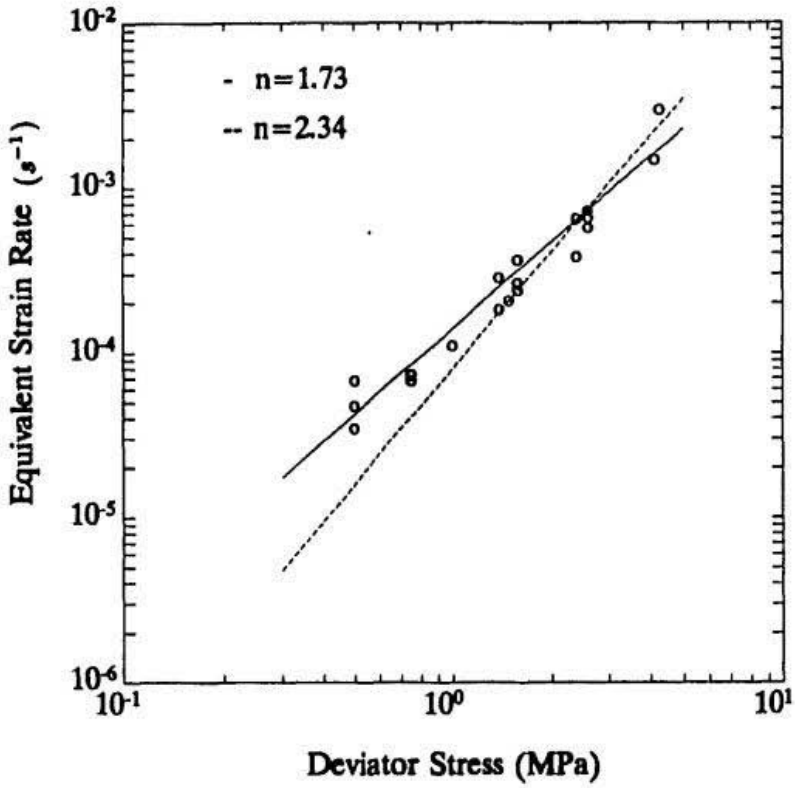

Figure 4.24: Logarithmic Plot of Equivalent Strain-Rate and Deviator Stress. The Coefficients and Power Exponents for the Superimposed Lines are Presented in the Legend.

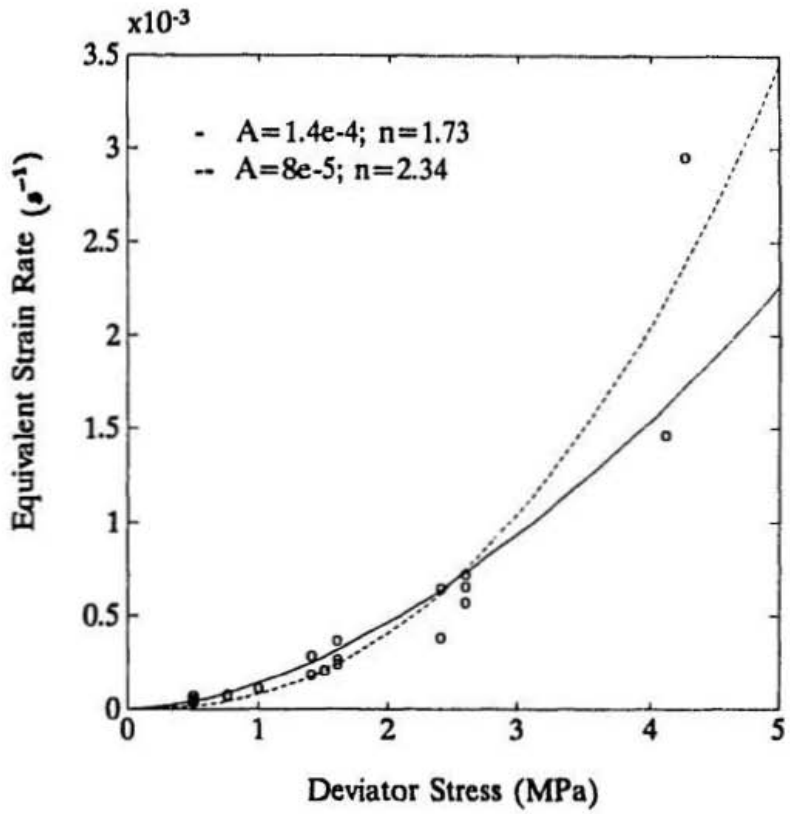

Figure 4.25: Non-linearity of Equivalent Strain-Rate with Deviatoric Stress.

The trend of non-linearity independent of confinement is quite promising with respect to utility and simplicity for implementation into finite element routines; see for example Jordaan et al. (1990b) or Xiao (1991). Although the samples have not yet fully recovered the transient stage, approximately 60% of the total strain is permanent creep for the higher applied deviators. Since for short time intervals and rapid loading the viscous element associated with delayed elasticity carries most of the load in the Kelvin unit, the recoverable strain could be modelled as a dashpot unit with reduced viscosity. Thus, numeric computations in mathmatical models such as FEM could be simplified — Jordaan et al., (1991b). In the development of a user defined material specification for the finite element program ABAQUS, McKenna et al. (1990) yielded an empirical function to describe the multiaxial strain behaviour of ice based on the results of Dorris (1991). The equation related the ratio of volumetric to equivalent strain-rate with the ratio of volumetric to von Mises stress and was expressed as,

$$\frac{\dot{\epsilon_v}}{\dot{e}} = 0.25exp\left[1.5\frac{\sigma_v}{S}\right], \tag{4.4}$$

where $\dot{\epsilon_v}$ is the volumetric strain-rate,

$\dot{e}$ is the equivalent strain-rate,

σ_v is the volumetric stress and

S is the von Mises stress.

Data used for the relationship were calculated from the plateau section of the stress-strain curve where the volumetric strain and axial stress had stabilized to nominally constant values. The empirical equation (Eq. 4.4) used to fit the data of Dorris (1991) and experimental results from the present test series are illustrated in Figure 4.26.

Lower stress ratios indicate a larger applied deviatoric stress for a given confining pressure, whereas lower strain-rate ratios represent creep dominanted deformation. The folding of the datapoints, in the present study, with increasing stress ratio arises from the independence of dilatational strain rate with hydrostatic confinement which effectively horizontally expands the data. Analysis based on volumetric and shear ratios may not be appropriate when the ice is substantially damaged. This is evident from the present test results where dilatation is independent of the mean stress. Although noting the limited data set available, the disparity indicates that the deformational response may be linked to stress-path history, as well as, current damage state and stress. For example, if the material state is initially within the regime of Dorris' data, then subject to a drop in confining pressure concurrent with a damaging path and then subsequently loaded under hydrostatic confinement, the deformational behaviour may exhibit characteristics observed in the present test series. Furthermore, Equation 4.4 could be only valid for cases were there is a low level of damage in the material.

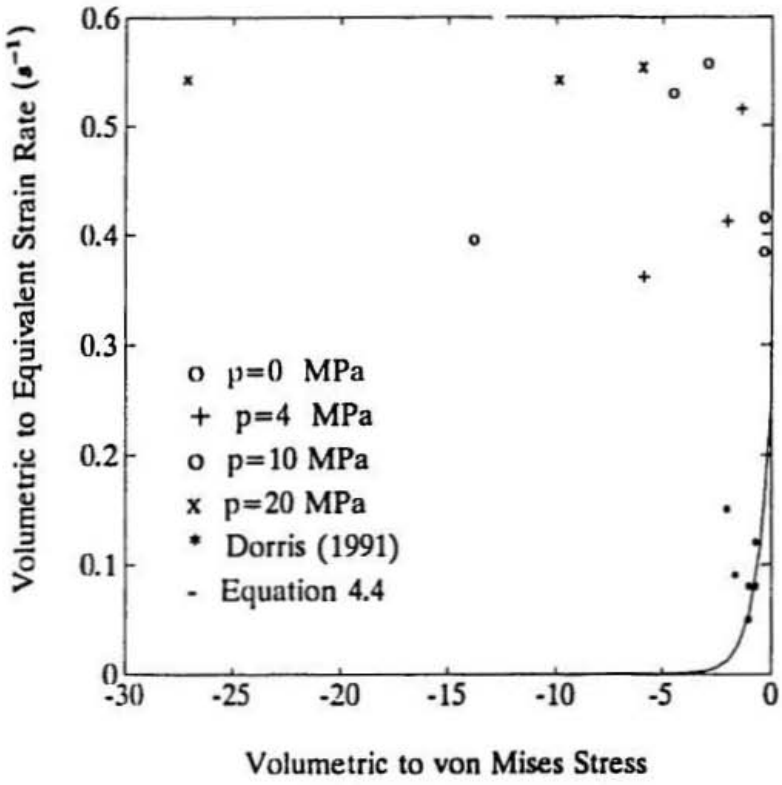

Figure 4.26: Ratio of bulk strain-rate to von Mises strain-rate as a function of the ratio of volumetric stress to von Mises stress. *McKenna et al., (1990)*

4.2 Relation to Observed Field Events

The considerable enhancement of creep strain and non-linearity of volumetric and shear deformation rates exhibited by the pre-damaged ice samples, independent of the confining pressure studied, has significant implications when considering full-scale interaction events. Medium-scale indentation tests; such as Hobson's Choice Ice Island (1989,1990), showed that peak local pressures attained magnitudes up to 70 MPa with steep gradients across load cells (Frederking et al., 1990). Intuitively, the present experimental results indicate that it is possible to have significant deformation in regions of moderate confinement during full-scale interactions where the deviatoric stresses and damage levels are expected to be much greater.

Figure 4.27 schematically illustrates a hypothesized failure process involved during penetration of an ice feature by a spherical indentor; much like the field program at Pond Inlet (1984). During fast crushing and clearing events, the progression of damage is considered to begin near the free edges of contact, possibly coupled by spalling events, with the pulverization front moving rapidly inward. The spatial distribution of these 'critical' zones and crushed regions fluctuate in time, which could be represented as a random process, are considered to be responsible for the dynamic activity associated with ice crushing. These mechanisms would also operate for other interaction geometries, such as those investigated during the Hobson's Choice Ice Island indentation tests (Figures 2.14–2.15; Frederking et al. (1990)). In general, for a predominantly crushing mode of failure, the overall picture is an ice feature with varied spatial and temporal distribution of critical zones which are a function of the stress-path, damage state, volumetric stress and deviatoric stress.

Density measurements reported by Meaney et al. (1991), load-time histories and video recording of the failure surface during indentation support this characterization.

These critical zones, typically associated with areas of moderate to high confinement, are seen as the key to dynamic fluctuations in load and local peak pressures exerted during ice–structure interaction events. The intense creep response observed during the present laboratory investigations can be also inferred from thin sections taken from Hobson's Choice (1990) medium scale indentation tests; see also Meaney et al. (1991). Ice cores were removed, from the same horizontal plane, of test face TFF-01, with a lateral center-to-center spacing of approximately 100 mm. Thin sections of each core are shown in Figure 4.28. The numbers in millimetres represent the depth away from the ice–structure interface.

The 'contact' zone reveals that the level of damage is significant near the ice-indentor interface and decreases in severity away from the failure surface. The crushing has created pockets of a finer grained matrix on the order of a millimetre; in comparison with the parent structure of 5–10 mm. Apart from the degree of pulverization, this feature is not too dissimilar from the grinding action evident in Figure 3.8. Thus, the 'contact' zone should not be considered intact or characteristic of the parent structure. In contrast, for the crushed zone there exists a distinct boundary or demarcation separating the pulverized material and the relatively undamaged region behind the layer. Although the crushed layer has undergone significant damage, the ice is still competent as a material. This was evident from uniaxial compressive tests

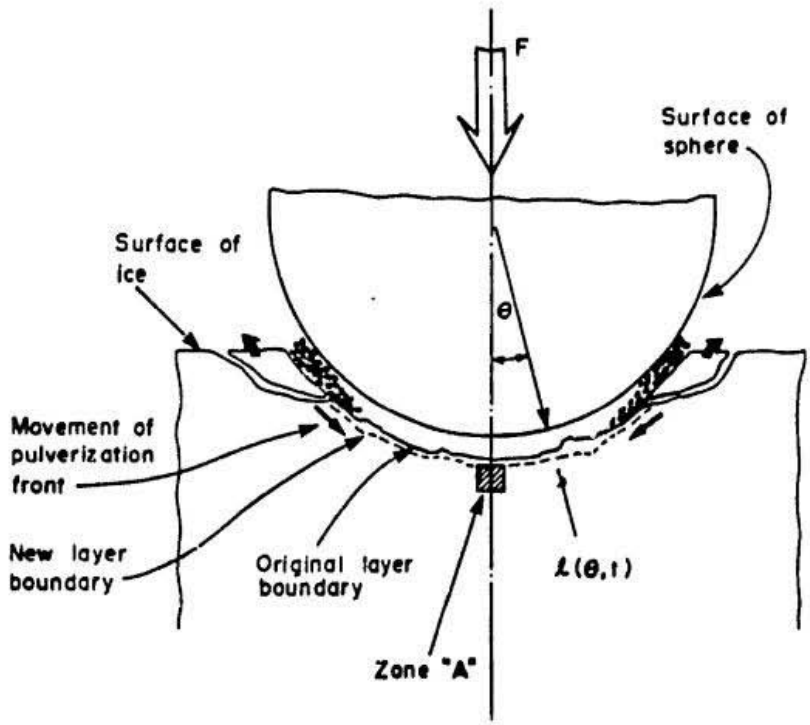

Figure 4.27: Failure Process for a Spherical Indentor Penetrating an Ice Feature. *Jordaan et al., (1990b)*

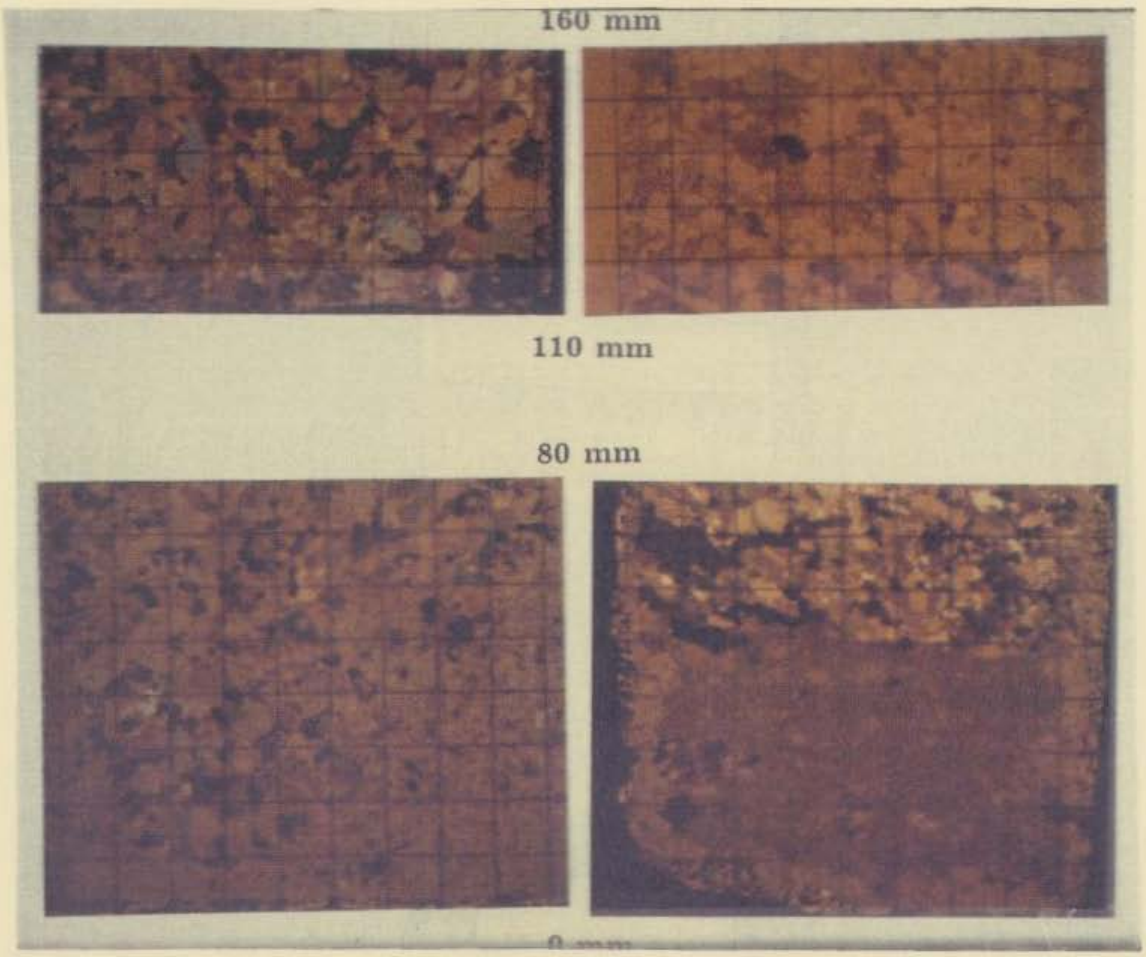

Figure 4.28: Horizontal Thin Sections of Samples Taken from Test Face TFF-01, (a) Thin Section of Core Taken from 'Contact' Zone, (b) Thin Section of Core Taken from Crushed Layer Region. The Superimposed Grid is 10 mm × 10 mm

of recovered ice cores from the crushed layer; see Kenny et al. (1991). The congealed nature of the material within the crushed layer could be related to a pressure melting or a sintering mechanism, which can be viewed as a reverse of the damaging process.

On closer inspection, Figure 4.28 illustrates the regional distribution of damage state. For the region behind the crushed layer (Figure 4.28 (b)) there is a lower degree of damage, at the same depth from the ice-indentor interface, than that for the ice located in the 'contact' zone. From this evidence, one can hypothesize that the considerable creep enhancement observed during the laboratory test program can also be seen during large scale events. That is, the crushed layer appears to act as a buffer zone for the mechanical energy where the deformation is concentrated, and intense creep limits the damage experienced by the ice mass behind the crushed layer through energy dissipation. Although the ice cores were removed from the test face within relative proximity (100 mm), the thin sections suggest fundamentally different deformational processes. Respectively, these mechanisms, appear to be related to a fracture controlled or damaging criterion and crack-enhanced creep process.

The regions generally associated with relatively lower damage levels are considered to be critical zones or 'hot spots' which actively fluctuate in position within the failure zone. This was supported by evidence from the pressure transducers, load cells and video recording of the failure surface during indentation. Similar contact phenomena were evident during tests conducted by Geotech where crushed ice was compressed between two flat plates over a range of displacement rates (Finn et al. (1989)) and crushing tests reported by Fransson et al. (1991) and Joensuu and Riska

(1988). Also, Kennedy (1990) performed incremental extrusion analysis of a crushed layer, with uniformly varying and irregular layer thicknesses, aimed at simulating ice–structure interactions. The analysis revealed that peak pressures were associated with zones where the crushed ice layer was thin. However during indentation tests at Hobson's Choice Ice Island in 1990, superimposing the final recorded pressures on the failure surface of test faces showed that the peak local pressures were not exclusively associated with the 'critical' zones. Nevertheless, the steep pressure gradients evident across the contact face, which can be related to shear, could govern the stochastic evolution of critical zones which results in significant damage, intense accelerated creep and rapid clearing of crushed material. Thus, it is conceivable that the significantly enhanced non-linear deformation, observed in the present test series, could operate at full-scale. Presently the key area for future research is the development of realistic ice-load models based on knowledge from field events, both medium- and full-scale as well as controlled laboratory tests.

4.2.1 Modelling Mechanical Behaviour: Preliminary Analysis

From an engineering viewpoint, there is a variety of philosophies which can be employed in describing the material behaviour of ice; these can range from empirical models to theoretical analysis. There are inherent advantages for each methodology with respect to simplicity, practicality and utility.

Empirical methods can be quite useful over the range of parameters investigated but the governing equations are limited to the available database and extrapolation

is highly speculative. An example of this, in ice mechanics, is the well known equation for ice indentation developed by Korzhavin. The equation utilizes empirical contact coefficients and reasonably predicts small-scale interactions (e.g. impacts with bridge piers) but the limits of application are evident when analyzing full-scale events where the ice forces are considerably overestimated. The main drawback with empirical methods is that there is limited analysis of the physics involved and thus the restricted scope of application. At the other extreme, material behaviour modelled by formalizing a hypothesis into a general theory of material behaviour which can be extremely powerful in terms of application (e.g. theory of elasticity) but may be particularly cumbersome or require rigorous analysis.

The complexity of ice–structure interaction events points to numerical methods, such as finite element and probabilistic analysis for solving engineering design problems. Although assumptions and idealizations are required, it is the generality in application which makes finite element modelling of ice–structure interaction events so appealing. Damage mechanics recognize the changing structure of the ice as a result of the stress and strain history and corresponding changes in the deformational behaviour.

There have been a number of proposed models to describe the compressive deformation in ice, see for example Karr (1985), Jordaan and McKenna (1991b) and Schapery (1991). These models have been typically founded on theories of continuum damage mechanics and viscoelasticity. The models attempt to describe the structural degradation in the material which results in a loss of deformational resistance. In the development of damage models there are two key parameters which

must be defined; namely, the cause of damage in the material (e.g. crack density) and the measures of effect on the overall mechanical behaviour (e.g. change in elastic modulus). Typically the accumulation of damage is incorporated into the model through some damage evolution law. Since the process was generally associated with the formation of microcracks, initial attempts to define a primary descriptor of damage were developed based on the rate theory of fracture (McKenna et al., 1989) and the following expression was proposed,

$$\dot{N} = \dot{N}_o \left[(S - \sigma_c)/\sigma_o\right]^m , \tag{4.5}$$

where $\dot{N}$ is the rate of crack nucleation ,

$\dot{N}_o$is the rate constant,

S is the von Mises stress (MPa),

σ_c is the critical stress for crack nucleation (MPa),

σ_o is the normalizing stress (MPa), and

m is a constant.

This was developed in light of work conducted by Budiansky and O'Connel (1976), where an isotropic damage parameter was found to be dependent upon the volumetric crack density and average crack size. Small-scale experiments have shown that crack density may not be an ideal or adequate descriptor when the material becomes significantly damaged. This can be appreciated by looking back at Figure 3.8 where considerable pockets of fine-grained material are interdispersed throughthout the cracked matrix. A series of uniaxial compressive tests, conducted by the author

at Memorial, supported this observation through thin section analysis. Individual samples were deformed, under a constant strain-rate of 10^{-4} s^{-1}, to a preset strain level (0.0005, 0.001, 0.002, 0.005, 0.01, 0.02), after which the specimen was sectioned and analysed for crack characterization. Similar to observations by Cole (1991) and Kalifa et al. (1989) the cracks were predominantly aligned in the direction of the compressive axis and that the maximum rate of microcracking occurred around peak stress. For an axial strain of 0.02 there was evidence of fine intergranular particles. The presence of these particles, commonly observed during high strain-rate compression tests, within the developed shearband, indicates a grinding process and represents another form of damage. The crushed material generated at the contact zone, evident during medium-scale indentation tests, has varied physical characteristics throughout the zone in which the accumulated damage cannot be described only in terms of microcrack density — discussed in the following section. Thus, the definition of an appropriate parameter needs to be further addressed.

Indeed excellent work conducted by Schapery (1991) considers the stress path in the formulation of a damage measure for a constitutive model describing viscoelastic deformation. In the model, a parameter S_σ accounts for the accumulation of damage in the material which is defined as,

$$S_\sigma = \int_0^t \left(\frac{\sigma}{\sigma_o}\right)^q dt, \tag{4.6}$$

where σ is the applied stress (MPa),

σ_o is a stress constant (MPa),

q is the stress exponent.

Having formalized a descriptor on the nature and degree of damage, the influence or effect of that damage on the overall stress-strain response of the material needs to be addressed. One such possible measure could be the change in the elastic modulus defined as,

$$E = E_o(1 - \lambda), \tag{4.7}$$

where E is the damaged modulus (MPa),

E_o is the initial modulus of intact material (MPa),

λ is the damage parameter.

The parameter λ is bounded by $0 \leq \lambda \leq 1$, where 0 represents no damage and 1 is total loss of elastic stiffness. This simple approach to damage mechanics does not take into account the creep properties of ice, inherent strain-rate dependence or the possibility of frictional work across crack surfaces. Investigations by Weertman (1969), on non-interacting cracks, found that for higher crack densities the creep rate was proportional to σ^n. Jordaan and McKenna (1991b) suggest that an exponential form might be worth exploring, such as

$$\dot{\epsilon} = \dot{\epsilon}_o exp(\beta N), \tag{4.8}$$

where $\dot{\epsilon}$ is the strain-rate (s^{-1}),

$\dot{\epsilon_o}$ is the reference strain-rate for intact ice (s^{-1}),

β is a constant enhancement parameter, and

N is crack density (# cracks).

Similarly Schapery (1991) incorporates the effects of damage through a function $g(\sigma)$, which is determined experimentally. In the model proposed by Jordaan and McKenna (1991b), a Burgers rheological model is used to describe the deformation of intact ice where the enhanced deformation due to damage, in the Hookean springs and non-linear dashpots, is incorporated through a creep enhancement parameter (β). The $exp(\beta N)$ term is similar to the $g(\sigma)$ parameter as defined by Schapery (1991).

Although further experiments need to be conducted to develop calibrated damage effect parameter, as a function of damage state and stress history, the numerical technique provides an elegant, yet rigorous treatment of the progressive damaging process in ice. Presumably, a family of non-linear curves, similar to those presented in Figures 4.21–4.22 would exist, for various damage and stress states, where the response could be represented by some functions of the form,

$$\begin{aligned} \dot{\epsilon_v} &\propto [S, \sigma_v, S_\sigma], \\ \dot{e} &\propto [S, \sigma_v, S_{sigma}]. \end{aligned} \tag{4.9}$$

From the present test series $g(\sigma)$ is dependent upon the damage state and deviatoric stress, although friction across crack faces and pressure melting may play a greater role at higher volumetric stresses. The calibration of the function $g(\sigma)$ could be conducted following Schapery (1991) or through empirical fits (i.e. power law, exponential form) of the rheological elements. Through this philosophy, future work should concentrate on identifying the critical parameters which characterize the progressive damaging process and creep enhancement under multiaxial stress states. Thus working towards the ultimate goal of developing a realistic ice-load constitutive model applicable for a number of design scenarios.

Chapter 5

Conclusions and Recommendations

Ice–structure interaction events are extremely complex processes not only with respect to the failure mechanisms involved but also the material behaviour of ice. Consequently, the development of an ice-load model, applicable for a range of interaction scenarios, necessitates the utilization of numerical methods and probabilistic analysis in design methodologies. Field observations and medium-scale indentation tests have provided invaluable information regarding the dynamics of the ice crushing process, spatial and temporal distribution of local peak pressures, as well as characterization of the failure zone. The key now is the parallel development of experimental programs which facilitate the formulation of a realistic predictive ice-load model. The methods have intrinsic advantages and, more importantly, neither are followed to the exclusion of the other.

The 'critical' zones generated during ice crushing events are generally associated with regions of moderate confinement and considered to be the seat of ice-induced vibrations, key in the magnitudes and distribution of local peak pressures, as well as the focal point where zones of lower pressure crushed material and spall areas would be developed. The aim of the present test series was to investigate the influence of damage on the deformational response of ice subject to hydrostatic stress state. General conclusions based on the experimental results detailed in this work may be summarized as follows:

1. The rate and magnitude of creep strain, both axial and lateral, is significantly enhanced due to the presence of microcracks (i.e. damage) independent of confinement (0-20 MPa).

2. The deformational response of pre-damaged ice was dominated at higher applied stress levels by viscous creep. This points to possible simplification of the generalized visco-elastic model for ice.

3. Equivalent shear strains and volumetric strains exhibited non-linear behaviour with deviatoric stress due to damage and was independent of confinement (0-20 MPa).

4. Results from the present experimental program have significant implications when considering full-scale events where it is possible to have significantly enhanced deformation due to damage under confinement at 'critical' zones.

In closing, further work should be conducted to better understand the influence of the damaging process on the deformational behaviour of ice subject to multiaxial stress state. Specifically, the interrelationship between load history, variable damage state and stress path needs to be addressed; (e.g. proportional loading).

References

Ashby, M.F. and Hallam, S.D. (1986). "The Failure of Brittle Solids Containing Small Cracks Under Compressive Stress States", **Acta Metallurgica**, Volume 34, Number 3, pp. 497–510.

Ashby, M.F. and Duval, P. (1985). "The Creep of Polycrystalline Ice", **Cold Regions Science and Technology**, Volume 11, Number 3, pp. 285–300.

Barnes, P., Tabor, D. and Walker, J.C.F. (1971). "The Friction and Creep of Polycrystalline Ice", Proceedings, **Royal Society London**, A, Volume 324, pp. 127–155.

Blenkarn, K.A. (1970). "Measurement and Analysis of Ice Forces on Cook Inlet Structures", Proceedings, 2nd Annual Offshore Technology Conference, **OTC '70**, Volume II, pp. 365–378.

Brown, (1926). "Experiments on Strength of Ice", **Report of Joint Board of Engineers on St. Lawrence Waterway Project**, Appendix F, Ottawa, ON, Canada.

Budiansky, B. and O'Connell, R.J. (1976). "Elastic Moduli of a Cracked Solid", Proceedings, **International Journal of Solids and Structures**, Volume 12, pp. 81–97.

Cannon, N.P., Schulson, E.M., Smith, T.R. and Frost, H.J. (1990). "Wing Cracks and Brittle Compressive Fracture", **Acta Metallurgica et Materialia**, Volume 38, Number 10, pp. 1955–1962.

Cole, D.M. (1991). "Microfracture and the Compressive Failure of Polycrystalline Ice", Proceedings, Symposium on Ice-Structure Interaction, **IUTAM/IAHR**, St. John's, NF, Canada, pp. 231–249.

Cole, D.M. (1988). "Crack Nucleation in Polycrystalline Ice", **Cold Regions Science and Technology**, Volume 15, Number 1, pp. 79–87.

Cole, D.M. (1986). "Effect of Grain Size on the Internal Fracturing of Polycrystalline Ice", **CRREL Report 86-5**, U.S. Army Cold Regions Research and Engineering Laboratory, Hanover, NH, U.S.A., 79 p.

Cole, D.M. (1985). "Grain Size and the Compressive Strength of Ice", Proceedings, 4th International Conference on Offshore Mechanics and Arctic Engineering, **OMAE '85**, Houston, TX, U.S.A., Volume II, pp. 220–226.

Costin, L.S. (1985). "Time-Dependent Damage and Creep of Brittle Rock", Proceedings, **2nd Session of Damage Mechanics and Continuum Modelling**, ASCE, Detroit, MI, U.S.A., pp. 25–38.

Dorris, J.F. (1991). "A Plasticity Model for the Crushing of Ice", Proceedings, Symposium on Ice-Structure Interaction, **IUTAM/IAHR**, St. John's, NF, Canada, pp. 311–337.

Dougill (1985). "Constitutive Relations for Concrete and Rock: Applications and Extensions of Elasticity and Plasticity Theory", In Mechanics of Geomaterials: Rocks, Concretes and Soils, Editor Z.P. Bažant, **IUTAM William Prager Symposium**, John Wiley and Sons Ltd., pp. 21–46.

Duval, P., Kalifa, P. and Meyssonnier, J. (1991). "Creep Constitutive Equations for Polycrystalline Ice and Effect of Microcracking", Proceedings, Symposium on Ice–Structure Interaction, **IUTAM/IAHR**, St. John's, NF, Canada, pp. 55-67.

Flügge, (1967). **Viscoelasticity**, Blaisdell.

Frederking, R., Jordaan, I.J. and McCallum, J.S. (1990). "Field Tests of Ice Indentation at Medium Scale Hobson's Choice Island, 1989", Proceedings, 10^{th} International Symposium on Ice, **IAHR '90**, Espoo, Finland, Volume 2, pp. 931–944.

Fransson, L., Olofsson, T. and Sandkvist, J. (1991). "Observations of the Failure Process in Ice Blocks Crushed by a Flat Indentor ", Proceedings, 11^{th} International Conference on Port and Ocean Engineering Under Arctic Conditions, **POAC '91**, St. John's, NF, Canada, Volume 1, pp. 501–514.

Gagnon, R.E. and Sinha, N.K. (1991). "Energy Dissipation Through Melting in Large Scale Indentation Experiments on Multi-Year Sea Ice", Proceedings, 10^{th} International Conference on Offshore Mechanics and Arctic Engineering, **OMAE '91**, Houston, TX, U.S.A., Volume 4, pp. 157–161.

Gold, L.W. (1972). **The Failure Process in Columnar-Grained Ice**, Technical Paper Number 369, Division of Building Research, National Research Council Canada, Ottawa, ON, Canada, 108 p.

Hallam, S.D. (1987). "The Role of Fracture in Limiting Ice Forces", 3^{rd} State of the Art Report, **IAHR Working Group on Ice Forces**, CRREL Special Report 87-17, Editor T.J.O. Sanderson, Hanover, NH, U.S.A., 1–33.

Häusler, F.U., Earle, E.N. and Gerchow, P. (1988). "Uniaxial and Biaxial Compressive Strength of Ice Sampled From Multi-Year Pressure Ridges", Proceedings, 9^{th} International Conference on Port and Ocean Engineering Under Arctic Conditions, **POAC '88**, Fairbanks, AK, U.S.A., Volume I, pp. 1–12.

Hawkes, I. and Mellor, M. (1972). "Deformation and Fracture of Ice Under Uniaxial Stress", **Journal of Glaciology**, Volume 11, Number 61, pp. 103–131.

Hobbs, P.V. (1974). **Ice Physics**, Oxford University Press, Bristol, UK, 837 p.

Horii, H and Nemat-Nasser, S. (1985). "Compression-Induced Microcrack Growth in Brittle Solids: Axial Splitting and Shear Failure", **Journal of Geophysical Research**, Volume 90, Number B4, pp. 3105–3125.

Horii, H. and Nemat-Nasser, S. (1983). "Overall Moduli of Solids with Microcracks: Load-Induced Anistropy", **Journal of Mechanics and Physics of Solids**, Volume 31, Number 2, pp. 155–171.

Iyer, S. (1989). "A State of the Art Review of Local Ice Loads for the Design of Offshore Structures", 4th State of the Art Report, **IAHR Working Group on Ice Forces**, CRREL Special Report 89-5, Editor G.W. Timco, Hanover, NH, U.S.A., pp. 1–57.

Jefferies, M.G. and Wright, W.H. (1988). "Dynamic Response of the Molikpaq to Ice–Structure Interaction", Proceedings, 7th International Conference on Offshore Mechanics and Arctic Engineering, **OMAE '88**, Houston, TX, U.S.A., Voluem 4, pp. 201–220.

Joensuu, A and Riska K. (1988). **Jään ja rakenteen välinen kosketus (Contact Between Structure and Ice)**, Report M-88, TKK/LRT, Helsinki University of Technology, Faculty of Mechanical Engineering, Laboratory of Naval Architecture and Marine Engineering, in Finnish, Otaniemi, Finland, 57 p.

Johnson, R.C. and Benoit, J.R. (1987). "Iceberg Impact Strength", Proceedings, 19th Offshore Technology Conference, **OTC '87**, Houston, TX, U.S.A., pp. 417–423.

Jones, S.J. (1982). "The Confined Compressive Strength of Polycrystalline Ice", **Journal of Glaciology**, Volume 28, Number 98, pp. 171–177.

Jordaan, I.J., Kennedy, K.P., McKenna, R.F. and Maes, M.A. (1991a). "Loads and Vibration Induced by Compressive Failure of Ice", Proceedings, 6th International Specialty Conference, **ASCE**, Hanover, NH, U.S.A., pp. 638–649.

Jordaan, I.J. and McKenna, R.F. (1991b). "Processes of Deformation and Fracture of Ice in Compression", Proceedings, Symposium on Ice–Structure Interaction, **IUTAM/IAHR**, St. John's, NF, Canada, pp. 283–309.

Jordaan, I.J., Stone, B.M., McKenna, R.F. and Fuglem, M.K. (1990a). "Effect of Microcracking on the Deformation of Ice", Prediction and Performance in Géothechnique, Proceedings, **43rd Canadian Geotechnical Conference**, Université Laval, Québec City, QC, Canada, Volume 1, pp. 387–393.

Jordaan, I.J., McKenna, R.F., Duthinh, D., Fuglem, M., Kenndey, K., Maes, M.A. and Marshall, A. (1990b). **Devlopment of New Ice Load Models**, Report Submitted to Canada Oil and Gas Lands Aministration (COGLA) and Centre for Cold Ocean Resources Engineering (C-CORE), October 26, 1990, 206 p.

Jordaan, I.J. and McKenna, R.F. (1988). "Constitutive Relations for Creep of Ice", Proceedings, 9th International Ice Symposium, **IAHR**, Sapporo, Japan, Volume 3, pp. 47–58.

Jordaan, I.J. and Timco, G.W. (1988). "Dynamics of the Ice Crushing Process", **Journal of Glaciology**, Volume 34, Number 118, pp. 318–326.

Karr, D.G. (1985). "A Damage Mechanics Model for Uniaxial Deformation of Ice", Proceedings, 4th International Conference on Offshore Mechanics and Arctic Engineering, **OMAE**, Volume 2, pp. 227-233.

Kalifa, P., Jones, S.J. and Slade, T.D. (1990). "Microcrack Nucleation in Granular Ice Under Uniaxial Compression: Effect of grain Size and Temperature", **Annals of Glaciology**, Volume 15, 1991, pp. 222-229.

Kalifa, P., Duval, P. and Ricard, M. (1989). "Crack Nucleation in Polycrystalline Ice Under Compressive Stress States", Proceedings, 8th International Conference on Offshore Mechanics and Arctic Engineering, **OMAE**, Houston, TX, U.S.A., Volume IV, pp. 13–21.

Kennedy, K.P. (1990). **Dynamic Activity and Crushed Ice Behaviour in Medium-Scale Ice–Structure Interactions**, M.Eng. thesis, Memorial University of Newfoundland, St. John's, NF, Canada, 158 p.

Kenny, S., Meaney, R., Stone, B. and Jordaan, I.J. (1991). **Failure Zone Characterization: Medium-Scale Field Indentation Program, Hobson's Choice Ice Island 1990**, Report prepared for Institute for Mechanical Engineering, National Research Council Canada, Ottawa, ON, Canada, 34 pp.

Kheisin, D.E. and Cherepanov, N.V. (1970). "Change of Ice Structure in the Zone of Impact of a Solid Body Against the Ice Cover Surface", Proceedings, **Problemy Arktiki i Antarktiki**, Issue 34, pp. 79–84.

Kry, P.R. (1978). **Continuous Crushing of Ice**, Esso Resources Canada Limited, Report IPRT-28ME-78.

Kurdyumov, V.A. and Kheisin, D.E. (1976). "Hydrodynamic Model of the Impact of a Solid on Ice", Prikladnaya Mekhanika, Volume 12, Number 10, pp. 103–109.

Likhomanov, V.A. and Kheisin, D.E. (1971). "Experimental Analysis of a Solid Against Ice", Proceedings, **Problemy Arktiki i Antarktiki**, Issue 38, pp. 103–111.

Lindholm, J-E., Riska, K and Joensuu, A. (1990). **Contact between Structure and Ice: Results from Ice Crushing Test with Flexible Indentor**, Report M-101, TKK/LRT, Helsinki University of Technology, Faculty of Mechanical Engineering, Laboratory of Naval Architecture and Marine Engineering, Otaniemi, Finland.

Määttänen, M.P. (1977). "Ice Force Measurements at the Gulf of Bothnia by the Instrumented Kemi I Lighthouse", Proceedings, 4th International Conference on Port and Ocean Engineering Under Arctic Conditions, **POAC '77**, St. John's, NF, Canada, Volume II, pp. 730–740.

McKenna, R.F., Jordaan, I.J. and Xiao, J. (1990). "Analysis of Damage and Energy Flow in the Crushed Layer During Rapid Ice Loading", Proceedings, 10th International Symposium on Ice, **IAHR '90**, Espoo, Finland, Volume 3, pp. 231–245.

McKenna, R.F., Meyssonier, J. and Jordaan, I.J. (1989). "Peak Pressures from a Damage Model for Ice in Compression", Proceedings, 8th International Symposium on Ice, **OMAE**, The Hague, Netherlands, Volume IV.

Meaney, R., Kenny, S. and Sinha, N.K. (1991). "Medium-Scale Ice-Structure Interaction: Failure Zone Characterization", Proceedings, 11th International Conference on Port and Ocean Engineering Under Arctic Conditions, **POAC '91**, St. John's, NF, Canada, Volume 1, pp. 126–140.

Meyssonnier, J. and Duval, P. (1989). "Creep Behaviour of Damaged Ice Under Uniaxial Compression: A Preliminary Study", Proceedings, 10th International Conference on Port and Ocean Engineering Under Arctic Conditions, **POAC '89**, Luleå, Sweden, Volume 1, pp. 225–235.

Murrell, S.A.F, Sammonds, P.R. and Rist, M.A. (1991). "Strength and Failure Modes of Pure Ice and Multi-Year Sea Ice Under Triaxial Loading", Proceeding, Symposium on Ice–Structure Interaction, **IUTAM/IAHR**, St. John's, NF, Canada, pp. 339–361.

Nadreau, J.-P., Mawwar, A.M. and Wang, Y.S. (1988). "Triaxial Testing of Freshwater Ice at Low Confining Pressures", Proceedings, 7th International Conference on Offshore Mechanics and Arctic Engineering, **OMAE '88**, Houston, TX, U.S.A., Volume IV, pp. 117–124.

Riska, K. (1991). "Theoretical Modelling of Ice-Structure Interaction", Proceedings, Symposium on Ice–Structure Interaction, **IUTAM/IAHR**, St. John's, NF, Canada, pp. 595–618.

Riska, K., Rantala, H. and Joensuu, A. (1990). **Full Scale Observations of Ship–Ice Contact**, Report M-97, TKK/LRT, Helsinki University of Technology, Faculty of Mechanical Engineering, Laboratory of Naval Architecture and Marine Engineering, Helsinki University of Technology, Otaniemi, Finland, 54 p.

Sanderson, T.J.O (1988). **Ice Mechanics: Risks to Offshore Structures**, Graham and Trotman Limited, London, UK, 253 p.

Schapery, R.A. (1991). "Models for the Deformation Behaviour of Visoelastic Media with Distributed Damage and Their Applicability to Ice", Proceedings, Symposium on Ice–Structure Interaction, **IUTAM/IAHR**, St. John's, NF, Canada, pp. 191–230.

Schulson, E.M. (1990). "The Brittle Compressive Fracture of Ice", **Acta Metallurgica et Materialia**, Volume 38, Number 10, pp. 1963–1976.

Schulson, E.M., Gies, M.C. and Lasonde, G.J. (1989). "The Effect of the Specimen-Platen Interface on the Internal Cracking and Brittle Fracture of Ice Under Compression: High-Speed Photography", **Journal of Glaciology**, Volume 35, Number 121, pp. 378–382.

Sinha, N.K. (1991). "Kinetics of Microcracking and Dilatation in Polycrystalline Ice", Proceedings, Symposium on Ice–Structure Interaction, **IUTAM/IAHR**, St. John's, NF, Canada, pp. 69–87.

Sinha, N.K. (1990a). "Is Miniumum Creep Rate a Fundamental Material Property?", Proceedings, 9th International Conference on Offshore Mechanics and Arctic Engineering, **OMAE '90**, Houston, TX, U.S.A., Volume IV, pp. 283–288.

Sinha, N.K. (1990b). "Microfracturing and Creep Dilation in Polycrystalline Columnar-Grained and Equiaxed Ice", Proceedings, 4th International Conference, **Creep and Fracture of Engineering Materials and Structures**, Swansea, U.K., pp. 345–354.

Sinha, N.K. (1988). "Experiments on Anisotropic and Rate-Sensitive Strain Ration and Modulus of Columnar-Grained Ice", Proceedings, 7th International Conference on Offshore Mechanics and Arctic Engineering, **OMAE '88**, Houston, TX, U.S.A., Volume IV, pp. 354–360.

Sinha, N.K. (1984). "Intercrystalline Cracking, Grain-Boundary Sliding, and Delayed Elasticity at High Temperatures", **Journal of Materials Science**, Volume 19, pp. 359–376.

Sinha, N.K. (1978). "Short-Term Rheology of Polycrystalline Ice", **Journal of Glaciology**, Volume 21, Number 85, pp. 457–473.

Stone, B.M., Jordaan, I.J., Jones, S.J. and McKenna, R.F. (1989). "Damage of Isotropic Polycrystalline Ice Under Moderate Confining Pressures", Proceedings, 10th International Conference on Port and Ocean Engineering Under Arctic Conditions, **POAC '89**, Luleå, Sweden, Volume 1, pp. 408–419.

Sunder, S.S. and Wu, M.S. (1990). "Crack Nucleation Due to Elastic Anistropy in Polycrystalline Ice", **Cold Regions Science and Technology**, Volume 18, Number 1, pp. 29–47.

Szyszkowski, W. and Glockner, P.G. (1985). "Modelling the Time-Dependent Behaviour of Ice", **Cold Regions Science and Technology**, Volume 11, Number 1, pp. 3–21.

Wang, Y.S. (1981). "Uniaxial Compression Testing of Arctic Sea Ice.", Proceedings, International Conference on Port and Ocean Engineering Under Arctic Conditions, **POAC '81**, Québec City, QC, Canada, Volume 1, pp. 346–355.

Weertman, J. (1969). "Effect of Cracks on Creep Rate", Transactions of the **ASM**, Volume 62, pp. 502–511.

Winkler, M.M. and Dorris, J.F. (1990). "Discussion of Recent Work to Develop a More Realistic Pressure–Area Curve for Ice", Proceedings, 9th International Conference on Offshore Mechanics and Arctic Engineering, **OMAE '90**, Houston, TX, U.S.A., Volume IV, pp. 231–235.

Xiao, J. (1991). **Finite Element Modelling of Damage Processes in Ice–Structure interaction**, M.Eng. thesis, Memorial University of Newfoundland, St. John's, NF, Canada, 95 p.

Appendix A

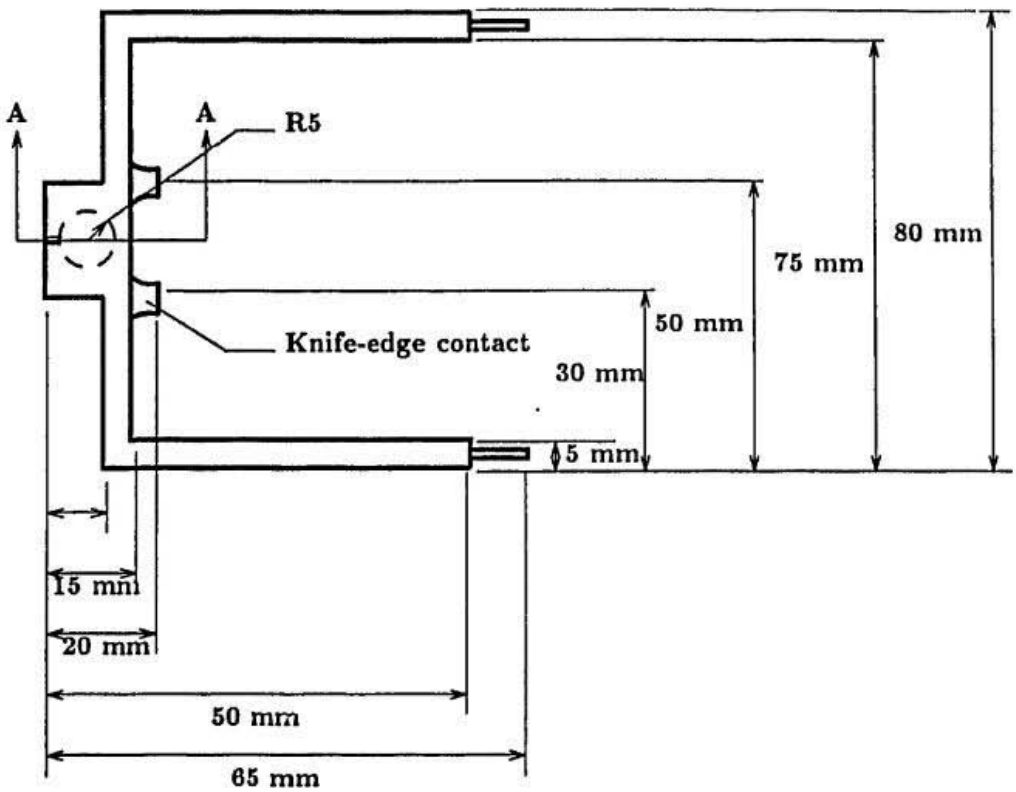

ALUMINUM MOUNTING COLLAR FOR AXIAL LVDT

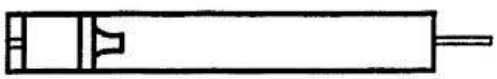

SECTION A–A

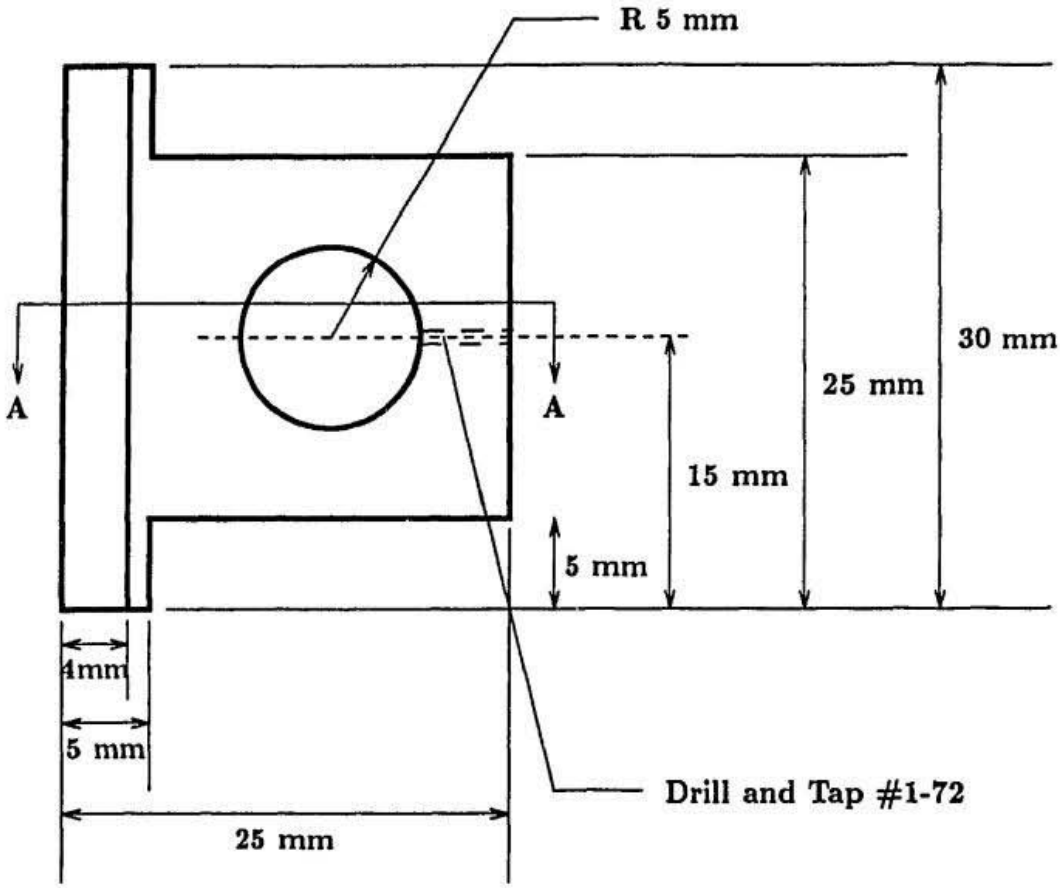

ALUMINUM MOUNTING COLLAR FOR LATERAL LVDT

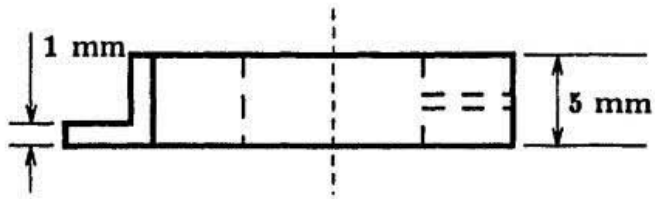

SECTION A-A

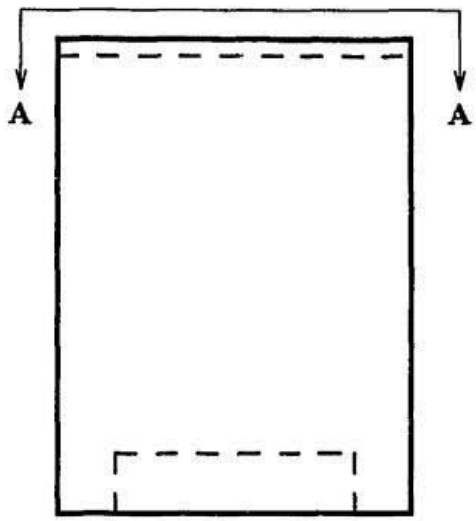

BRASS ENDCAP FOR MOUNTING ICE SAMPLE

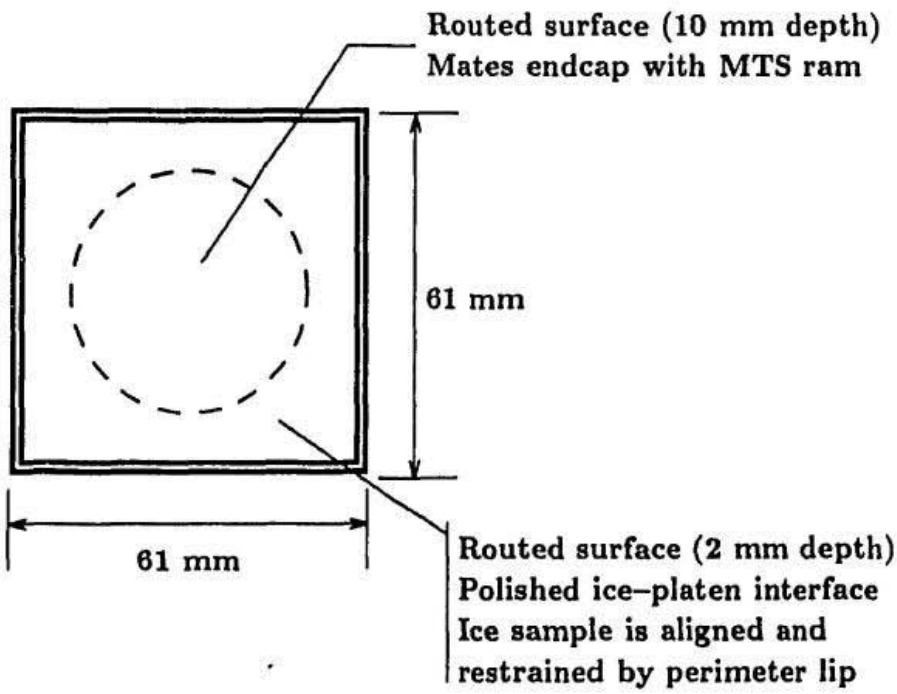

SECTION A-A